The effects of atmospheric stability on wind farm layout optimization

by

D. Dane

in partial fulfilment of the requirements for the degree of

Master of Science
in Sustainable Energy Technology

at the Delft University of Technology,
to be defended publicly on July 22, 2021, at 10:00 AM

Student number:	4384377
Supervisor:	Dr. ir. D.J.N. Allaerts
Thesis committee:	Prof. dr. S.J. Watson
	Dr. ir. D.J.N. Allaerts
	Dr. S. Basu
Date:	July 5, 2021

Wind Energy Group, Faculty of Aerospace Engineering, Delft University of Technology

Abstract

The power production of downstream wind turbines in a wind farm is significantly impacted by wake effects of upstream turbines. Improving the layout optimization process could reduce these wake losses and therefore result in more efficient wind farms. The wakes are also affected by atmospheric stability conditions, as stable conditions lead to a reduced wake recovery, and unstable conditions lead to an improved wake recovery. The topic of atmospheric stability has quickly gained more attention in wind energy research over the recent years. However, there is still little research done that focuses specifically on the effects of atmospheric stability on the wind farm layout optimization process.

This thesis aims to determine the effects of atmospheric stability on the optimal layout of a wind farm and to quantify the potential benefits of considering stability conditions in the layout optimization process. A stability-dependent Jensen wake model is developed, using a stability-dependent wake decay coefficient based on the non-dimensional Obukhov length. The developed model is implemented in FLORIS, a wake modeling utility for Python, to calculate the wind field and the annual energy production (AEP). A simplistic layout optimization method is used, in which the positioning of wind turbines relative to each other is fixed and only the orientation of the entire wind farm is varied. To quantify the potential benefits of considering stability conditions, the layout optimization is done twice for each analyzed case: once using the determined stability conditions and once using the assumption of neutral stability conditions. The resulting benefit of considering stability effects is expressed as the potential AEP gain.

The results of the first cases looked promising, showing potential AEP gains of 7.4%, 5.6%, and 9.2%. However, these cases consist of unrealistic wind conditions and were mostly intended to study the effects of different stability conditions on the resulting optimal layout. For example, it is found that it is more beneficial to reduce wake overlap for stable conditions than for unstable conditions, which results in stable wind directions playing a dominant role in the optimization process. Cases with semi-realistic wind conditions showed significantly lower potential AEP gains of 0.1% and 0.7%. Finally, a real case based on meteorological data from an offshore site in the Netherlands resulted in a potential AEP gain of 0.0%.

It is concluded that the benefits of considering stability effects in the layout optimization process are likely to be insignificant. In most cases, the layout optimization under neutral stability conditions already optimizes for wind directions with stable conditions, as stable conditions tend to be more frequent in wind directions with high wind speeds. It is expected that there can be a small potential AEP gain in cases with unusual stability distributions that differ significantly from the described trend. However, even in such cases it is likely that the benefits are still very small.

Table of Contents

List of Figures

List of Tables

Nomenclature

Latin symbols

A_0	Rotor swept area	R	Specific gas constant
A_w	Cross-sectional area of wake	Ri	Richardson number
c_p	Specific heat capacity	Ri_B	Bulk Richardson number
C_T	Thrust coefficient	s	Turbine spacing
D	Rotor diameter	T	Temperature
g	Gravitational acceleration	T_v	Virtual temperature
h	Hub height	u	Wind speed (ambient)
k_w	Wake decay coefficient	u_*	Friction velocity
k^*	Growth parameter	v	Wind speed (wake)
L	Obukhov length	w	Wind speed (vertical)
p	Air pressure	x	Downwind distance
q	Specific humidity	z	Height
r	Radius of wake	z_0	Surface roughness

Greek symbols

Θ	Potential temperature	κ	Von Kármán constant
Θ_v	Virtual potential temperature	ρ	Air density

Abbreviations

AEP	Annual Energy Production
CFD	Computational Fluid Dynamics
DOWA	Dutch Offshore Wind Atlas
FLORIS	FLOw Redirection and Induction in Steady State
IWFBL	Infinite Wind Farm Boundary Layer
KNMI	Koninklijk Nederlands Meteorologisch Instituut / Royal Netherlands Meteorological Institute
LES	Large Eddy Simulation
MABL	Marine Atmospheric Boundary Layer
NREL	National Renewable Energy Laboratory
RANS	Reynolds-Averaged Navier Stokes
TKE	Turbulent Kinetic Energy
WAsP	Wind Atlas Analysis and Application Programme

1. Introduction

The total installed capacity of wind energy reached 743 GW in 2020 (GWEC, 2021). The installed capacity doubled between 2013 and 2019 and increased by a factor of over 30 compared to 2000 (WWEA, 2020). In 2020, the newly installed capacity reached a record of 93 GW, which is a 53% year-on-year increase compared to 2019 (GWEC, 2021). The installed capacity of wind energy increases rapidly. Despite this rapid growth, it is estimated that the rate of new installed capacity must be three times faster to limit global warming to well below 2° C above pre-industrial levels (GWEC, 2021). This limit is a goal that was set in the 2015 Paris climate agreement, which is an agreement by 196 parties to combat climate change (UNFCCC, n.d.). To meet this goal, it is not only important to install more wind farms, but also to keep optimizing the design of these wind farms. Improving the layout optimization process for wind farms leads to higher energy yields, resulting in a more cost-effective energy generation and a more efficient use of the available space and resources.

The layout of a wind farm is generally optimized based on known distributions of wind speed and wind direction at a given site (Samorani, 2010). The performance of wind turbines within a wind farm is heavily impacted by the wake effects of upstream turbines. Studies by Barthelmie et al. (2009) and Stevens et al. (2014) showed that downstream wind turbines in a wind farm roughly have a 40% reduced power output compared to wind turbines in the front row. The topic of wake effects is well-known in the field of wind energy research and there are many methods developed for simulating these wake effects. In layout optimization, engineering models such as the Jensen model (Jensen, 1983) or the Gaussian model (Bastankhah and Porté-Agel, 2014) are often used. However, more detailed engineering models are still developed, such as the curled wake model developed by Martínez-Tossas et al. (2019) and a controls-oriented model by King et al. (2020) that includes yaw-induced wake recovery and secondary steering. Wake effects are strongly influenced by atmospheric stability, with unstable conditions leading to fast wake recovery and stable conditions leading to slow wake recovery (Abkar and Porté-Agel, 2015). These stability effects have a large impact on the performance of wind turbines within a wind farm. Alblas et al. (2014) show in their study that the power output of a wind farm in stable conditions is 10-20% lower than in unstable conditions. Similarly, Barthelmie and Jensen (2010) found a 9% decrease in wind farm efficiency when comparing stable with unstable conditions. Research on atmospheric stability in wind energy applications has become increasingly popular over the recent years (Borvarán et al., 2020; Krutova et al., 2020; Ghaisas et al., 2017). However, there is still little research that focuses specifically on the impact of atmospheric effects on the layout optimization process. One of the few examples is a recent study by Guo et al. (2021), which has some parallels with the work presented in this thesis. In their study, the layout optimization is performed for different stability conditions. Their results show a significant change in the optimal layout compared to the assumption of neutral stability conditions and an increase in power generation of 0.94%.

This thesis aims to determine the effects of atmospheric stability on the optimal layout of a wind farm and to quantify the potential benefits of considering stability conditions in the layout optimization process. A stability-dependent Jensen wake model is developed by implementing a stability-dependent wake decay coefficient. Calculations of the wind field and the annual energy production (AEP) are done using FLORIS, a wake modeling utility for Python (FLORIS, 2020). A simplistic layout optimization method is used, in which the positioning of wind turbines relative to each other is fixed and only the orientation of the entire wind farm is changed. The optimization method is applied to five cases, which range from very simplistic to finally a realistic case based on meteorological data from an offshore site in the Netherlands. For each case, the layout optimization is done with and without the consideration of stability conditions. The resulting benefits of considering stability conditions, compared to assuming neutral stability conditions, are quantified by a parameter introduced as the potential AEP gain.

To achieve the aim of this thesis, the following goals are set:

- To develop a simple layout optimization method that includes stability-dependent wake modelling
- To analyze the effects of different stability conditions on wakes in a wind farm and how these effects change the resulting optimal layout
- To determine the optimal layout and the potential AEP gain for four hypothetical cases and for one real case using wind conditions based on meteorological data.
- To compare the performance of the stability-dependent Jensen and Gaussian wake models

The report is structured as follows. In chapter 2, the required theoretical background is given, which is mainly focused on wake modelling, atmospheric stability, and the relation between these two topics. In chapter 3, the layout optimization process is described and the method to determine the potential AEP gain is introduced. The stability effects on the wakes and on the resulting optimal layout are analyzed in detail. The AEP results for the first four cases are presented in separate sections. In chapter 4, a stability-dependent Gaussian wake model is developed and compared to the stability-dependent Jensen wake model. The calibration of the stability-dependent growth parameter and a validation using the AEP results are described. The stability-dependent Gaussian wake model is applied to two cases and the results are compared with the results from the Jensen model. Additionally, the influence of the turbine spacing and the ambient wind speed on the potential AEP gain is determined for both models. In chapter 5, the potential benefits of considering stability conditions are determined for a realistic case. The wind conditions for this final case are based on meteorological data from an offshore site in the Netherlands. The method to determine the stability conditions is explained, after which the wind conditions are analyzed. The AEP and optimization results are then presented. In chapter 6, the conclusions are summarized per chapter. A general conclusion is also given, which directly addresses the main goals of this thesis. Finally, some recommendations for future projects are given.

2. Theoretical Background

In this chapter a theoretical background is presented, which is mainly focused on wake modelling, atmospheric stability, and the relation between these two topics. In section 2.1, the Jensen wake model and the Gaussian wake model are described. In section 2.2, some basic concepts of atmospheric stability are explained, and the most common stability parameters are described. Section 2.3 focuses on the wake decay coefficient; the only adjustable parameter in the Jensen wake model, which represents the wake recovery rate. Commonly used values for this coefficient are given, and a model to implement a stability-dependent wake decay coefficient is presented. In section 2.4 the relation between atmospheric stability and wind speed is described. Finally, in section 2.5, some general information is given about the wake modeling software FLORIS, which is used in this thesis.

2.1 Wake models

Wake models are engineering models that provide a computationally inexpensive method for calculating the wind field in a wind farm, which is particularly useful for layout optimization applications. When wind flows through a wind turbine rotor, the kinetic energy of the wind is partly extracted by the rotor. This extracted energy causes the rotor to move and results in the generation of electrical energy, referred to as wind energy. The extraction of kinetic energy from the wind causes the wind speed to be lower behind the wind turbine, which results in a wake downstream of the turbine. In a wind farm, these wakes have a significant impact on the incoming wind speed for subsequent wind turbines. It is therefore crucial for the development of wind farms to have a good understanding of the size and shape of these wakes and the downstream velocity deficits within these wakes. In general, there are two main approaches to modelling these wakes. The first approach is to use computational fluid dynamics (CFD). An example of this is to accurately calculate the flow field by solving the Reynolds-averaged Navier-Stokes (RANS) equations. Another commonly used method is large eddy simulation (LES) in which filtered Navier-Stokes equations are used to remove small scale flow effects. The main disadvantage of CFD is that it requires large computational power, which often leads to long computation times. The second approach is to use analytical models or engineering models. These models are approximations of reality, which are made empirically by describing what is observed. The physics in these models is often simple, but they still give fairly accurate results for specific parameters, for example if only the wind speed far from the turbine is required. Studies by Barthelmie et al. (2011) show that both the CFD approach and the engineering models have similar accuracy when it comes to predicting wake losses. For wind farm layout optimization, it is particularly useful to have a fast way of calculating the wind field. This is because for each step in the optimization process, the positions of the turbines or the wind conditions can be different, which means that for each step the wind field has to be calculated. This is the main reason for using engineering models in this thesis. In the following sections, two specific wake models are described in detail. Section 2.1.1 considers the Jensen wake model, the main wake model used in this thesis. Section 2.1.2 considers the Gaussian wake model, which is only used in chapter 4, where its performance is compared to the Jensen model.

2.1.1 Jensen wake model

The Jensen wake model, which was introduced by N.O. Jensen in 1983, is one of the most widely used wake models due to its simplicity and relatively good accuracy. The main idea of the model is based on the following two assumptions. Firstly, the wake has a conical shape of which the initial diameter is equal to the diameter of the rotor. The diameter and thus the width of the wake increases linearly with increasing downstream distance from the rotor. Secondly, the wind speed is constant over the cross-section of the wake. Due to conservation of mass, the wind speed increases with downstream distance. The balance of mass is given in equation 2.1.

$$\pi r_0^2 v_0 + \pi(r^2 - r_0^2)u = \pi r^2 v \tag{2.1}$$

A visualization of the wake model is given in figure 2.1. In both equation 2.1 and figure 2.1, v is the wind speed within the wake at distance x downstream from the turbine, v_0 is the initial wind speed right behind the rotor, r is the radius of the wake at distance x, r_0 is the initial radius equal to half the rotor diameter, u is the ambient wind speed, and α is the wake expansion coefficient.

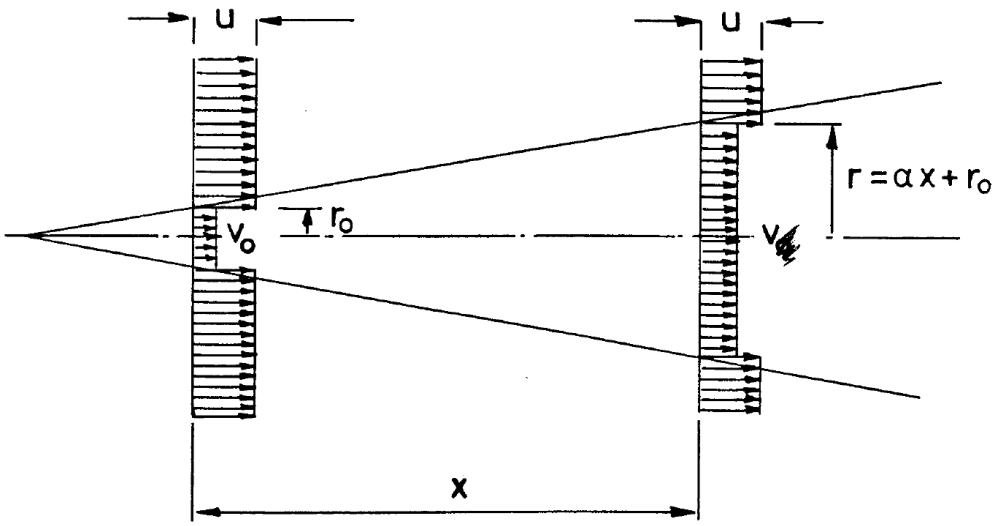

Figure 2.1. Schematic of the Jensen wake model with definition of symbols. (Jensen, 1983)

Using the mass balance in equation 2.1, an expression for the wind speed in the wake can be found. For this expression, an assumption from actuator disc momentum theory is used to define the initial wind speed behind the rotor as $v_0 = 1/3 * u$. Substituting this for v_0 in equation 2.1 results in an expression for the wind speed as given in equation 2.2.

$$v = u\left(1 - \frac{2}{3}\left(\frac{r_0}{r_0 + \alpha x}\right)^2\right) \tag{2.2}$$

To test the accuracy of the model, Jensen compared velocity deficits for a single turbine with measurements by Vermeulen (1979). For this comparison, a wake expansion coefficient of 0.1 was used. The agreement between the model and the measurements was found to be excellent for the wake

centerline velocity deficits. There was, however, a large dissimilarity between the top-hat shape of the velocity profile of the model and the more bell-shaped curve of the measurements. Jensen shows that a better agreement is found if a cosine-bell distribution is applied as a modulation to the wake function. However, he also reasons that for practical purposes, the over and under-estimation of the wake deficits of the top-hat shape are likely to cancel out. He therefore does not add the distribution as a requirement for the model and only gives a recommendation of using such a distribution when a more precise calculation is required. The Gaussian wake model described in section 2.1.2 is an example of such a wake model that does use a gaussian distribution for the radial velocity deficits. The Jensen model keeps the top-hat shaped velocity profile that resulted from the assumption of constant wind speed over the cross-section of the wake. Nowadays, it is exactly this top-hat velocity profile that is so characteristic for the Jensen wake model.

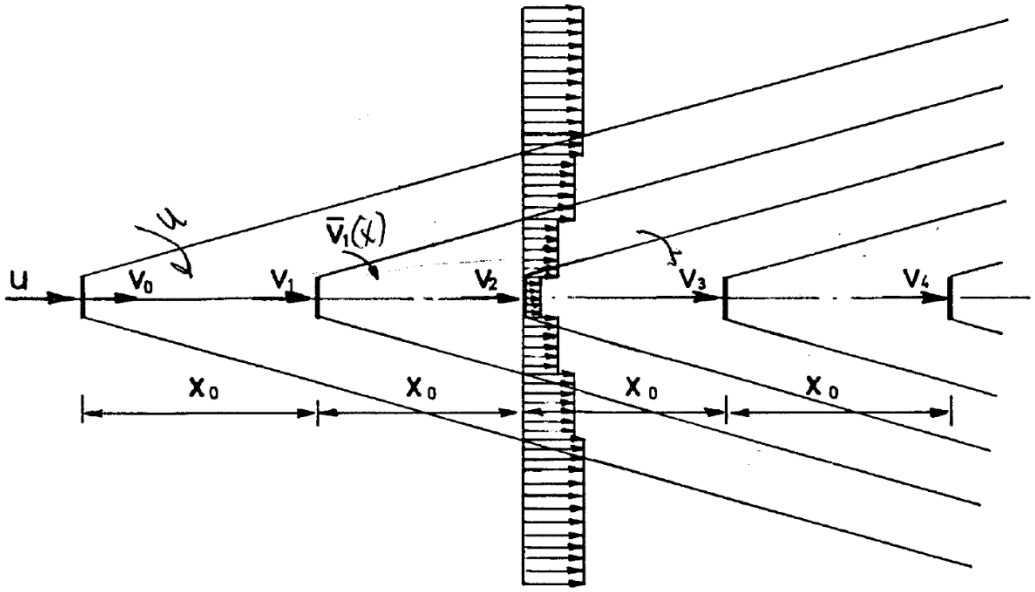

Figure 2.2. Schematic of the Jensen wake model with wake interaction. (Jensen, 1983)

The wake model is expanded by adding a method to determine wake interaction between multiple turbines. A visualization of this method is given in figure 2.2, for a case in which there are several turbines in a straight line behind each other. The main idea behind it is that the wind speed in the wake of the first turbine at the downstream distance x of the second turbine is now the incoming wind speed for the second turbine. For the second turbine, instead of having an ambient wind speed u, this ambient wind speed is the wind speed v_1 from the wake of first turbine. This also means that the wind speed right after the second turbine is $1/3 * v_1$. In principle, this method can be applied to as many turbines as required, however the calculations become complicated quickly. Jensen therefore assumes that the ambient wind speed seen by subsequent turbines is equal to u, the real ambient wind speed. This assumption means that the wake recovery is overestimated. Using this method, an asymptotic expression is found for the wind speed v_∞ incoming on turbines on later rows. This expression is given in equation 2.3. The expression is no longer dependent on x, but rather on x_0, which is the distance between the turbines. It

is found that this asymptotic value is already reached after the first two turbines, meaning that any turbine from the third row on will operate at this wind speed.

$$v_\infty = u\left(1 - \frac{2y}{1-y}\right) \qquad with \qquad y = \frac{1}{3}\left(\frac{r_0}{r_0 + \alpha x_0}\right)^2 \tag{2.3}$$

The model was further developed by Katic et al. in 1987 to take into account the turbine characteristics. The main goals were to improve the accuracy of the model and to improve the efficiency of wind turbine cluster configurations. It is again stated that the wind speed in the cross-section of the wake is constant, because the goal is not to describe the wind field as accurately as possible, but rather to find a good estimate for the wind speed incoming on other turbines, specifically for the purpose of estimating the AEP. An expression for the velocity deficit of the new model is given in equation 2.4 and now includes the thrust coefficient C_T. The wake expansion coefficient α is replaced by the wake decay coefficient k_w and the radius r is replaced by the diameter D. The velocity deficit is normalized and given by $1 - v/u$. For example, if the ambient wind speed is 10 m/s and the wind speed at some distance x in the wake is 8 m/s, the resulting velocity deficit is 0.2.

$$1 - \frac{v}{u} = \frac{1 - \sqrt{1 - C_T}}{(1 + 2k_w x/D)^2} \tag{2.4}$$

To add the velocity deficits of multiple wakes, a sum of squares of the velocity deficits is used. The assumption behind this is that the energy deficit of the mixed wake is equal to the linear sum of the energy deficits of the individual wakes. The resulting velocity deficit for a combination of two wakes is given in equation 2.5. In this equation, v_1 and v_2 are the velocities in the individual wakes and v is the velocity in the mixed wake.

$$\left(1 - \frac{v}{u}\right)^2 = \left(1 - \frac{v_1}{u}\right)^2 + \left(1 - \frac{v_2}{u}\right)^2 \tag{2.5}$$

Katic et al. compared the model with test examples from more sophisticated models from a comparison study by Ainslie in 1982. They found that the results are generally in agreement with the other models. The main problem is determining the wake decay coefficient, as it is influenced by factors such as ambient turbulence, turbine-induced turbulence, and atmospheric stability. However, they also conclude that the overall power output is relatively insensitive to the wake decay coefficient. The reason for this is that a small value for this coefficient results in a large power reduction for a small angle, while a large value results in a small power reduction for a large angle. Therefore, the wake decay coefficient is mainly important for calculations in very specific wind directions, but this importance is reduced when all wind directions are considered. Finally, they conclude that this model is a practical tool for wind farm developers interested in AEP estimations, but that other models should be used for other aspects like turbulence, loads and economics.

2.1.2 Gaussian wake model

The Gaussian wake model that is considered in this thesis is introduced by Bastankhah and Porté-Agel in 2014. They start by describing the Jensen wake model and point out that there are two important limitations to this model. The first is the top-hat shape of the velocity deficit profile, which is simply not a realistic representation of the velocity deficits observed in wind turbine wakes (Chamorro and Porté-Agel, 2010). The second is that Jensen (1983) claimed to use conservation of momentum to derive his model, while Bastankhah and Porté-Agel show in their paper that it was actually only conservation of mass that was used. They follow up with an expression for the velocity deficit proposed by Frandsen (2006) as given in equation 2.6. Frandsen did use momentum conservation to derive this expression, but still assumed a top-hat shaped velocity profile. In this expression, A_0 is the rotor swept area and A_w is the cross-sectional area of the wake, which is a function of distance x.

$$1 - \frac{v}{u} = \frac{1}{2}\left(1 - \sqrt{1 - 2\frac{A_0}{A_w}C_T}\right) \tag{2.6}$$

The derivation for the Gaussian model starts with the assumption that the velocity deficit has a Gaussian shape, regardless of the incoming wind conditions. The expression for the velocity deficit therefore takes the form of equation 2.7. In this expression, $C(x)$ is the maximum velocity deficit at the wake centerline, which is the peak of the Gaussian curve, r is the radial distance from the wake centerline, and σ is the standard deviation of the velocity deficit profile.

$$1 - \frac{v}{u} = C(x)\exp\left(-\frac{r^2}{2\sigma^2}\right) \tag{2.7}$$

To find an expression for $C(x)$, mass and momentum conservation is used in which viscous and pressure terms are neglected. Combined with the total force on the turbine, this results in the expression for $C(x)$ given in equation 2.8. An assumption is made for a linear expansion of the wake.

$$C(x) = 1 - \sqrt{1 - \frac{C_T}{8(\sigma/D)^2}} \qquad with \qquad \frac{\sigma}{D} = k^*\frac{x}{D} + \varepsilon \tag{2.8}$$

The growth parameter k^* in equation 2.8 is similar to the wake decay coefficient for the Jensen model, however there is an important difference. In the Jensen model this coefficient is $k_w = dr/dx$, which represents the growth rate of the wake radius. In the Gaussian model this coefficient is $k^* = d\sigma/dx$, which represents the growth rate of the standard deviation. The value for the standard deviation right behind the turbine is given by ε as x approaches zero. The expression for ε is a function of the thrust coefficient and is given in equation 2.9.

$$\varepsilon = 0.25\sqrt{\beta} \qquad with \qquad \beta = \frac{1}{2}\left(\frac{1+\sqrt{1-C_T}}{\sqrt{1-C_T}}\right) \tag{2.9}$$

Combining equation 2.7 and 2.8 results in the expression for the velocity deficit of the Gaussian wake model, as given in equation 2.10. In this expression, y is the spanwise coordinate, z is the vertical coordinate, and z_h is the wind turbine hub height.

$$1-\frac{v}{u}=\left(1-\sqrt{1-\frac{C_T}{8(k^*x/D+\varepsilon)^2}}\right)exp\left(-\frac{1}{2(k^*x/D+\varepsilon)^2}\left(\left(\frac{z-z_h}{D}\right)^2+\left(\frac{y}{D}\right)^2\right)\right) \tag{2.10}$$

The results of the model are compared with five different LES and experimental case studies. It is concluded that the velocity profiles that are obtained are in acceptable agreement with the LES and experimental data. In contrary, top-hat shaped models like the Jensen model generally underestimate the velocity deficit at the wake centerline and overestimate the velocity deficit at the edges of the wake. The new Gaussian model is also more consistent and accurate when it comes to power estimation, compared to the Jensen model, which is often sensitive to the position of turbines and the wind direction.

2.1.3 Summary

The most important equations from this section are equations 2.4 and 2.10. These equations describe the velocity deficits in the wake for the Jensen model and the Gaussian model, respectively. The Jensen model is the main model used throughout this thesis, and is made stability-dependent using the wake decay coefficient. The stability-dependent wake decay coefficient is introduced in section 2.3.2 and is first applied in chapter 3. The Gaussian model is used only in chapter 4, where its performance is compared with the Jensen model.

2.2 Atmospheric stability

Atmospheric stability is a measure for the tendency of the atmosphere to suppress or enhance vertical motion. There are three main types of stability conditions, which are neutral, stable, and unstable conditions. In a stable atmosphere, vertical motion is naturally suppressed, while in an unstable atmosphere, vertical motion is enhanced. In this section, the basic concepts and equations that are required to understand atmospheric stability are explained. The equations and figures in this section are taken from the book Wind Energy Meteorology by Emeis (2018), unless stated otherwise.

2.2.1 Air density

Air pressure is a measure for the amount of air above a certain area. Going higher up in the atmosphere, this air mass becomes smaller and therefore the air pressure decreases. Under the assumption that there is no vertical motion, the change in air pressure with height is described by the hydrostatic equation given in equation 2.11. In this equation, p is air pressure, z is height, g is the gravitational acceleration, ρ is air density, R is the specific gas constant of air, and T is the absolute temperature.

$$\frac{\partial p}{\partial z}=-g\rho=-\frac{gp}{RT} \tag{2.11}$$

It is important to note that air density is not constant, but instead is dependent on both temperature and pressure (and therefore height). As an example, the air density is plotted in figure 2.3 for different air temperatures and pressures for typical near-surface conditions. Air density decreases as temperature increases, which means that warm air is less dense than cold air. Similarly, air density also decreases as height increases, which means that under the assumption of constant temperature, air density is lower at greater heights. However, generally speaking the air temperature is lower at greater heights, which implies that the density should increase somewhat. This balance between the decrease of air density due to an increase in height, and the increase of density due to a decrease in temperature, immediately raises an interesting aspect of atmospheric stability. It is also one of the key aspects for the parameterization of atmospheric stability, as is shown later in section 2.2.2.

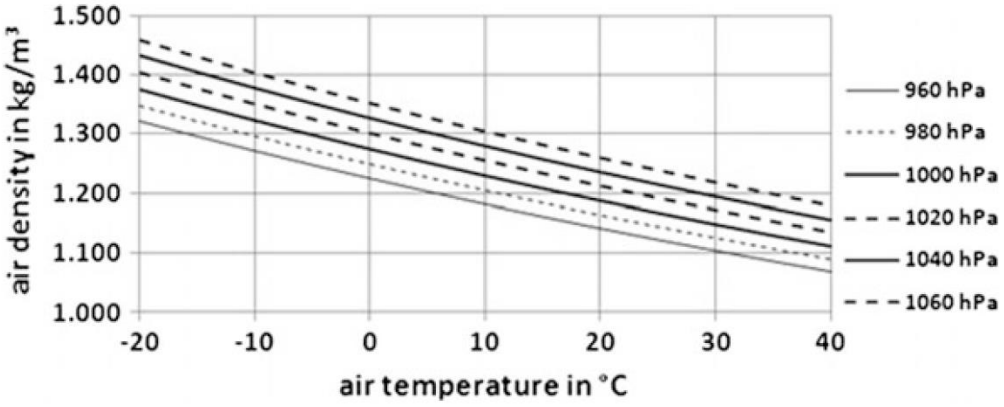

Figure 2.3. Air density for different temperatures and pressures for typical near-surface conditions. (Emeis, 2018)

Next to temperature and height, there is a third important factor that influences air density, which is humidity. Humid air is less dense than dry air. The virtual temperature T_v is used to compare the temperature of different air masses with different humidities. It is defined as the temperature at which a dry air mass has the same density as a humid air mass with temperature T and humidity q. Since humid air is less dense, this virtual temperature is always higher than the temperature of the humid air. An expression for the virtual temperature is given in equation 2.12. The specific humidity q is expressed in kg of water vapor per kg of air.

$$T_v = T(1 + 0.609q) \tag{2.12}$$

The difference between the dry air temperature and the virtual temperature depends on temperature and humidity. The saturation level of water in air depends strongly on the temperature, which means that the difference between the amount of water contained in saturated cold air and saturated warm air is large. This difference is clearly visible in figure 2.4, which shows the temperature increment from the dry air temperature to the virtual temperature, for different air temperatures and humidities.

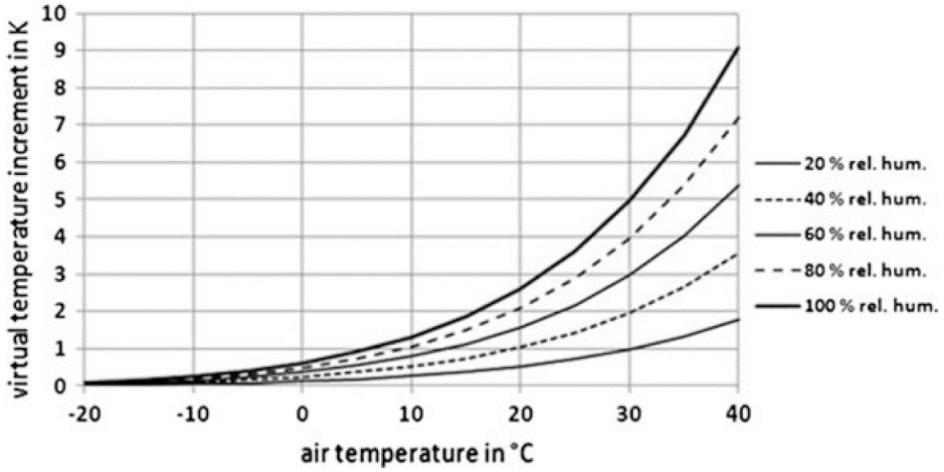

Figure 2.4. Temperature difference between dry air temperature and virtual temperature for different air temperatures and humidity levels. (Emeis, 2018).

2.2.2 Potential temperature

In section 2.2.1 it is mentioned that there is an interesting balance for the air density with increasing height, which is a balance between the decrease in air density due to a decrease in pressure with height and an increase in air density due to a decrease in temperature with height. In this section, this balance is explained in more detail, and it is used to define a stability parameter. The decrease of pressure with height is given earlier in the hydrostatic equation in equation 2.11. In neutral conditions, the decrease of temperature with height is described using an adiabatic vertical temperature gradient. An expression for this gradient is given in equation 2.13, in which c_p is the specific heat of air.

$$\frac{\partial T}{\partial Z} = -\frac{g}{c_p} \tag{2.13}$$

It is described that in a stable atmosphere, vertical motion is naturally suppressed, while in an unstable atmosphere, vertical motion is enhanced. To explain the concept of stability, an example is given first. As a first case, imagine that the atmosphere would only have a negative temperature gradient and a constant pressure. If an air parcel with a slightly higher air temperature than its environment is released in such an atmosphere, it would go up, since it has a lower density than the surrounding air. As soon as it has gone up, the temperature difference between the air parcel and the environment is larger and therefore the air parcel is accelerated upwards even more. This effect keeps getting stronger, therefore this is a clear example of an unstable atmosphere that enhances vertical motion. As a second case, imagine an atmosphere with a constant temperature and a negative pressure gradient. If an air parcel with a slightly higher density is released in such an atmosphere, it would fall down, since it is heavier than the surrounding air. However, as this parcel is falling down, it reaches a point where its density is lower than the density of the surrounding air. This causes the air parcel to be pushed up again, up to the point where it becomes heavier than the surrounding air and it starts to fall down again. This process keeps repeating and the air parcel stays at roughly the same height. It is therefore a clear example of a stable atmosphere that suppresses vertical motion.

In reality, both gradients are present and therefore the atmospheric stability depends on the balance between these two gradients. If the temperature gradient is strong enough relative to the pressure gradient, it is likely that vertical motion is enhanced, resulting in an unstable atmosphere. And vice versa, if the pressure gradient is strong enough, this results in a stable atmosphere. The potential temperature Θ, given in equation 2.14, is introduced to quantify this balance and to determine whether the atmosphere is stable or unstable. In this equation, p_0 is the surface pressure.

$$\theta = T\left(\frac{p_0}{p}\right)^{\frac{R}{cp}} \tag{2.14}$$

The potential temperature is defined such that it is constant with height in a neutral atmosphere. The atmosphere is considered stable if the potential temperature increases with height, so when $\partial\theta/\partial z > 0$. The atmosphere is considered unstable if the potential temperature decreases with height, so when $\partial\theta/\partial z < 0$. The following example is used to give a quantitative feeling for the balance between the temperature gradient and the pressure gradient. The potential temperature is linearly proportional with air temperature and inversely proportional with air pressure to the power of (R/c_p). If the air temperature decreases by 10%, it is multiplied by a factor of 0.9. To keep the potential temperature constant, the air pressure would also have to be multiplied by this same factor of 0.9, but raised to the power of $(R/c_p)^{-1}$. Using typical values for c_p = 1005 J kg^{-1} K^{-1} and R = 287 J kg^{-1} K^{-1}, gives a ratio between these values of roughly 3.5. This means that the air pressure in this situation would have to be multiplied by a factor of $0.9^{3.5}$ = 0.69. This example shows that if the air temperature decreases by 10%, the air pressure in a neutral atmosphere decreases by approximately 31%. If the air pressure decreases less than this 31%, it means that the temperature gradient is relatively stronger than the pressure gradient, which results in an unstable atmosphere. If the air pressure decreases more than this 31%, the pressure gradient is relatively stronger than the temperature gradient, which results in a stable atmosphere.

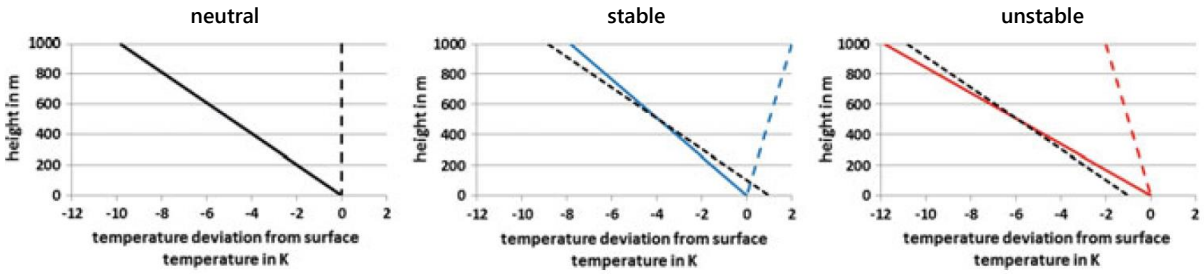

Figure 2.5. Virtual temperature profiles for neutral (left), stable (middle) and unstable (right) classes. The air temperature is plotted with full lines. The potential temperature is plotted with long dashes. A shifted version of the adiabatic temperature profile of the neutral class is plotted with short dashes in the stable and unstable classes. This profile intersects the air temperature profile at 500 m and is used as a reference for stability. (Emeis, 2018).

A visualization of the potential temperature in the three stability classes is given in figure 2.5. The air temperature is plotted with full lines. The potential temperature is plotted with long dashes. The adiabatic decrease in air temperature of the neutral class (left) is plotted with short dashes on the stable class (middle) and on the unstable class (right). It is clearly shown in these plots that the potential temperature is constant with height for the neutral class, and that it increases or decreases with height for the stable and unstable classes, respectively. The plots can also be used to explain the stability effects. An air parcel that follows adiabatic temperature changes is described by the black full curve on the left plot. If this same air parcel is put at a height of 500 m in the stable atmosphere, the temperature change is shown with the short dashes in the middle plot. If the air parcel is moved upwards, its temperature is lower than the temperature of the surrounding air at the same height, causing it to return to its initial position. When it is moved downwards, its temperature is higher than the surrounding air, which also causes it to return to the initial position. This shows that the atmosphere is stable with an increasing potential temperature. Similarly, the right plot can be used to show that the atmosphere is unstable for a decreasing potential temperature.

To account for humidity, the method that is used for the virtual temperature in section 2.2.1 is applied to the potential temperature. The new parameter Θ_v is introduced as the virtual potential temperature, given in equation 2.15. The reasoning that is used for the virtual temperature is the same, therefore the expressions for both parameters are practically the same.

$$\theta_v = \theta(1 + 0.609q) \tag{2.15}$$

2.2.3 Non-dimensional stability parameters

The potential temperature is almost never used directly as a stability parameter. It is often more practical to have a non-dimensional stability parameter. In this section, two non-dimensional stability parameters are introduced that both use the potential temperature. The first is the Richardson number and the second is the non-dimensional Obukhov length.

The Richardson number Ri is a measure for the ratio between buoyancy effects and wind shear effects. There are different forms of the Richardson number. The first form that is introduced is the gradient Richardson number, which is given in equation 2.16. In this expression, u is the wind speed component in the mean wind direction and $\partial u/\partial z$ is the wind shear. The squared wind shear is an indication of the kinetic energy available to cause turbulence (Stull, 2017). Similar to the potential temperature, the sign of the Richardson number determines the stability, with $Ri > 0$ indicating a stable atmosphere and $Ri < 0$ indicating an unstable atmosphere.

$$Ri = \frac{g\frac{\partial \theta_v}{\partial z}}{\theta_v\left(\frac{\partial u}{\partial z}\right)^2} \tag{2.16}$$

For real situations it is often impossible to measure the wind speed at many different heights to determine the wind shear. It is more common that measurements are taken at fixed heights with a relatively large vertical distance between them. For this reason, the bulk Richardson number Ri_B is introduced, as is given in equation 2.17. The bulk Richardson number uses the delta operator to indicate differences between two points, rather than gradients. This form of the Richardson number is the most frequently used in boundary layer studies. When the bulk Richardson number is applied to air layers directly above the surface, it can be simplified further by removing the delta operator from the height z and the wind speed u, as both values are zero at the surface.

$$Ri_B = \frac{g\Delta\theta_v\Delta z}{\theta_v(\Delta u)^2} \tag{2.17}$$

Before introducing the second non-dimensional stability parameter, it is important to introduce the friction velocity u_*. The friction velocity is used as a velocity scale in boundary layer meteorology and is dependent on the turbulent momentum flux, which depends on fluctuations in the different wind components. Fluctuations in the mean wind direction are given by u' and fluctuations in the vertical wind direction are given by w'. The friction velocity is defined as the square root of the turbulent momentum flux at the surface, as given in equation 2.18. In this expression the subscript 0 indicates that surface values of u' and w' are used.

$$u_* = \sqrt{\overline{u'w'}_0} \tag{2.18}$$

The second stability parameter is the Obukhov length L, given in equation 2.19. The Obukhov length itself is, as the name suggests, not a non-dimensional parameter and is interpreted as the height at which the production of turbulence by buoyancy is equal to the production of turbulence by wind shear. The constant κ is the von Kármán constant, which is generally set to 0.4. The term $\overline{\theta_v{}'w'}_0$ in the right denominator is the surface heat flux, which is similar to the turbulent momentum flux.

$$L = \frac{\theta_v}{\kappa g}\frac{u_*^3}{\overline{\theta_v{}'w'}_0} \tag{2.19}$$

The Obukhov length is made non-dimensional by using the height z. Instead of dividing the Obukhov length L by z, it is more practical to divide z by L. The reason for this is that it results in the same characterization of stability classes as found for the Richardson number and the potential temperature. This means that the non-dimensional Obukhov length z/L represents a neutral atmosphere when $z/L = 0$, a stable atmosphere when $z/L > 0$, and an unstable atmosphere when $z/L < 0$. The expression for the stability parameter z/L is given in equation 2.20.

$$\frac{z}{L} = \frac{\kappa g z}{\theta_v}\frac{\overline{\theta_v{}'w'}_0}{u_*^3} \tag{2.20}$$

2.2.4 Summary

Sections 2.2.1 and 2.2.2 are mostly intended as an introduction to atmospheric stability for readers with little knowledge on the topic, providing background information for some of its basic concepts. The most important equations from this section are equations 2.17 and 2.20, which give expressions for the bulk Richardson number Ri_B and the non-dimensional Obukhov length z/L, respectively. The non-dimensional Obukhov length is the main stability parameter used in this thesis. The stability classes and boundaries that are used, are introduced in the general methodology in chapter 3. The stability-dependency of the wake decay coefficient is also based on this stability parameter, as is shown in the section 2.3.2 of the theoretical background. The bulk Richardson number is only applied in chapter 5, in which it is required to determine the stability conditions from meteorological data.

2.3 Wake decay coefficients

The wake decay coefficient k_w is the only adjustable parameter in the Jensen wake model and can be used to calibrate the model to match certain observations. The choice of the wake decay coefficient is important, as it can significantly impact the predicted AEP of a wind farm. In the Jensen model, the wake decay coefficient represents the expansion of the wake with downwind distance. A high value results in a fast expansion of the wake, which means that the velocity deficit in the wake decreases rapidly with distance. The rate at which the velocity deficit is reduced is referred to as the wake recovery. The wake decay coefficient is therefore a measure for wake recovery, with high values resulting in a fast wake recovery and low values resulting in a slow wake recovery. Atmospheric stability also has an impact on wake recovery, with stable conditions resulting in a slower wake recovery, and unstable conditions resulting in a faster wake recovery, compared to neutral conditions (Abkar and Porté-Agel, 2015).

In many studies and applications, a constant wake decay coefficient is used. The coefficient in these cases is determined by the wind conditions over a year or an even longer period, such that the predicted AEP matches the observed AEP for a specific site. Examples of studies that use a constant wake decay coefficient are discussed in section 2.3.1. Another option is to use a wake decay coefficient that is not constant, but rather dependent on the actual wind conditions. Usually, the coefficient in these cases is dependent on some stability parameter. Studies that consider the effects of stability on wake recovery are discussed in section 2.3.2.

2.3.1 Constant wake decay

The goal for this section is to show that there is not one correct value for the wake decay coefficient and to give an indication of the range of values that are found in literature. In the study where Jensen introduced his wake model (Jensen, 1983), he suggested a value of 0.1 for the wake decay coefficient. He does not give any specific reasoning for choosing this value, other than indicating that for usual wakes the entrainment constant (as it was referred to in this paper) should be approximately 0.1. The results of the model are compared to measurements by Vermeulen (1979) and show excellent agreement for this value. However, the results are also compared to measurements of the Nibe-wake project by

Højstrup (1983). To calibrate the model with these measurements, the wake decay coefficient has to be set to 0.07. Even though Jensen states that the calibration is probably not justified due to some uncertain assumptions, the difference between these two values already shows that there is a significant discrepancy between the correct values when matching observations. In a follow-up study by Katic et al. (1987), in which Jensen was also involved, a value of 0.075 is used. However, different types of turbines are used, and it is concluded that for some turbines a value of 0.11 fits much better, indicating that the type of turbine also affects wake recovery. The explanation given is that the turbine with the higher coefficient had different rotor blades that likely induced additional turbulence. It is also concluded in this paper that the overall AEP for a wind farm is relatively insensitive to small changes in the wake decay coefficient.

In 1992 Frandsen suggested an empirical expression for the wake decay coefficient based on site parameters, as given in equation 2.21. In this expression, h is the hub height and z_0 is the surface roughness. The fact that this wake decay coefficient is dependent on the surface roughness, immediately shows that there is a large difference between the wake recovery offshore and onshore. For offshore sites, the surface roughness is typically considered to be 0.0002 m, whereas for onshore sites this value can differ between 0.03 m for grassland, 0.5-1.0 m for forests and over 2 m for urban areas (Stull, 2017). For typical offshore (z_0=0.0002 m) and onshore (z_0=0.05 m) sites, this results in wake decay coefficients of 0.038 and 0.066, respectively, at a hub height of 100 m.

$$k_w = \frac{0.5}{\ln\left(h/z_0\right)} \tag{2.21}$$

In 1987 the Department of Meteorology and Wind Energy at the Risø National Laboratory in Denmark released the first version of the Wind Atlas Analysis and Application Programme (WAsP). WAsP is a commercial software that can be used for almost anything related to wind energy, for example for wake modelling, wind resource assessment or energy yield calculations. Nowadays, the development of WAsP is done by the Department of Wind Energy at the Technical University of Denmark and it has become an industry standard in the field of wind energy. The WAsP-recommended value for the wake decay coefficient is 0.075 for onshore sites and 0.04-0.05 for offshore sites (DTU Wind Energy, n.d.). Many studies that use the Jensen wake model either use these recommended values or, when using different values, compare their results with cases that use the recommended values. It can therefore be said that the WAsP-recommended values are currently a baseline reference for the comparison of wake decay coefficients.

The WAsP-recommended values are generally accepted to be a good estimate for the wake decay coefficients for offshore sites. However, there can still be significant differences between the values that are found when matching the predicted AEP to the observed AEP for different sites. For offshore sites, the differences between surface roughness values are generally smaller than for onshore sites. This is because for onshore sites there can be different types of vegetation or even geographical features, while for offshore sites the differences in surface roughness values are caused mainly by waves. This means

that for offshore sites, the differences between the found wake decay coefficients are primarily the result of differences in atmospheric stability conditions. This statement is further supported by comparing the results from the following two studies. Barthelmie and Jensen (2010) studied wake losses at the Nysted offshore wind farm and found a wake decay coefficient of 0.03 to best match the observations. Similarly, Gaumond et al. (2014) studied the Horns Rev offshore wind farm and found a coefficient of 0.04. It is interesting to note that the wind conditions at the Nysted wind farm are generally more stable than at the Horns Rev wind farm. This is also another indication that stable conditions result in a slower wake recovery and therefore in more wake losses. According to Peña and Rathmann (2013), the overall effect of stability on wind speed in a wind farm is larger than the effect of surface roughness. They reason that, since surface roughness is generally considered a major factor in wind farm development, atmospheric stability should be considered as an important factor as well.

2.3.2 Stability-dependent wake decay

One of the most important aspects of wake modelling is wake recovery, which in the Jensen wake model is reflected by the wake decay coefficient. Wake recovery is dependent on site parameters, such as the surface roughness, but more importantly on wind conditions, such as the atmospheric stability. It is explained in section 2.2 that in a stable atmosphere, vertical motion is suppressed, while in an unstable atmosphere, vertical motion is enhanced. This vertical motion affects the mixing of air between layers with the ambient wind speed and air in the wake. This means that during stable conditions there is reduced mixing, resulting in a slower wake recovery, while during unstable conditions there is increased mixing, resulting in a faster wake recovery. As mentioned in section 2.3.1, the effects of atmospheric stability on velocity deficits in a wind farm are estimated to be greater than the effects of surface roughness and should therefore be considered as a major factor in wind farm development (Peña and Rathmann, 2013).

The goal of this thesis is to study the effects of atmospheric stability on the wind farm layout optimization process. It is therefore crucial to find a relation between the stability conditions and the wake recovery, and to be able to quantify this relation between the wake decay coefficient and some stability parameter. The main work that is used to find a relation between the wake decay coefficient and the Obukhov length is by Peña and Rathmann (2013) and Peña et al. (2014). Their work is based on the infinite wind farm boundary layer (IWFBL) model by Frandsen (1992) and is extended to take atmospheric stability into account. Peña and Rathmann (2013) used the IWFBL model by Frandsen, which was intended for neutral conditions only, and added a local atmospheric stability correction function, based on work by Emeis (2010). They found the expression for the wake decay coefficient given in equation 2.22. In this expression, κ is the von Kármán constant, which is generally set to 0.4 and $\Psi(z/L)$ is the stability correction function, which depends on the non-dimensional Obukhov length.

$$k_w = \frac{\kappa}{\ln(z/z_0) - \Psi(z/L)} \tag{2.22}$$

The stability correction function, given in equation 2.23, is obtained from Paulson (1970). It depends on the stability parameter z/L and the coefficients a and b, which are determined empirically. The values that are used for these coefficients are $a = 5$ and $b = 16$ and are obtained from Högström (1988).

$$\Psi(z/L) \begin{cases} = 2\,ln\left(\frac{1+x}{2}\right) + ln\left(\frac{1+x^2}{2}\right) - 2\,arctg(x) + \frac{\pi}{2} & for \quad \frac{z}{L} < 0 \\ = 0 & for \quad \frac{z}{L} = 0 \\ = -a\frac{z}{L} & for \quad \frac{z}{L} > 0 \end{cases} \qquad (2.23)$$

$$with \qquad x = \left(1 - b\frac{z}{L}\right)^{1/4}$$

Peña and Rathmann (2013) used this new expression for a stability-dependent wake decay coefficient and implemented it in a modified Park wake model, which is based on the Jensen wake model. The Park wake model is evaluated for an infinite array of wind turbines, for which the wind speed, turbine spacing, surface roughness, and stability conditions can be adjusted. They compared the model with the IWFBL model by Frandsen and the IWFBL model by Emeis (2010). It is worth noting that in their study, the wind speed reduction (or velocity deficit) is only determined far downstream, since the wake model is compared with infinite wind farm models. The results show that the recommended WAsP values for the wake decay coefficient are generally too high for cases with a low surface roughness. The coefficients are further adjusted to match the velocity deficits given by the IWFBL model of Frandsen. It is found that the adjusted values are much lower than the WAsP-recommended values for all roughness lengths and a wide range of neutral to stable conditions. Peña et al. (2014) used the modified Park wake model to compare the stability-dependent wake decay coefficient and the WAsP-recommended value of 0.05. In this follow-up study, the wakes are modelled individually, and the simulation layout is based on the Horns Rev I offshore wind farm. The resulting velocity deficits are compared, using power data from the wind farm. The power of each individual turbine is used to estimate the wind speed at that turbine. The power of the front turbine is used as a proxy for the ambient wind speed. Data from a nearby met mast is used to determine the bulk Richardson number, which is then converted to the stability parameter z/L, which is required to determine the stability-dependent wake decay coefficient. The results show a good agreement between the simulations and the observed velocity deficits in the wind farm. Interestingly, the stability-dependent model was closer to the observations for turbines in the last rows, while the model using the WAsP-recommended values was closer for turbines in the first rows. This makes sense, as the stability-dependent values are based on an infinite farm model, which therefore should more accurately predict velocity deficits in situations that resemble an infinite farm. It is, however, noted that the wind speed reduction that would be obtained using the IWFBL model is not approached by any of the simulated cases. This is likely because they account for multiple wind directions, rather than just one wind direction parallel to the row. It is also found that, as expected, the velocity deficits for both the simulations and the observations are largest for stable conditions and smallest for unstable conditions. The energy yield for the two different approaches for the wake decay coefficient is not determined, therefore no conclusion is made on which value gives a better overall prediction of the total power generation.

Another method for adding stability effects to the Jensen wake model is used by Schmidt et al. (2016). In this study, two methods for calculating the AEP for an existing onshore wind farm are compared. The wind farm is located in North America and the input data for both methods is generated using a one-year mesoscale simulation of the site. The first method uses CFD and the second method uses the Jensen wake model. To implement the stability effects in the Jensen model, an empirical model for determining the velocity deficit is used. This model is introduced by Salimi (2016) and is obtained by fitting parametrized curves to the wake centerline velocity deficits from CFD RANS simulations of an actuator disk model. The model describes a function f, given in equation 2.24, which is multiplied by the incoming wind speed to obtain an additional velocity deficit due to stability effects. In this equation, s is the non-dimensional downwind distance given in number of rotor diameters ($s = x/D$), and a and b are coefficients determined by s and the following constants: $c_1 = 0.1695$, $c_2 = 2.156$, $c_3 = 6.73$, $c_4 = 0.033$, $c_5 = 0.0026$, $c_6 = 0.074$, and $c_7 = -0.011$.

$$f\left(s, \frac{z}{L}\right) = a(s)\sqrt{\left|\frac{z}{L}\right|} + b\frac{z}{L} \qquad with \quad \begin{cases} a(s) = c_1 \exp\left[-\left(\frac{s-c_2}{c_3}\right)^2\right], & b = c_4 \quad for \ \frac{z}{L} > 0 \\ a(s) = c_5 s - c_6\,, & b = c_7 \quad for \ \frac{z}{L} < 0 \end{cases} \tag{2.24}$$

The additional velocity deficit is added to the velocity deficit obtained by the Jensen model to determine the stability-dependent total velocity deficit. For example, if for stable conditions the factor is 0.1 and the incoming wind speed is 10 m/s, then an additional velocity deficit of 1 m/s should be taken into account as a result of stability effects. For unstable conditions, this factor is negative, resulting in a reduced total velocity deficit. The results of both the CFD method and the wake models are compared with power data of the wind farm. It is found that the stability corrected wake model predicted the AEP more accurately than the neutral wake model. It is, however, also found that both methods underestimate the wind speeds at the turbine locations and therefore do not accurately predict the AEP. One possible reason that is given for this is that the power data obtained for that year could be coincidently biased towards high values. Other reasons are that the terrain at which the site is located is too complex for the used models or that the 10° resolution of the wind sectors was too coarse to observe significant wake effects. It is concluded that the results of the wake models are in agreement with the CFD results, but that more detailed simulations are required to adequately predict the performance of the wind farm at this complex site.

2.3.3 Summary

The wake decay coefficient reflects the wake recovery rate in the Jensen wake model. There is not one single value that most accurately predicts the wake effects for any given site. Instead, the wake decay coefficient is a site-specific parameter, which is often determined by matching predictions to observations. In case no site-specific values are determined, the WAsP recommended values of 0.075 for onshore sites and 0.05 for offshore sites are widely considered to be a good reference. Since the goal of this thesis is to study the effects of atmospheric stability on the wind farm layout optimization process, it is crucial to have a relation between the wake decay coefficient and the stability conditions. The most important equation from this section is therefore equation 2.22, which gives the expression for the wake

decay coefficient k_w as a function of the stability parameter z/L. The values for the stability-dependent wake decay coefficients that are obtained from this expression are given in table 3.1 in chapter 3.

2.4 Relation between atmospheric stability and wind speed

Wind speed is the most important parameter for the power production of any wind farm. It is generally beneficial to optimize the layout of a wind farm for the wind directions that have the highest occurrence and the highest average wind speeds. However, it is described in sections 2.2 and 2.3 that atmospheric stability also has a significant influence on the power production, due to effects on the wake recovery. It is important to understand the relation between atmospheric stability and wind speed. For example, it could be that high wind speeds are more likely to be stable. This would mean that these high wind speeds are less beneficial than expected when assuming neutral conditions. The information presented in this section is used to develop the semi-realistic wind conditions of case 4 in section 3.5 and to analyze the wind conditions obtained from the meteorological data presented in section 5.3.

The first study that is highlighted in this section is by Archer et al. (2016). This study focuses on wind speed, atmospheric stability, and turbulent kinetic energy (TKE) in the marine boundary layer (MABL) of the northeastern U.S. Two data sets, which use different measurement methods, are compared to find which parameters are suitable as a proxy for atmospheric stability, with the main stability parameter based on the Obukhov length. It is found that the shape of the wind speed profile is often non-logarithmic in unstable conditions, but very rarely non-logarithmic in stable conditions. It is concluded that a non-logarithmic wind speed profile is a good qualitative proxy for unstable conditions, but that having unstable conditions does not necessarily mean that the profile cannot be logarithmic. In this study, the atmospheric stability conditions are plotted against many different parameters, such as the wind direction, hour of day, month, but also the wind speed. The plot for atmospheric stability for the different wind speed bins is shown in figure 2.6. It is found that for this site the MABL is predominantly unstable, with 61% unstable, 21% neutral, and 18% stable conditions. Neutral conditions are found more at low wind speeds and are most uncommon at intermediate wind speeds. This is an interesting finding, since wind farms operate mostly at these intermediate wind speeds and this observation implies that the assumption of neutral stability is wrong for a large part of the operating time. It is also found that unstable conditions generally have lower wind speeds than neutral and stable cases, and that this observation is most distinct during summer months. The highest frequency of stable conditions is during spring (25%) and the highest frequency of unstable conditions is during fall (77%) and winter (63%). This is likely due to large temperature differences between water and air resulting in unstable atmospheric conditions. Wharton and Lundquist (2012) obtained similar results when comparing the mean wind speeds for all stability classes. They found that the lowest mean wind speeds occur in the spring and summer months during unstable conditions.

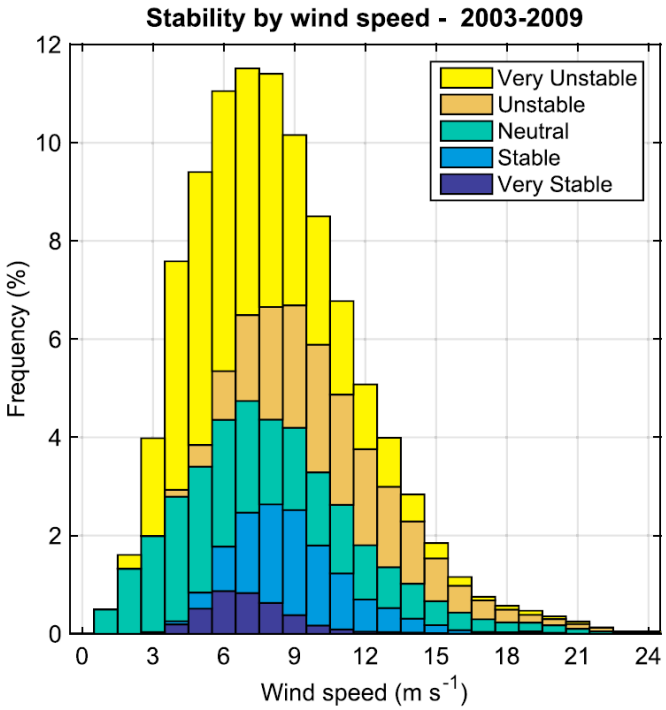

Figure 2.6. Frequency of atmospheric stability classes for different wind speeds. The data is from multi-level measurements on the Cape Wind met mast in the northeastern U.S. (Archer et al., 2016).

A study that clearly shows a relation between stability and wind speed is by Rodrigo et al. (2018). The goal of this study is to establish a process for evaluating meso-micro methodologies for wind resource assessment. A range of methods that couple meso and microscale models is studied to find a trade-off between accuracy and computational cost. These models are not particularly relevant for this thesis, however, they are compared with observed distributions of atmospheric stability versus wind speed, which are relevant. The data is from the Cabauw onshore met mast in the Netherlands, which is characterized by horizontally homogenous conditions and a surface roughness of 0.15 m. The bin-based normalized stability distributions are shown in figure 2.7, in which blue and red represent stable and unstable conditions, respectively. The occurrence of the different wind speeds is shown with a gray line. The reference height is 80 m and the stability parameter used is the non-dimensional Obukhov length z/L. These observations show a clear relation between atmospheric stability and wind speed. Unstable conditions are most common at low wind speeds, while stable conditions are most common at intermediate wind speeds. Neutral conditions become more common as the wind speed increases. These findings are in agreement with what is generally observed in literature. Emeis (2018) states that atmospheric stability and wind speed are usually correlated; unstable conditions are often found in low wind speeds, while stable conditions are more frequent in higher wind speeds. Holtslag et al. (2014) show similar results to the observations shown in figure 2.7, with unstable conditions clearly favoring lower wind speeds and stable conditions favoring higher wind speeds.

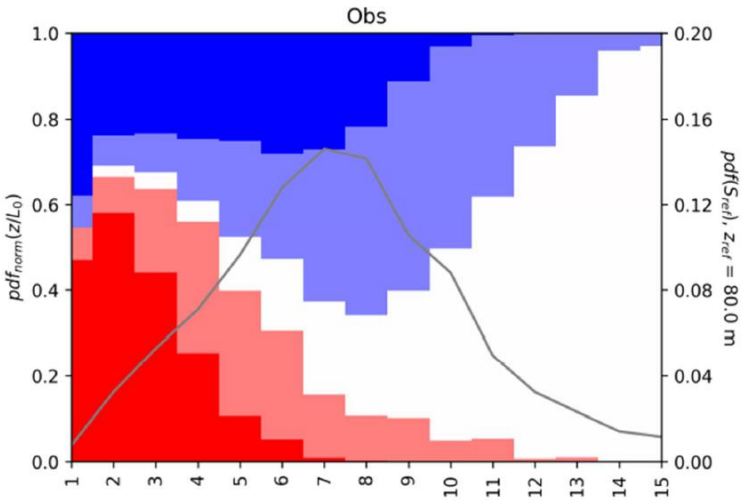

Figure 2.7. Bin-based normalized stability distributions (left vertical axis) based on observations from the Cabauw onshore met mast in the Netherlands. Blue and red represent stable and unstable conditions, respectively. The probability density function of the wind speed (right vertical axis) is shown with a gray line. The reference height is 80 m. (Rodrigo et al., 2018).

2.5 Wake modeling software: FLORIS

The wake modeling software used in this thesis is FLORIS (FLOw Redirection and Induction in Steady State), which is a wake modeling utility in Python that is developed by NREL. The software is completely open-source, which is one of the main reasons for choosing this software. Another reason is the fact that it is developed for Python, which conveniently allows modification of the code and therefore also the implementation of new features, such as the required stability-dependent wake decay coefficient. FLORIS is designed as a computationally inexpensive modeling tool for steady-state wake characteristics in wind farms. There are many different models implemented in FLORIS, including models for velocity deficits, wake deflection, wake steering, and turbulence. A few examples of models included in FLORIS are the Jensen wake model, the Gaussian wake model, the Curl model, and the Gauss-Curl-Hybrid model. Additionally, there are also tools for flow visualization, AEP calculations, layout optimization and other options.

The inputs for FLORIS are divided into three main sections: wake, turbine, and farm. Firstly, the wake section is where the wake model is defined. As mentioned before, there are many different options for which wake model is used and more complex models also include more options, such as wake steering and added turbine-induced turbulence. The Jensen model is the most simple model and includes only one adjustable parameter; the wake decay coefficient, which is set to 0.05 by default. Secondly, the turbine section is where the specifications of the turbine are defined. This includes geometrical parameters such as the hub height and the rotor diameter, but also performance parameters such as the power and thrust curves. The default turbine in FLORIS is the NREL 5MW reference turbine, which is described in more detail in section 2.5.1. Finally, the farm section is where both the layout of the wind

farm and the wind conditions are defined. Individual turbines are modelled by setting the farm layout to a 1x1 wind farm. When modelling multiple wind directions and wind speeds, for example in an AEP calculation, the flow field is reinitialized for each step. Such a step generally takes less than a second for wind farms of 100 turbines. It is stated by Bay et al. (n.d.) that the computation time for the wake of an individual turbine is 0.0018 s for the Jensen model and 0.0025 s for the Gaussian model.

2.5.1 NREL offshore 5-MW baseline wind turbine

The NREL offshore 5-MW baseline wind turbine, referred to in this thesis as the NREL 5MW reference turbine, is presented in a technical report by Jonkman et al. (2009). The turbine was designed to be a baseline reference to standardize offshore wind turbine specifications. It is useful to have a reference model that is used by multiple research teams, as it makes it easier to compare the results from different studies by eliminating effects caused by specific turbine models. Many studies use the model, and it can therefore be said that it has successfully become a baseline reference in wind energy research.

The wind turbine is a conventional three-bladed wind turbine. Some examples of main properties are the hub height of 90 m, the rotor diameter of 126 m, and a rated wind speed of 11.4 m/s. Table A.1 includes all of the gross properties and is given in appendix A. Some of the steady-state responses, including the power curve and the thrust curve, are given in figure A.1. The model is mainly based on the REpower 5M wind turbine, but it is a combination of other existing wind turbine prototypes and conceptual models from other projects. The conceptual models were used for additional information, because not all the required detailed data was available from the turbine manufacturers.

3. Layout optimization with stability-dependent Jensen wake model

The main goal of this chapter is to use a simple optimization method to determine the potential AEP gain that is achieved by considering stability effects in the layout optimization process. The wind conditions in the cases in this chapter range from very simple with only one wind direction, to semi-realistic with wind conditions based on wind statistics from a real site. The purpose of the first three cases is to serve as a proof of concept for considering stability in layout optimization and to give a benchmark value for the potential AEP gain in extreme cases. The wind conditions in these cases are therefore unrealistic, and the relation between wind speed and stability is not based on any of the literature findings described in section 2.4. The fourth, semi-realistic case is used to provide a more accurate indication of the potential AEP gain for real sites.

In section 3.1, the general method that is used for all cases is explained. In section 3.2, the first case is presented and used to introduce some of the reasoning and terminology that is used throughout this chapter. The effects of the stability-dependent wake decay coefficient are shown, and a method to quantify the benefits of considering stability effects is introduced. In section 3.3 the second case is presented, which consists of two wind directions with different stability conditions. An extensive analysis is given on the differences between the neutral and the non-neutral case, and on which stability condition plays a dominant role in the resulting optimal layout. In section 3.4, the extreme case for any combination of two wind directions is found, which results in the highest possible potential AEP gain. Finally, in section 3.5, the optimization method is applied to a semi-realistic case, which is based on a wind resource map of the North Sea.

3.1 General methodology

In this section, the simple optimization method that is used is explained. The base layout of the wind farm, the used wind turbine, and the definition of the stability classes are also described.

3.1.1 Layout optimization method

Throughout this thesis, a simplistic layout optimization method is used. In this method, the positioning of wind turbines relative to each other is fixed and only the orientation of the entire wind farm is varied. This means that the number of rows, the number of turbines per row, and the turbine spacing are all fixed. The only free parameter in this optimization method is the orientation of the wind farm (relative to north). There are two main reasons for choosing this method over the more conventional approach of optimizing the position of each individual turbine. The first reason is that the traditional layout optimization method often results in a rather random looking wind farm layout. One of the goals of this

thesis is to determine the effects of stability conditions on the optimal layout. This analysis would be almost impossible for such seemingly random layouts, as it difficult to quantify changes between different stability conditions. The used method provides the option to concisely quantify the change in the optimal layout. For example, rotating the farm by 3° results in a 5% increase in AEP. The second reason is to reduce computation times. With the traditional layout optimization method, a 3x3 wind farm has 18 free parameters to optimize, while a 9x9 wind farm has 162 free parameters to optimize. This means that it takes significantly longer to optimize larger wind farms. With the used method, all wind farm layouts only have one free parameter. Larger farms will still have longer computation times due to an increased complexity of wake effects, but this applies to both methods. Additionally, by introducing stability effects into the optimization process, the number bins required to describe the wind condition is increased by a factor of 5. This generally means that the computation time is also increased by roughly the same factor. Using this method, the expected increase in computation time is compensated by reducing the number of free variables.

The layout optimization method is used to determine the optimal layout, which for this method can also be referred to as the optimal orientation. The optimal orientation is considered to be the orientation that results in the highest annual energy production (AEP). To find the optimal orientation, the AEP is calculated in case-specific wind conditions for a farm orientation of 0° to 90° in steps of 1°. A visualization of this process is given in figure 3.1. The cases are generally defined by their wind conditions, as both the used farm layout and the variation of the farm orientation are the same for all cases. The used layout is a 9x9 square grid with a turbine spacing of 7D. The only exception is in section 4.4, in which the goal is specifically to study the effect of different layouts. The used turbine for all cases is the 5MW reference wind turbine, developed by NREL to be used as a reference to standardize baseline offshore wind turbine specifications. More information on this wind turbine is given in section 2.5.1.

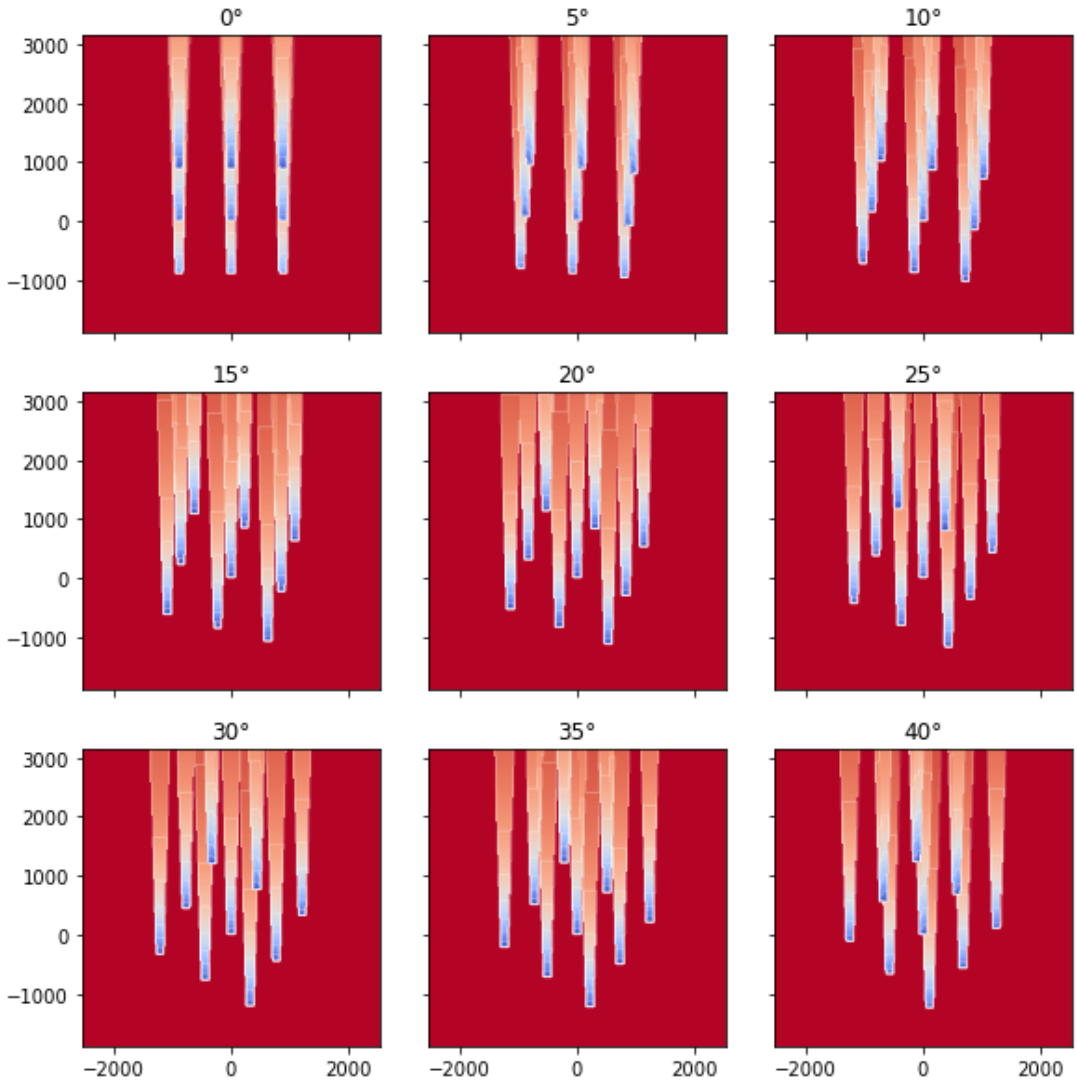

Figure 3.1. Visualization of some steps in the optimization process. In this example, the wind farm orientation is rotated from 0° to 40° in steps of 5°. In the used method, the orientation is changed from 0° to 90° in steps of 1°.

3.1.2 Definition of stability classes

One of the goals of this thesis is to study the effects of atmospheric stability on the resulting optimal layout of a wind farm. It is therefore important to understand how the stability classes are defined and how the AEP is affected by wind conditions with different stability classes. The stability classes are defined using the non-dimensional Obukhov length as a stability parameter. As described in section 2.2, the Obukhov length L is a common stability parameter that is used in combination with height z, which is usually the hub height, to create a non-dimensional stability parameter z/L. The stability classes used in this thesis are shown in table 3.1 and are based on values found in Schmidt (2016), Peña et al. (2014) and Brand (2008). The AEP is calculated using the Jensen wake model in FLORIS. The Jensen wake model, described in section 2.1, is one of the most widely used wake models due to its simplicity and yet relatively good accuracy. FLORIS is a wake modeling tool in Python developed by NREL and is described in more detail in section 2.5. In the Jensen wake model, the velocity deficit in the wake of the turbine is determined by the width of the wake, which is determined by the wake decay coefficient described in

section 2.3. The wake decay coefficient is one of the most important parameters in this study, since its dependency on the atmospheric stability directly impacts the AEP and therefore the optimization results. To calculate the wake decay coefficients for different values of z/L, equation 2.22 is used, which is described in more detail in section 2.3.2. Some examples of the used values for the stability-dependent wake decay coefficient for each stability class are shown in table 3.1.

Table 3.1. Definition of the stability classes and some characteristic wake decay coefficients.

stability class	**range of z/L**	**characteristic z/L**	**characteristic k_w**
very unstable	z/L < -0.5	-1.0	0.0336
unstable	-0.5 ≤ z/L ≤ -0.1	-0.5	0.0327
neutral	-0.1 < z/L < 0.1	0	0.0307
stable	0.1 ≤ z/L ≤ 0.5	0.5	0.0258
very stable	0.5 < z/L	1.0	0.0222

3.2 Case 1: One wind direction

In this section the first case is presented, which is the most basic case of just one wind direction with one stability condition. For example, only neutral wind coming from the south (180°). There are two main goals in this case. The first is to determine how the stability-dependent wake decay coefficient changes the shape of the wakes and how this affects the optimal orientation. The second is to quantify the benefits of considering stability in the optimization process by introducing a parameter referred to as the potential AEP gain.

Three different wind conditions are compared as sub-cases within this case. For all three sub-cases the wind speed is 9 m/s and the wind direction is exactly north (0°). The only difference between these sub-cases is the atmospheric stability condition that is used, which is very unstable ($z/L = -1$), neutral ($z/L = 0$) and very stable ($z/L = 1$). Note that for all cases in sections 3.2, 3.3, and 3.4, these are the only stability conditions that are used. The prefix "very" is often omitted to improve readability, which means that the very unstable case is simply referred to as the unstable case. It is also important to mention that for this specific case with only one wind direction, the 45° orientation is a symmetry axis, meaning that any rotation beyond 45° will result in the same physical situation as that same rotation before 45°. For example, an orientation of 50° gives the same result as 40°. For this reason, the orientation range of 0° to 90° that is considered in general throughout the chapter, is narrowed down to a 0° to 45° range in this section.

3.2.1 Neutral case

Before comparing the different sub-cases, the neutral case is presented. The resulting optimal orientation for the neutral case is 8° with an AEP of 1642 GWh. As a comparison: the worst possible orientation is 0° with an AEP of 373 GWh. The AEP for all orientations between 0° and 15° is given in table 3.2 in section 3.2.3. The optimal orientation for each sub-case is within this range. A small range of orientations is given to provide an indication of the variation between the AEP for different orientations. From this table it is clear that there is a big difference between the 7° and the 8° orientation. Initially, it was thought that the reason for this difference is that the 8° orientation is the first orientation for which the wakes of the turbines in a certain row no longer overlap with any of the turbines in the next row. To visualize this effect, the wake plots of the 6°, 8°,10° and 12° orientations for the neutral case are shown in figure 3.2. The wake plots are zoomed in on a smaller section of the wind farm to more clearly demonstrate if there is any overlap. It is clear from these wake plots that there is still an overlap at the 8° orientation. The first orientation that has no more overlap is 10° and for the 12° orientation there is a clear gap between the wake and the next turbine. It is worth noting that the impact of this wake overlap, even at the edge of a wake, is typically large due to the top-hat shaped velocity deficit distribution of the Jensen wake model. This effect is smaller for the Gaussian wake model, which is used in chapter 4.

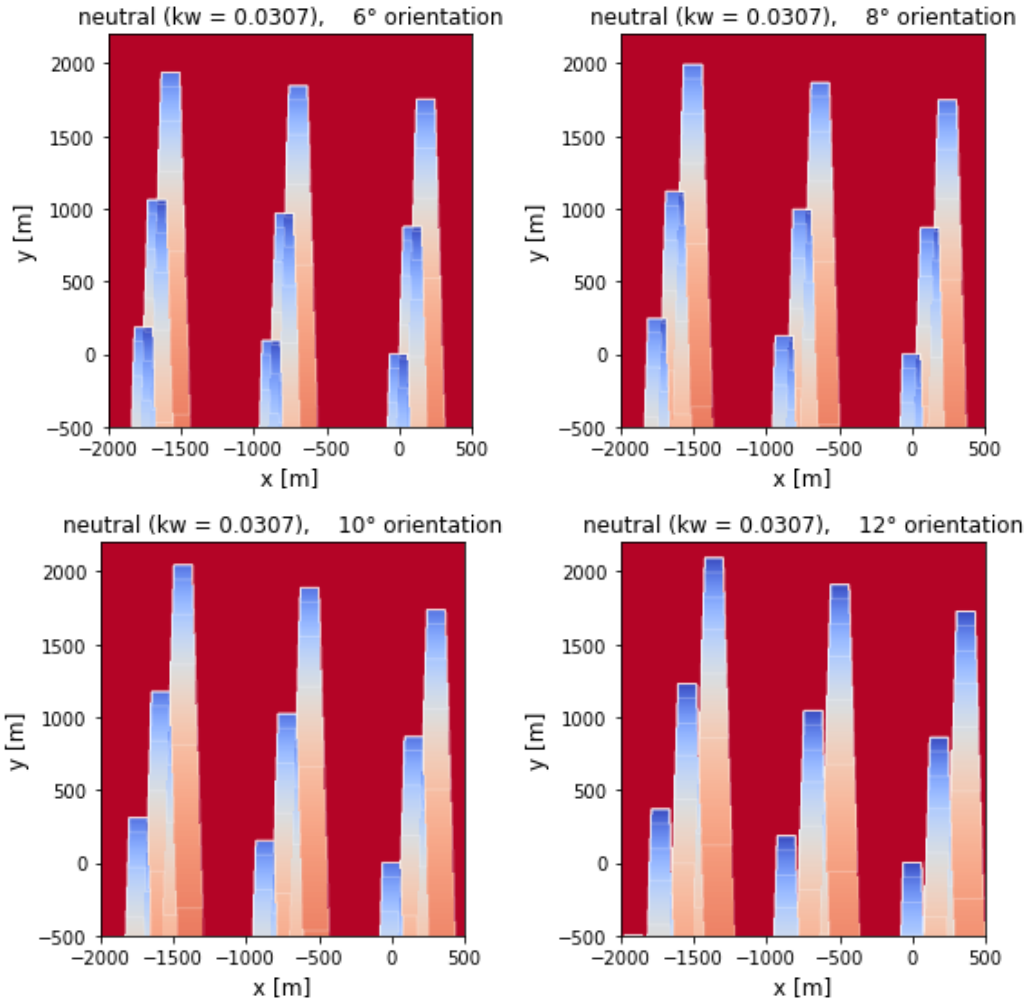

Figure 3.2. Zoomed-in wake plots for the 6°, 8°,10° and 12° orientation for the neutral case.

To further understand why the 8° orientation is optimal for this neutral case, it is important to understand what happens if the orientation angle increases. Rotating the wind farm reduces the negative effect of wakes on turbines in the next row, as shown in figure 3.2. However, it also introduces a new negative effect, which is increased by increasing the orientation. By rotating the wind farm further, the wakes of the turbines on the first rows start to overlap with turbines on the last rows. The velocity deficit at any position in a wake is determined by the distance from the turbine; at smaller distances the velocity deficit is larger. As the orientation angle increases, the wakes of turbines in the first row start to overlap with turbines that are closer to that row. This means that the negative effect becomes larger. To visualize this effect, parts of the wake plots for the 12°, 16°, 20° and 24° orientations are shown in figure 3.3. The optimal orientation in this simple case is a balance between the two described wake effects. Clearly, avoiding overlap on any turbine right after another turbine is important, since the velocity deficits at these short distances are large. However, it is not important enough to make it the only criterion, as a balance between the two effects results in the optimal orientation of 8°.

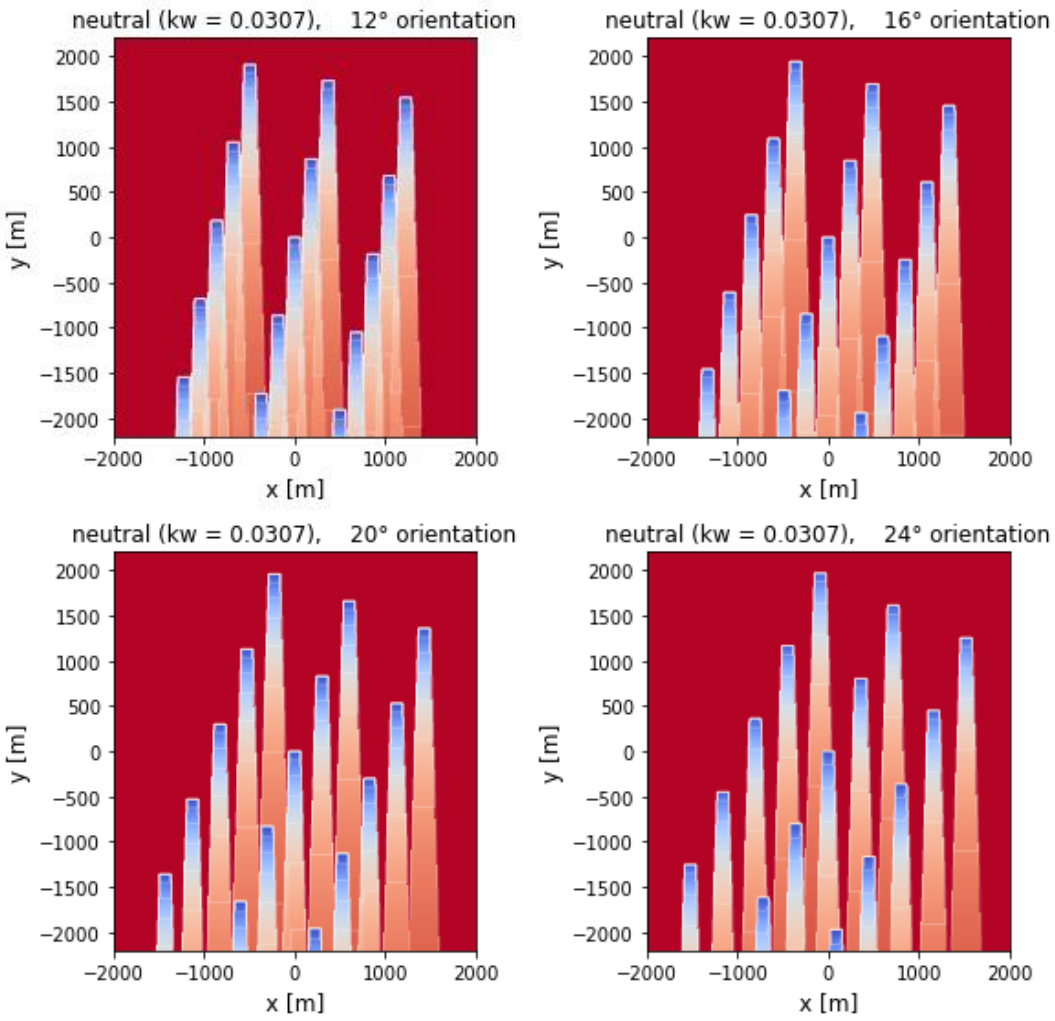

Figure 3.3. Zoomed-in wake plots for the 12°, 16°, 20° and 24° orientations for the neutral case.

3.2.2 Comparison of three sub-cases

The unstable, neutral, and stable cases have wake decay coefficients of 0.0336, 0.0307 and 0.0222, respectively. To visualize the effect of these different stability-dependent wake decay coefficients, zoomed-in wake plots of just two turbines are shown in figure 3.4. The orientation of the wind farm is the same for all three cases, the only difference between them is the stability condition. The three cases look very similar, however, it is still clear that the wake in the stable case is narrower than the wake in the unstable case. This is of course expected, as the width of the wake is determined by the wake decay coefficient. The result is that the stable wake has a slower wake recovery, which means there will be a larger velocity deficit at the same distance downstream in the wake, compared to the neutral or unstable wake. This effect is also visualized by the overall slightly more blue color of the stable wake. Unstable wakes have the benefit of increased wake recovery, it is therefore less negative if there is an overlap with a downstream turbine. However, the downside is that there is an increased chance of getting overlap, due to the increased width of the wake. The stable wake has the opposite benefits and downsides; due to the narrower wakes, there is a reduced chance of getting overlap. However, if there is an overlap, it will have a larger negative effect. Even though the differences between these cases seem small, it will be clear by the end of this section that they can have a large impact on the potential energy production.

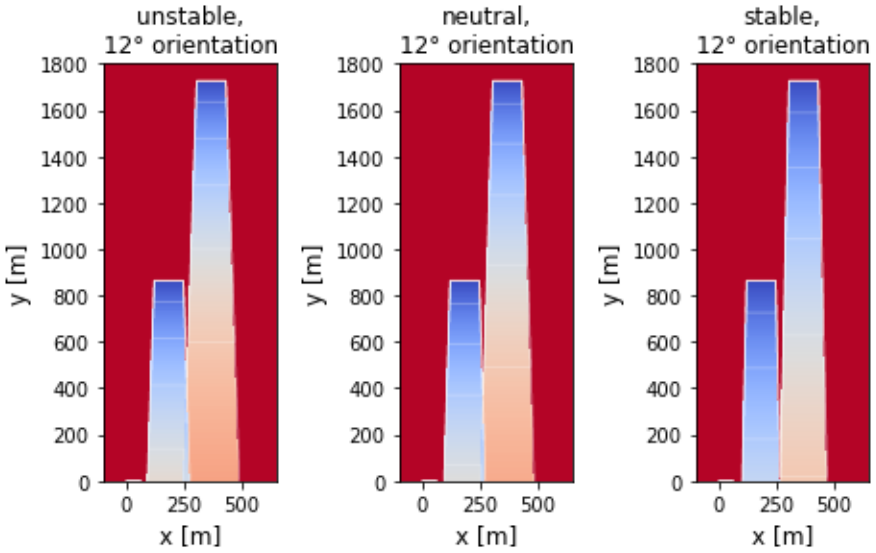

Figure 3.4. Comparison of the wakes for the unstable, neutral, and stable case.

As mentioned in section 3.1.1, to determine the optimal orientation, the AEP is calculated for orientations of 0° to 90° in steps of 1°. The AEP results for the orientations between 0° and 15° are shown in table 3.2. The neutral and stable case have the same optimal orientation of 8°. The unstable case has a larger optimal orientation of 10°. The increased optimal orientation angle of the unstable case can be explained using the same two effects that are described in section 3.2.2. Firstly, the width of the unstable wake is larger than the width of the neutral wake. This means that to avoid overlap with turbines in the next row (similar to what is shown in figure 3.2), the orientation angle has to be larger. Secondly, increasing the orientation angle causes the wakes of turbines on the first row to start overlapping with turbines on the last rows. However, due to the increased wake recovery in unstable wakes, this effect is far less negative

than it is for the neutral case. The reduced velocity deficit over longer distances, causes the balance between these two effects to shift more towards avoiding overlap on turbines in the next row. The result is an increased optimal orientation of 10° for the unstable case. For the stable case, one could expect the orientation angle to become smaller. However, in this particular case, reducing the orientation to 7° results in too much overlap on the turbine behind it. While increasing it only increases the negative effects of the second effect described before, especially since the reduced wake recovery causes increased velocity deficits over longer distances, compared to the unstable or neutral case. The result is that the optimal orientation of 8° is the same as the neutral case.

Table 3.2. AEP results for the unstable, neutral, and stable case for orientations from 0° to 15°.

	AEP [GWh]		
orientation	**unstable**	**neutral**	**stable**
0	666	604	373
1	666	604	373
2	666	604	386
3	712	657	514
4	985	949	860
5	1199	1176	1108
6	1190	1340	1296
7	1337	1495	1469
8	1495	**1642**	**1605**
9	1603	1600	1593
10	**1605**	1591	1538
11	1581	1582	1542
12	1539	1521	1494
13	1545	1525	1451
14	1551	1538	1481
15	1516	1522	1477

3.2.3 Definition of potential AEP gain

The goal of this chapter is not only to show the effects of stability on the wakes and the AEP, but also to quantify the benefit of considering stability in the optimization process. To do this, a new parameter is introduced: the potential AEP gain. The potential AEP gain is the highest possible percentage-wise increase in AEP that could be obtained when stability conditions are considered during the optimization process, relative to the AEP that is obtained under the assumption of neutral stability. This parameter is used throughout the rest of this thesis report, it is therefore important that it is clear how it is determined and what the reasoning behind it is. To further clarify this, an example is given that uses the results from the unstable and neutral case from table 3.2.

The AEP results for the different optimal orientation angles in table 3.2 show that the optimal AEP in the unstable case is 1605 GWh for the 10° orientation. The optimal AEP in the neutral case is 1642 GWh for the 8° orientation. Under the assumption of neutral stability, the developers of a wind farm would only find the values for the neutral AEP in the optimization process. The result is that an orientation of 8° would have been chosen for this wind farm. Now, imagine that on this particular site the wind conditions

are actually always unstable. This means that for the 8° orientation, the AEP that would have been obtained is 1495 GWh, since this is the AEP at the 8° orientation for the unstable case. The developers of this wind farm expected an AEP of 1642 GWh, which is much higher than the 1495 GWh obtained. However, these are not the two values that should be compared. The real question is: what AEP could the developers have obtained, if they had considered the stability conditions on this site? The answer to this question is in the optimization of the unstable case. The optimal orientation of 10° would have been chosen and an AEP of 1605 GWh would have been obtained. In this case the potential AEP gain is determined by the 1495 GWh that is obtained under the assumption of neutral stability and the 1605 GWh that is obtained by considering the stability conditions on the site. The resulting potential AEP gain for this case is $(1605 - 1495)/1495 = 7.4\%$. This means that for this simple (but extreme) case of one wind direction with unstable wind conditions, the AEP is increased by 7.4%. This significant increase is achieved just by taking the stability conditions into account during the optimization process and changing the resulting wind farm orientation from 8° to 10°.

In the other cases described in this report, there are no unstable, neutral, and stable sub-cases. Instead, there are only a neutral case and a non-neutral case. The non-neutral case represents the "real" wind conditions for that case, while the neutral case represents the assumption of neutral stability conditions. In general, the potential AEP gain is determined with the following two values. The first is the AEP in the non-neutral case at the non-neutral optimal orientation angle. The second is the AEP in the non-neutral case at the neutral optimal orientation angle. It is emphasized that the AEP in the neutral case is only used to determine the neutral optimal orientation angle, but the value of this AEP is never used in the potential AEP gain calculation, since it is not the AEP that would be obtained in the "real" wind conditions.

3.3 Case 2: Two wind directions

In this section the second case is presented. It is the first case that contains multiple wind directions with different stability conditions. More specifically, there are two wind directions that both have the same relative occurrence of 50%. The first is an unstable $(z/L = -1)$ wind from the 165° direction and the second is a stable $(z/L = 1)$ wind from the 195° direction. The wind rose and the stability rose for this case are shown in figure 3.5. Under the assumption of neutral stability, the wind conditions in this case are symmetrical. However, with the added stability conditions the case is no longer symmetrical. The main goal for this section is to show how the optimal orientation changes between the neutral case to the non-neutral case. The expectation is that there is some sort of preference orientation towards one of the stability conditions, for example if the optimal orientation angle for the non-neutral case is rotated more towards either the stable or unstable wind direction. The results from this case could be valuable for specific realistic cases in which there are wind directions with a certain dominant stability condition.

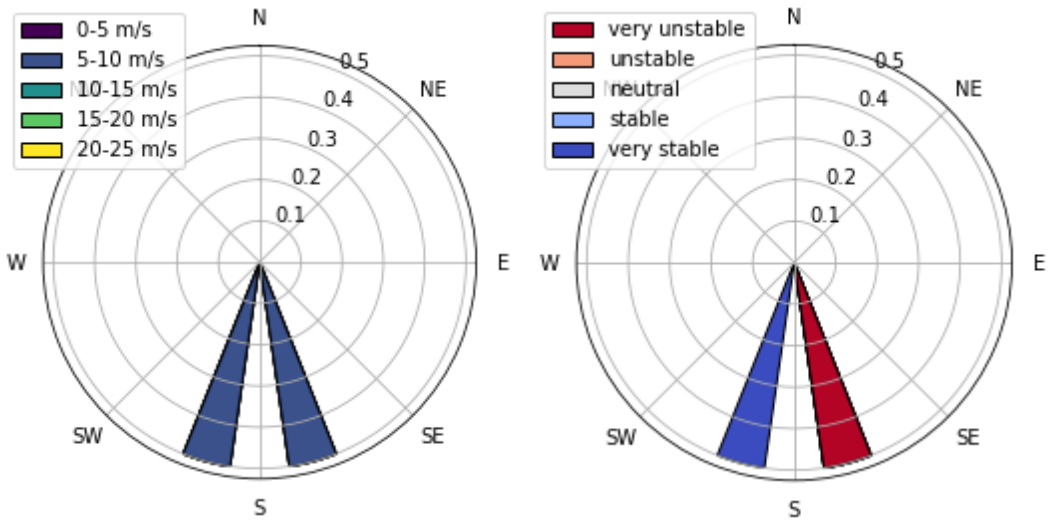

Figure 3.5. The wind rose (left) and the stability rose (right) for case 2.

3.3.1 Results

The results of the AEP calculations for all orientations are shown in table 3.3. This is the only case for which this table is shown in its entirety. This is done to point out some interesting findings and to give an idea of the differences between the AEP over the entire orientation range. For other cases similar tables are used, but they are not presented. The results are also visualized in figure 3.6, showing the AEP versus the orientation for both the neutral and the non-neutral case.

For the neutral case, there are two orientations that can both be considered as the optimal orientation as they give the same AEP, these are the 23° and the 67° orientations. The reason that they give the same AEP is again the result of a symmetry axis in the 45° orientation. Whenever the wind conditions are symmetrical around the north-south axis, the orientations from 0° to 45° are physically identical to the orientations from 90° to 45°; they are symmetrical in the 45° axis. This symmetry is clear from the neutral AEP results in table 3.3. The symmetry can be understood more intuitively using the following reasoning. When the square grid wind farm is rotated by 80° (clockwise) it is in exactly the same orientation as when it is rotated by -10° (counter-clockwise). If the wind conditions are symmetrical around the north-south axis, so in the 0° direction, it does not matter if the wind farm is rotated 10° (clockwise) or -10° (counter-clockwise). The physical situation for both orientations is exactly the same, it is just mirrored. The fact that this is only true for symmetrical wind conditions, is clear from the non-neutral AEP results in table 3.3. For example, it is shown that the non-neutral AEP for the 10° orientation is no longer the same as the non-neutral AEP for the 80° orientation. This results in the non-neutral case having just one optimal orientation of 23°.

Table 3.3. AEP results for the neutral and non-neutral case 2 for orientations from 0° to 90°.

	AEP [GWh] neutral	AEP [GWh] non-neutral		AEP [GWh] neutral	AEP [GWh] non-neutral
0	1522	1496	90	1522	1496
1	1487	1458	89	1487	1468
2	1478	1454	88	1478	1446
3	1484	1483	87	1484	1446
4	1514	1506	86	1514	1467
5	1513	1500	85	1513	1469
6	1538	1527	84	1538	1522
7	1616	1573	83	1616	1539
8	1460	1459	82	1460	1420
9	1307	1300	81	1307	1220
10	1224	1208	80	1224	1168
11	1111	1084	79	1111	1062
12	965	911	78	965	925
13	938	847	77	938	902
14	938	840	76	938	961
15	1020	915	75	1020	1052
16	1048	929	74	1048	1101
17	1053	954	73	1053	1042
18	1080	1019	72	1080	1070
19	1229	1193	71	1229	1209
20	1333	1310	70	1333	1303
21	1415	1403	69	1415	1330
22	1538	1522	68	1538	1447
23	**1622**	**1610**	67	**1622**	1524
24	1546	1551	66	1546	1601
25	1505	1482	65	1505	1549
26	1439	1367	64	1439	1405
27	1260	1262	63	1260	1293
28	1243	1230	62	1243	1180
29	1250	1246	61	1250	1168
30	1242	1243	60	1242	1151
31	1198	1197	59	1198	1110
32	1196	1179	58	1196	1136
33	1224	1191	57	1224	1260
34	1371	1272	56	1371	1349
35	1426	1380	55	1426	1477
36	1484	1475	54	1484	1531
37	1596	1599	53	1596	1546
38	1503	1539	52	1503	1502
39	1383	1381	51	1383	1388
40	1381	1325	50	1381	1357
41	1391	1332	49	1391	1371
42	1388	1331	48	1388	1368
43	1387	1330	47	1387	1362
44	1381	1371	46	1381	1421
45	1435	1447	45	1435	1447

As explained in section 3.2.4, the non-neutral case is considered to represent the "real" wind conditions at a site. The AEP values that are eventually obtained are determined by this non-neutral case, regardless of which assumption is used in the optimization process. To determine the benefit of considering stability in the optimization process, the resulting optimal orientation is compared with the optimal orientation obtained under the assumption of neutral stability. In this case, both the neutral and the non-neutral case have an optimal orientation of 23°. This could lead to the conclusion that there is no benefit in considering stability for this case. However, the neutral case had two identical optimal

orientations of 23° and 67°, this is important for the following reason. If development of a wind farm for this site is done under the assumption of neutral stability, both the 23° and the 67° orientation could be chosen, as they are equally beneficial. If the 23° orientation is chosen, the resulting AEP is 1610 GWh. The same AEP is obtained if the optimization of the wind farm is done using the stability conditions, as the resulting optimal orientation is also 23°. However, if the 67° orientation is chosen, the resulting AEP is 1524 GWh. This is significantly less than the AEP of 1610 GWh that is obtained using the stability conditions. As explained in section 3.2.4, the potential AEP gain is the highest possible gain in AEP when optimizing using stability conditions, relative to the assumption of neutral conditions. For this particular case, there is no way of knowing which orientation is chosen under neutral stability, since they are equally beneficial. It is concluded that the potential AEP gain for this case is $(1610 - 1524)/1524 = 5.6\%$, which is achieved by changing the orientation from 67° to 23°.

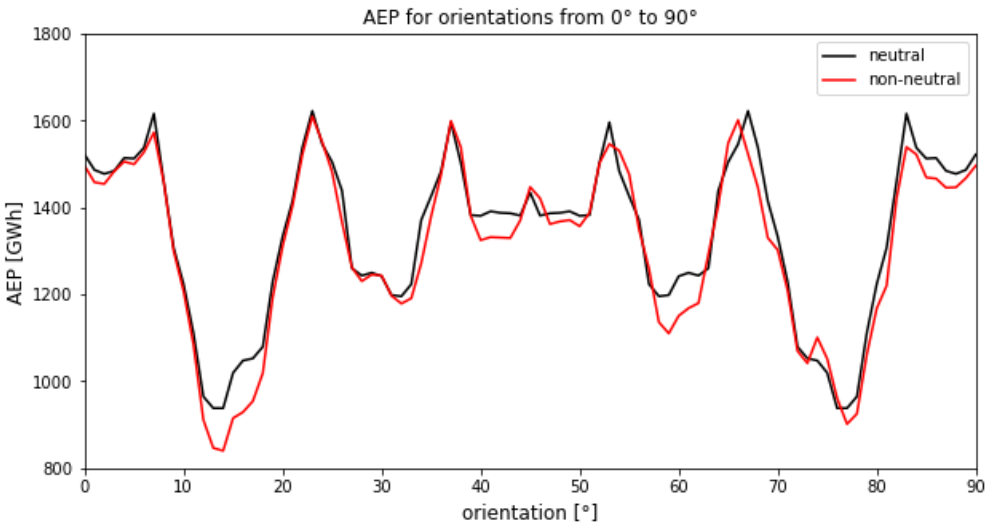

Figure 3.6. The AEP for each orientation in the neutral and non-neutral case 2.

3.3.2 Comparison of 23° and 67° orientation

As shown in table 3.3 in section 3.3.1, due to symmetry the 23° and the 67° orientation resulted in the same AEP for the neutral case. However, for the non-neutral case in which stability effects are considered, the two orientations showed significant differences in AEP of 1610 GWh and 1524 GWh, respectively. This difference in AEP is a direct indication of the importance of considering stability effects. In this section, the wake plots for these two specific directions are analyzed.

In figure 3.7, the wake plots for the 23° and the 67° orientations are shown for the neutral case. The wake plots for the 165° wind direction (unstable in non-neutral) are shown on the left and the wake plots for the 195° wind direction (stable in non-neutral) are shown on the right. It is important to note that for the 67° orientation, the wake plot of the 165° wind direction looks exactly like the mirrored wake plot of the 195° wind direction for the 23° orientation, and vice versa. This is of course again due to symmetry. There are two different layout orientations that can clearly be distinguished, which will be named for clarity throughout this section. The first is visible on the top-left and bottom-right in which the first row

of turbines is more or less diagonally positioned relative to the incoming wind direction. It is therefore referred to as the diagonal orientation. The second is visible on the top-right and bottom-left in which the first row of turbines is almost perpendicular to the incoming wind direction. The result is that the following turbines are more or less aligned with the wind direction and this orientation is therefore referred to as the aligned orientation. Regardless of which orientation (23° or 67°) is chosen or which stability conditions are used in this specific case, there is always one wind direction that faces a diagonal orientation and one wind direction that faces an aligned orientation. The rest of the analysis is focused on the difference between these two types of orientations and finding out if either one of these orientations is more favorable for stable or unstable conditions.

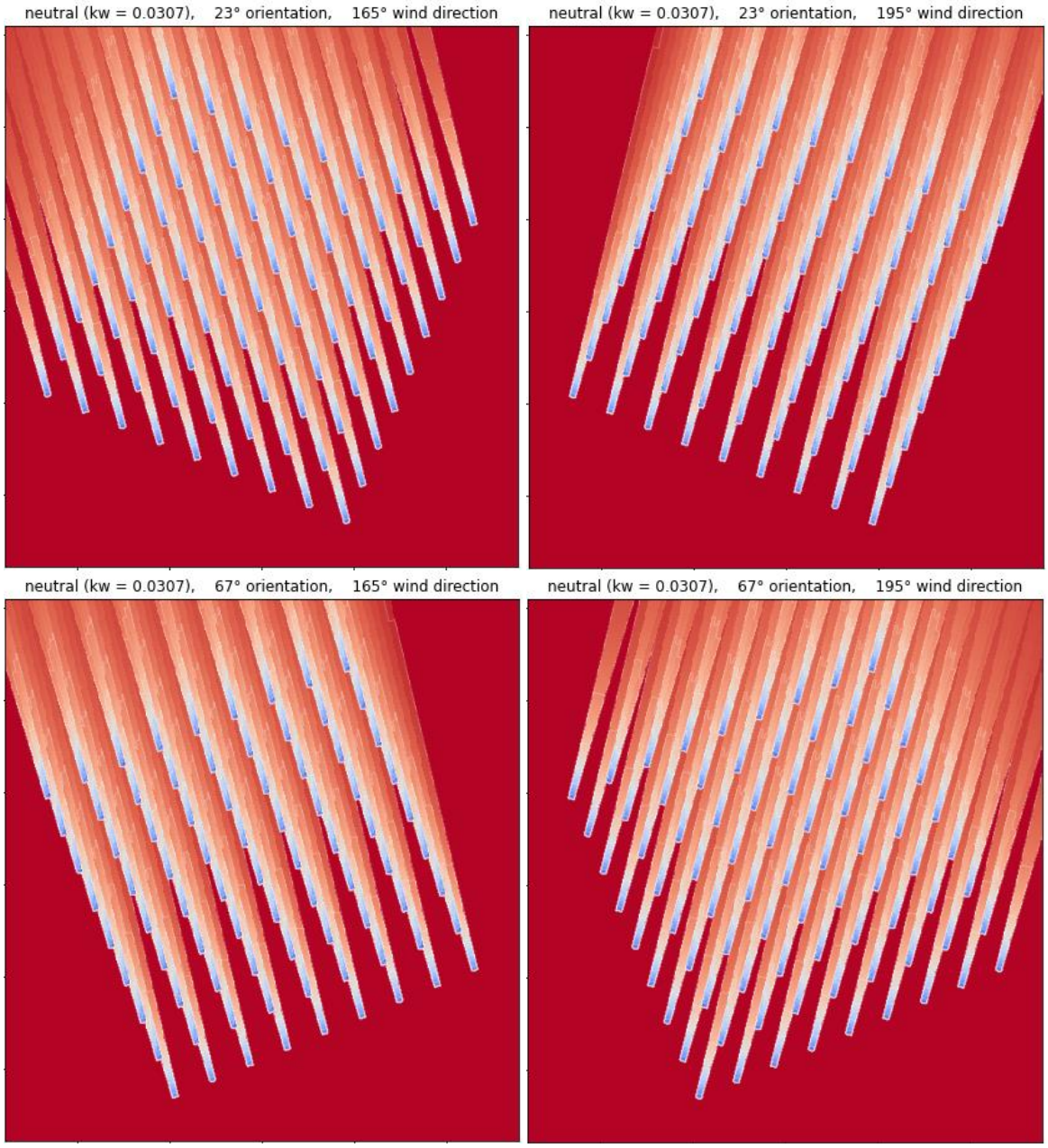

Figure 3.7. Wake plots for the neutral case with the 23° orientation at the top and 67° orientation at the bottom. The 165° wind direction is shown left and the 195° wind direction is shown right.

In figure 3.8, zoomed-in wake plots are shown for the diagonal and the aligned orientations. These wake plots focus specifically on the overlap of wakes of turbines in the first few rows on turbines in later rows. Both orientations seem to have advantages and disadvantages, but the main difference between them is the number of rows and therefore the distance before there is wake overlap. The aligned orientation has the advantage of delaying the overlap as long as possible. Only the turbines in the last three rows are fully in the wakes of previous turbines. The diagonal orientation has more wake overlap, with turbines after either three or four rows being fully in the wakes of previous turbines. However, the diagonal orientation has the advantage of having some turbines on the side corners. These specific turbines at the edges have less turbines behind them and therefore there are less wake losses. Overall, the aligned orientation seems to be the better orientation as it is also very similar to the optimal orientation found in case 1 (section 3.2) for one single wind direction.

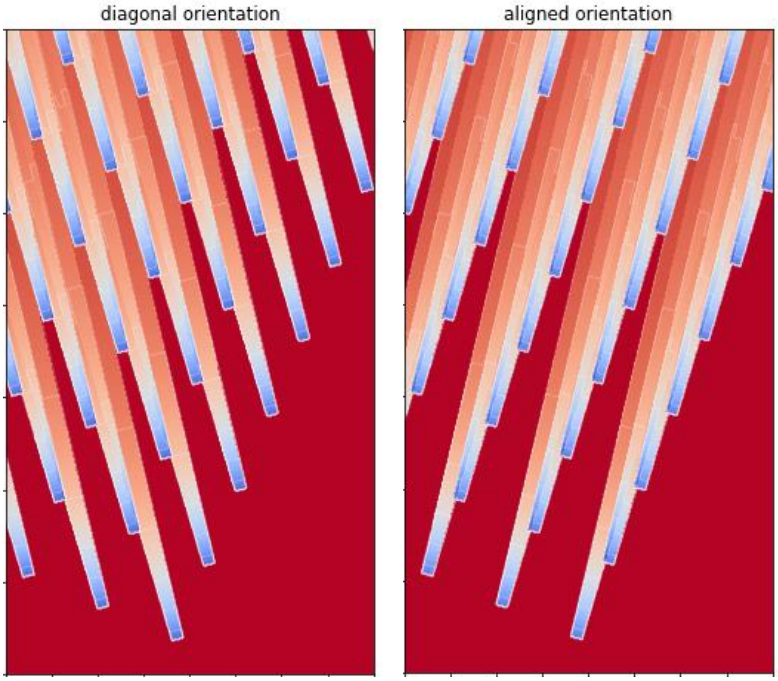

Figure 3.8. Zoomed-in wake plots of the 23° orientation for neutral conditions with on the left the diagonal orientation and on the right the aligned orientation.

The question that remains is how these two different orientations affect the layout optimization. For the neutral case, it does not matter which orientation (23° or 67°) is chosen, as both wind directions will face the same orientations with the same neutral stability conditions. However, for the non-neutral case, there is a significant difference in AEP between the 23° and the 67° orientation, therefore it does matter which wind direction (stable or unstable) faces the aligned and the diagonal orientation. Generally speaking, unstable wind is considered favorable for wind energy production due to its increased wake recovery. It could therefore be determined that the positive effects of the unstable winds should be maximized and that the unstable wind should be in the aligned direction. However, stable winds have a decreased wake recovery that could result in significant losses, so it could also be reasoned that these negative effects should be minimized and that the stable wind should be in the aligned direction. The final optimal layout

is the result of a balance between maximizing these positive effects and minimizing these negative effects. The results from section 3.3.1 show that the 23° orientation is better than the 67° orientation in the non-neutral case. This means that the unstable wind in the 165° direction faces the diagonal orientation and the stable wind in the 195° direction faces the aligned orientation. It is concluded that minimizing the negative effects of the stable wind direction is in this case the dominant factor for determining the optimal layout. This conclusion can intuitively be understood, as unstable wind is considered favorable precisely because of the fact that it has a better wake recovery. Due to this improved wake recovery, it is less negative if there is wake overlap for unstable winds, but this also means that it is less beneficial to optimize the layout for unstable winds specifically. It is more beneficial to optimize for stable winds instead, as the reduced wake recovery results in large velocity deficits over larger areas. Therefore, the benefit of reducing wake overlap for stable winds is greater than for unstable winds. With this reasoning, maximizing the positive effects of unstable conditions is only done by minimizing wake overlap. However, there is another way to benefit from the increased wake recovery of unstable winds. It is possible that, due to the improved wake recovery, wind turbines in unstable wind directions could be positioned closer together than wind turbines in stable wind directions. This could result in a more efficient use of the area and thus, in a higher AEP for real wind farm projects since these are usually restricted to a designated area. In this thesis, however, the turbine spacing is kept constant in all directions and this potential extra change to the layout is therefore not tested.

This case considered extreme wind conditions for which the results are limited to just two specific wind directions and stability conditions. The results for the optimal orientation, the potential AEP gain, and the optimization balance between the aligned and the diagonal orientations are only applicable to this case specifically. However, a qualitative conclusion is also found that shows that stable wind directions play a dominant role in wind farm layout optimization when stability effects are considered. This finding is applicable to realistic cases and could improve the AEP by reducing the wake losses of stable winds significantly.

3.4 Case 3: Finding the extreme case

In this section the third case is presented. The goal of this section is to find the extreme case with the wind conditions that result in the highest potential AEP gain. Similar to case 2, there are two wind directions with a constant wind speed of 9 m/s. There is one stable ($z/L = 1$) and one unstable ($z/L = -1$) wind direction. In case 2, the wind directions were fixed at 165° and 195°. These wind directions and the 30° angle between them were chosen arbitrarily, as the choice was not based on any findings in literature and there were no particular expectations for these specific conditions. The difference in this case is that all possible angles between the two wind directions are tested. The goal is to find the angle for which the effects of stability have the largest impact on the resulting optimal layout, which is quantified by the largest potential AEP gain.

3.4.1 Wind conditions

To test all possible wind conditions with one unstable and one stable wind direction, it is important to determine which combinations result in unique physical situations, such that the total number of combinations that have to be tested is reduced to the minimum. In this section, the unstable wind direction is referred to as A and the stable wind direction is referred to as B. With a step size of 1° in the variation of any wind direction, there are 360 possible values for A and 360 possible values for B. This results in a total number of 129,600 possible combinations of A and B. However, this number is quickly reduced using two steps. The first and most important of these steps is that A is fixed at 0°, while B is varied from 0° to 360°. This means that it is no longer needed to look at the two specific wind directions, but rather only at the angle between the wind directions, reducing the total number of combinations to 360. The reason why this is a valid operation is explained in an example. If A is 50° and B is 70°, the angle between the wind directions is 20°. The resulting optimal orientation for this combination could be 60° for neutral conditions and 63° for non-neutral conditions. The potential AEP gain is determined by the difference in AEP between the 60° orientation and the slightly further rotated orientation of 63°. Now, imagine A is 0° and B is 20°. The angle between the wind directions is still 20°, but the optimal orientation for this combination is now 10° for neutral conditions and 13° for non-neutral conditions. The potential AEP gain for the second example is again determined by the difference between in AEP between the two orientations, however this AEP gain is exactly the same as the AEP gain in the first example. This is true because the wind conditions for the first example are essentially the same as the wind conditions for the second example, assuming that the terrain is homogeneous. The only difference between these two examples is the initial orientation of the wind farm relative to wind direction A. However, this initial orientation does not influence the result, as the same difference in optimal orientation and AEP between the neutral and the non-neutral case is found. So, even though the optimal orientation is different between the 0° and 20°, and the 50° and 70° example, the potential AEP gain is the same. Since the goal is to find the case with the largest potential AEP gain, it is only required to look at the angle between the two wind directions rather than at all possible combinations. The second important step is that it does not matter which of the two wind directions is the stable one and which is the unstable one. This operation is valid due to symmetry and is also explained in a short example. If A is again 50° and B is again 70°, the same example is obtained as before, and this example is shown to be equal to the case of A being 0° and B being 20°. However, if A is 70° and B is 50° the wind directions are essentially swapped. Rearranging this case in the same way, setting A to 0°, results in B being 340° or -20°. This new case, in which A is 0° and B is -20°, is a mirrored version of the initial example with a mirrored optimal orientation, but again with exactly the same potential AEP gain. This step has two main results. The first is that it does not matter if the unstable or the stable wind is fixed in the 0° wind direction, it is therefore enough to only vary one of the two wind directions. The second is that the total number of combinations is reduced to 180. Overall, this means that to test all possible wind conditions, A is fixed at 0° and B is varied from 0° to 180°. Note that the unique case of a 0° angle means that the wind is unidirectional with an even distribution of stable and unstable conditions.

3.4.2 Results

The goal for this case is to find the angle between an unstable and a stable wind direction that results in the highest potential AEP gain. The potential AEP gain is determined for all possible angles between these two wind directions from 0° to 180° in steps of 1°. The results are shown in figure 3.9. Before addressing the values that are found, it is important to notice that there are clearly two more symmetries present in the results. These symmetries are at the 90° and the 45° angles and are caused by symmetries in the square grid layout of the wind farm. These symmetries in the layout were known, however it was initially not expected these would show up in the results for this particular case. This finding has an impact on the case, since it means that only the angles from 0° to 45° have to be considered, reducing the total number of unique physical situations to just 46. The results for this smaller range of angles are shown in figure 3.10. The potential AEP gain varies between 0.9% and 9.2%. The lowest AEP gain of 0.9% is obtained for multiple angles, for example 20° and 27°. The highest AEP gain of 9.2% is obtained for the 40° angle and is achieved by changing the orientation from 8° to 79° (or -11°). It is important to note that this does not mean that the 40° angle between two wind directions is better in any way. It only means that for the 40° angle it is important to consider stability effects in the optimization process, as the potential gain in doing so is 9.2%. While for the 20° angle the benefit of considering stability effects is only 0.9%. Even though the 40° angle has the highest single peak, another interesting result is the range between 22° and 25°, for which all the AEP gains are relatively high. The average potential AEP gain of all angles is 3.9%. Finally, it is important to realize that due to the symmetry effects mentioned earlier, the potential AEP gain for the 40° angle is equal to the 50°, 130° and 140° angles. This means that for any of those angles the benefit of considering stability is the greatest.

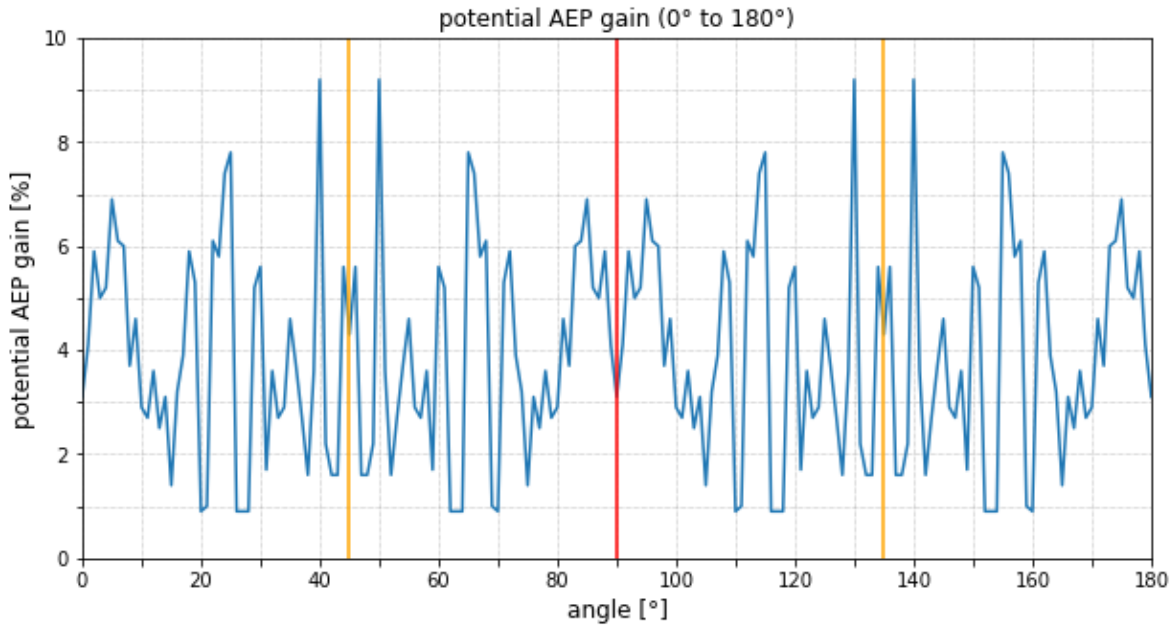

Figure 3.9. The potential AEP gain for angles between 0° and 180°. Symmetry at the 90° angle is highlighted with a red line and symmetry at the 45° and 135° angle is highlighted with orange lines.

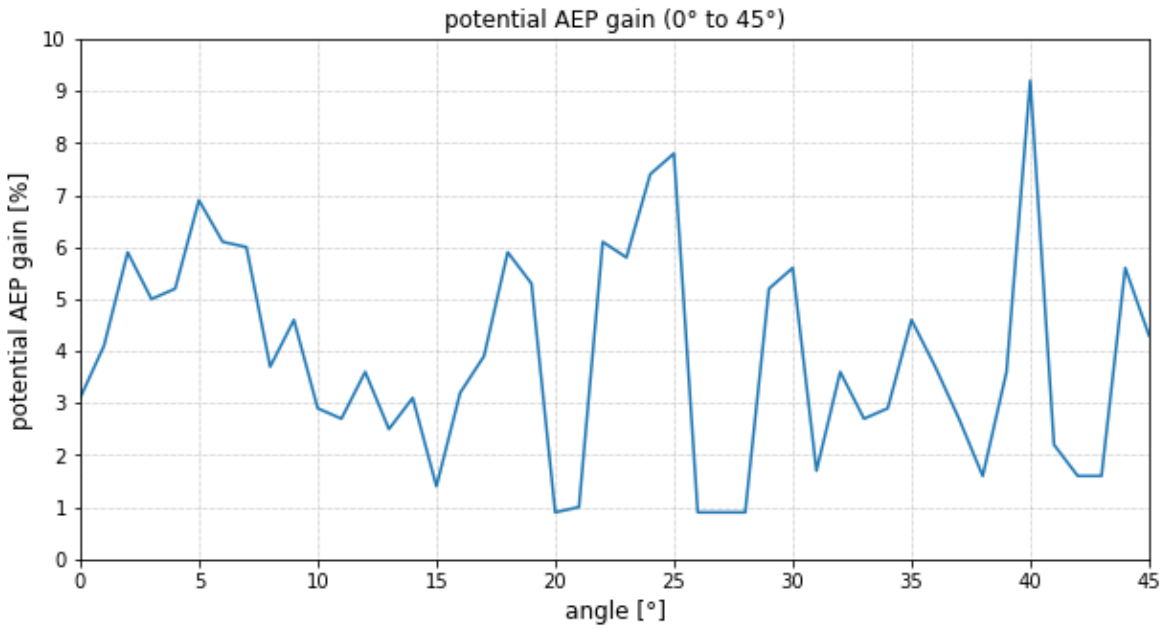

Figure 3.10. The potential AEP gain for angles between 0° and 45°. These angles contain all possible unique physical situations for any combination of two wind directions.

Similar to case 2, these results are strictly limited to this specific case in which there are two wind directions of which one is very unstable and one very stable. These wind conditions are highly unlikely to occur in reality and therefore any potential AEP gain obtained in real cases are likely to be much lower than the 9.2% that is found. However, the results from this case could still improve layout optimization for some specific sites. For example, on sites that have some distinct geographical features, like hills or beaches, where there could be a dominant stable wind from one direction and a dominant unstable wind from another direction. If the angle between these expected wind direction matches any of the high peaks from this case, there is a good chance that considering stability will result in improved AEP. However, even if this is not the case, it is likely that any site that contains some dominant stable or unstable wind direction will benefit from considering these stability effects. In case 4 in section 3.5, a semi-realistic case is considered that focuses more on how large this benefit could be in a more realistic scenario. In chapter 5, meteorological data is used to perform the analysis for real conditions.

3.5 Case 4: Semi-realistic wind conditions

In this section, the final case is presented. There are two main goals for this case. The first goal is to find the potential AEP gain for a more realistic case, to see if the effects of including stability in the optimization process is still significant for such a case. The second goal is to compare this case with a similar case in which there is a clear bias for certain stability classes in certain wind directions. The wind conditions in this case are based on results from Brand (2008), who made a wind resource map for the Dutch part of the North Sea by combining data from a numerical weather prediction model and measurements from meteorological stations. The distribution of average wind speed per wind direction

is given in table 3.4. The overall distribution of the stability classes is given in table 3.5. This case is considered semi-realistic for the following two reasons. Firstly, the resolution of the wind directions bins is relatively coarse with a bin size of 30°. The frequency and average wind speeds for these bins are given. It could have been an option to convert the data to a smaller bin size, by uniformly distributing the data for each 30° bin over smaller bins, however it was chosen not to do so, mainly to keep computation times to a minimum. This simplification does mean that the wind can only come from directions in steps of 30°, which is of course not realistic. Secondly, a stability class distribution is also given, however the frequency of the different stability classes is only given overall, and not for each wind direction specifically. Therefore, assumptions are made for the stability distribution per wind direction.

Table 3.4. The distribution of average wind speeds per wind direction from Brand (2008). The bin size is 30° and the value shown for wind direction is the center of the bin.

wind direction [°]	**0**	**30**	**60**	**90**	**120**	**150**	**180**	**210**	**240**	**270**	**300**	**330**
wind speed [m/s]	9.5	7.8	8.0	10.5	8.5	8.9	8.6	10.8	11.4	11.4	10.5	8.5
frequency [%]	6	5	5	7	7	8	12	15	12	10	7	6

Table 3.5. The overall stability distribution from Brand (2008).

stability class	**very unstable**	**unstable**	**slightly unstable**	**neutral**	**slightly stable**	**stable**	**very stable**
frequency [%]	35	23	7	2	5	25	3

3.5.1 Wind conditions

The data from Brand is used directly to obtain a wind rose for this case, as is shown in figure 3.11. However, to obtain a stability rose, the data from the overall stability distribution in table 3.5 has to be modified in two ways. Firstly, this stability distribution uses the stability classes “slightly unstable” and “slightly stable”, while these two classes are not used throughout this thesis. It is preferred to keep the stability classes consistent over all cases. This means that the occurrences of these two classes have to be redistributed over the unstable, neutral, and stable classes. Depending on the boundaries of the stability parameter, a slightly stable condition could either be a stable or a neutral condition. The boundary between the slightly stable and stable class used by Brand is roughly 0.06. The upper boundary of the slightly stable class used by Brand is higher than the lower boundary used for the stable class in this thesis. It is therefore decided that all “slightly”-occurrences are added to the neutral class. This results in a new stability distribution with five stability classes, as shown in table 3.6.

Table 3.6. The modified overall stability distribution with five stability classes.

stability class	**very unstable**	**unstable**	**neutral**	**stable**	**very stable**
frequency [%]	35	23	14	25	3

The second adjustment concerns the stability distribution over the different wind directions. This is done in two different ways to create two separate cases: one case in which the stability distribution is uniform

over the wind directions and one case in which there is a clear bias for certain stability classes in certain wind directions. For the uniform case, the stability classes are distributed over the wind directions in such a way that each individual wind direction has the same stability distribution, equal to the overall stability distribution. For the biased case, some wind directions are made dominantly stable, and some wind directions are made dominantly unstable or very unstable. There are more unstable wind directions, because overall there are more unstable wind conditions. The stability distribution per wind direction is made such that the overall distribution is the same as the uniform case; they both follow the distribution given in table 3.6. The stability roses for the uniform and the biased case are shown in figure 3.11.

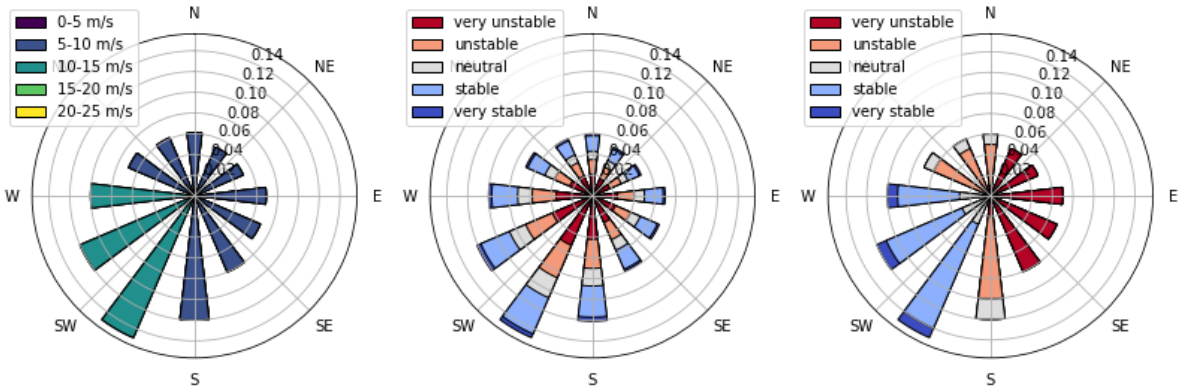

Figure 3.11. The wind rose (left), the uniform stability rose (middle), and the biased stability rose (right) for case 4.

3.5.2 Results

The results show that the potential AEP gain is larger in the biased case than in the uniform case. The potential AEP gain for the uniform case is 0.1%, which is achieved by changing the orientation from 82° to 52°. This result means there is practically no benefit in considering stability effects for these wind conditions. It is important to emphasize that this 0.1% is the gain when comparing the uniform case to the neutral case. This result is more or less expected, since the uniform distribution of stability conditions means that positive and negative effects of stable and unstable conditions are likely to cancel each other out. There are no wind directions for which there are either more unstable conditions to benefit from, or more stable conditions to reduce the wake losses for. This results in the AEP for the optimal orientation in the uniform case being only slightly higher than the AEP for the optimal orientation in the neutral case. The biased case, however, has a potential AEP gain of 0.7%, which is also achieved by changing the orientation from 82° to 52°. This result is significantly higher than the value of 0.1% in the uniform case. The reason that both cases have the same optimal orientation, is likely the result of the coarse wind direction bins of 30°. The results shows that if there are wind conditions in which certain stability conditions are more common in specific wind directions, the benefits of considering these stability effects in the optimization process are significantly larger than for wind conditions with uniformly distributed stability conditions.

The potential AEP gain of 0.7% for the biased case is significantly lower than the values between 5.6% and 9.2% found in previous cases. This is expected, as the wind conditions in previous cases are very unrealistic. These cases were mostly intended either for the clarification of certain concepts, or as a

benchmark to give an upper limit for potential AEP gain in extreme cases. It is expected that the value of 0.7% is a more realistic indication of the potential AEP gain in real cases. This expectation is tested in chapter 5, in which the layout optimization is done using meteorological data from a real site.

3.6 Chapter conclusions

In this section, the main results and conclusions from this chapter are summarized.

- For case 1, the optimal orientation is 8° for the stable case, 8° for the neutral case, and 10° for the unstable case. Due to an increased width, the unstable case requires an increased orientation to reduce wake overlap with turbines on the following rows. When considering neutral and unstable conditions, the potential AEP gain for this case is 7.4%.

- For case 2, the optimal orientation is either 23° or 67° for the neutral case, and 23° for the non-neutral case. Under the assumption of neutral stability, the 67° could have been chosen just as likely as the 23° orientation. In non-neutral conditions, the 23° orientation results in a significantly higher AEP than the 67° orientation. This results in a potential AEP gain of 5.6%.

- For case 2, an aligned and a diagonal orientation are defined. The aligned orientation has the advantage of delaying wake overlap as long as possible. The diagonal orientation has the advantage of having turbines on the side corners, which have less turbines behind them. Considering all wake effects, the aligned orientation is more favorable, which is further supported by the fact that it is close to the optimal orientation found in case 1.

- When considering stability effects in layout optimization, a balance between two new considerations is introduced. The first is to maximize the positive effects of the improved wake recovery in unstable conditions. The second is to minimize the negative effects of the reduced wake recovery in stable conditions. The benefit of reducing wake overlap is greater for stable winds than for unstable winds. This results in the stable conditions playing a dominant role in determining the optimal layout.

- For case 3, the potential AEP gain for all possible angles between two wind directions is determined. The highest potential AEP gain of 9.2% is found for an angle of 40°. The lowest potential AEP gain of 0.9% is found for multiple angles. This is considered the extreme case, and the gain of 9.2% is used as a benchmark for the maximum possible gain for any case.

- For case 4, the potential AEP gain is 0.1% for the uniform case and 0.7% for the biased case. The results show that if there are wind conditions in which certain stability conditions are more common in specific wind directions, the benefits of considering stability effects in the optimization process are significantly larger than for wind conditions with uniformly distributed stability conditions.

4. Layout optimization with stability-dependent Gaussian wake model

The main goal of this chapter is to develop a stability-dependent Gaussian wake model and to compare its performance with the stability-dependent Jensen wake model presented in chapter 3. For the Jensen wake model, many results appear to be highly sensitive to small changes in the orientation. This sensitivity is a direct result of the fact that in the Jensen wake model the velocity deficit is constant over the width of the wake. Therefore, a small change in the orientation could be the difference between either having an overlapping wake or not having an overlapping wake on subsequent turbines, with a significant difference in incoming wind speed as a result. The Gaussian wake model should reduce this sensitivity and provide a more realistic indication of the optimal orientation.

In section 4.1, the development of the stability-dependent gaussian wake model is described. The stability-dependency is implemented using just one parameter and is based on a simple calibration with the Jensen model. In section 4.2, this new model is validated by comparing the AEP results for each wind farm orientation for the Jensen and the Gaussian model. The velocity deficits at various downwind distances in the wake are also compared. In section 4.3, the stability-dependent Gaussian model is applied to the wind conditions presented in case 3 and case 4 of chapter 3. The potential AEP gain for these cases is determined and compared with the results obtained using the Jensen model. Finally, in section 4.4, the impact of changing the turbine spacing and the ambient wind speed on the potential AEP gain is determined for both the Jensen and the Gaussian model.

4.1 Stability-dependent growth parameter

The Gaussian wake model is made stability-dependent using the growth rate parameter k^*. The use of this parameter in the model is described in section 2.1.2 and it is found in equations 2.8 and 2.10. The growth rate in the Gaussian wake model is similar to the wake decay coefficient in the Jensen wake model. Therefore, the choice is made to use this parameter to implement the effects of atmospheric stability on the wake recovery, similar to what is done with the wake decay coefficient in the Jensen wake model. The stability-dependency of the growth rate k^* is not directly based on values found in literature. Instead, the stability-dependent Jensen wake model introduced in this thesis is used to calibrate the value of k^* for different stability conditions. The calibration process, which is based on the resulting AEP, is described in this section.

In FLORIS, there are four adjustable parameters (constants) for the Gaussian wake model. The growth rate k^* is not an individually adjustable parameter, instead it is linearly dependent on turbulence intensity and the constants k_a and k_b. These constants affect the wake expansion in the lateral and vertical

direction, respectively. The other two constants that can be modified by the user are α and β, which determine the dependence of the boundary between the near-wake and the far-wake region on turbulence intensity and on the turbine's induction factor, respectively. Since these constants affect the transition between the near-wake and the far-wake region, rather than the wake expansion, it is decided not to change these constants. It is preferred to have only one parameter for the calibration of the growth rate, and not to calibrate k_a and k_b separately. To allow such a direct calibration of the value of k^*, a scaling factor is used as the calibration parameter. This means that the wake expansion is scaled equally in the lateral and vertical direction. Using this set-up, the growth rate can be calibrated, without knowing the actual value of k^*, by applying a scaling factor to the default values of k_a and k_b, which in FLORIS are 0.38 and 0.004, respectively.

The calibration of the k* scaling factor is based on the resulting AEP of two wind farm layouts under various wind conditions. The benchmark for this calibration is the AEP obtained in the same wind conditions, using the stability-dependent Jensen wake model. The two main cases that are used, in terms of the wind rose, are a uniform case and a unidirectional case, both with a wind speed of 9 m/s. Each of these cases consist of a very stable ($z/L = 1$), neutral ($z/L = 0$), and very unstable ($z/L = -1$) sub-case, resulting in total of six different wind conditions. These cases are used in both a 5x5 and a 9x9 farm layout. This results in a total of twelve cases, with four cases per stability class for the calibration. For each case, the scaling factor is determined such that the resulting AEP is within 1 GWh of the AEP obtained with the Jensen model. For each of the three used stability classes, the average value of the four determined scaling factors is used as the final scaling factor for that stability class. The values for the unstable and the stable class are determined by linear interpolation between the neutral class and the respective very unstable and very stable classes. The resulting values for the stability-dependent k^* scaling factor for all stability classes are given in table 4.1. To visualize the difference between the Jensen and the Gaussian model, wake plots for the very stable and unstable conditions are shown in figure 4.1.

Table 4.1. The resulting values for the stability-dependent k* scaling factor.

stability class	very unstable	unstable	neutral	stable	very stable
k* scaling	1.12	1.06	1.01	0.80	0.58

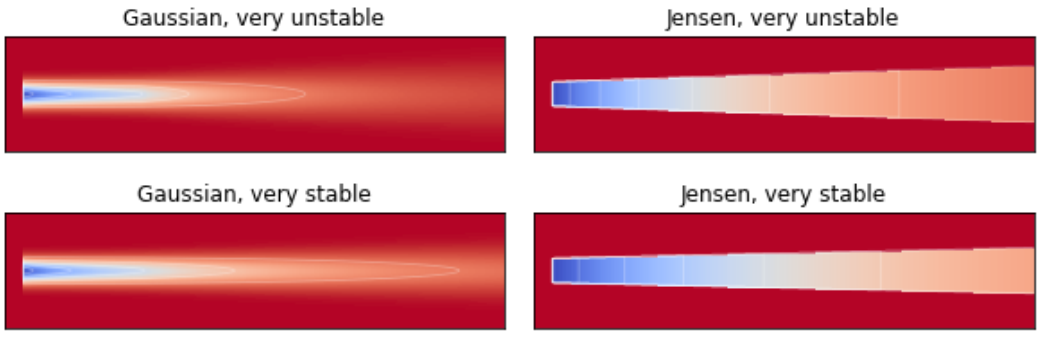

Figure 4.1. A comparison of the wake plots for a single wind turbine using the Gaussian wake model (left) and the Jensen wake model (right) for very unstable conditions (top) and very stable conditions (bottom).

4.2 Validation of stability-dependent Gaussian model

In this section, the stability-dependent Gaussian wake model is validated by comparing the resulting AEP for different orientations of a wind farm with results from the Jensen wake model. It is expected that the Gaussian model is less sensitive to small changes in the orientation, due to the gradually increasing velocity deficit from the outside to the center of the wake. This is different from the Jensen model, in which a wind turbine could have a significantly different incoming wind speed for small changes of orientation, since the velocity deficit is constant over the width of the wake. It is therefore expected that the Gaussian model results in a smoother AEP curve for the different orientations. This validation is not aimed at finding the exact same AEP results for each orientation for both models, since that would defeat the purpose of using a different model in the first place. Instead, the validation is performed to check if the differences between the implemented stability effects are similar to the stability-dependent Jensen wake model.

4.2.1 AEP results for case 1 wind conditions

The first step of the validation is to compare a case which consists of only one wind direction with one stability class, similar to case 1. This case is tested for multiple stability conditions, wind speeds, and turbine spacings for a 9x9 wind farm. The results of one of these tests are shown in figure 4.2 for the very stable and very unstable case for a wind speed of 9 m/s and a turbine spacing of 7D. The neutral case is left out for readability of the plot, but is closer to the unstable case than the stable case for both the Gaussian and the Jensen model. The AEP is only shown for orientations from 0° to 45°, as these are the only physically unique situations for a case with one wind direction. For all of the tested cases, the results generally show a good agreement between the two models for most orientations. The most remarkable differences are at orientations around 0°, 27°, and 45°. These are the orientations at which the wind direction is in some way aligned with the turbines, as is shown in figure 4.3. The Gaussian model results in a lower AEP than the Jensen model at these exact orientations, however, the Jensen model results in a lower AEP for a larger range around these orientations. This finding is as expected and is a direct result of the difference between the velocity deficits of the Gaussian and the Jensen model. In the Gaussian model, the deficit is largest at the wake centerline, therefore the AEP is lowest when the wind direction is exactly aligned with the turbines. For the Jensen model, the velocity deficit is constant over the width of the wake, therefore it does not matter if the wind direction is exactly aligned or if it is a few degrees off. This results in the more plateau-like curve of the Jensen model.

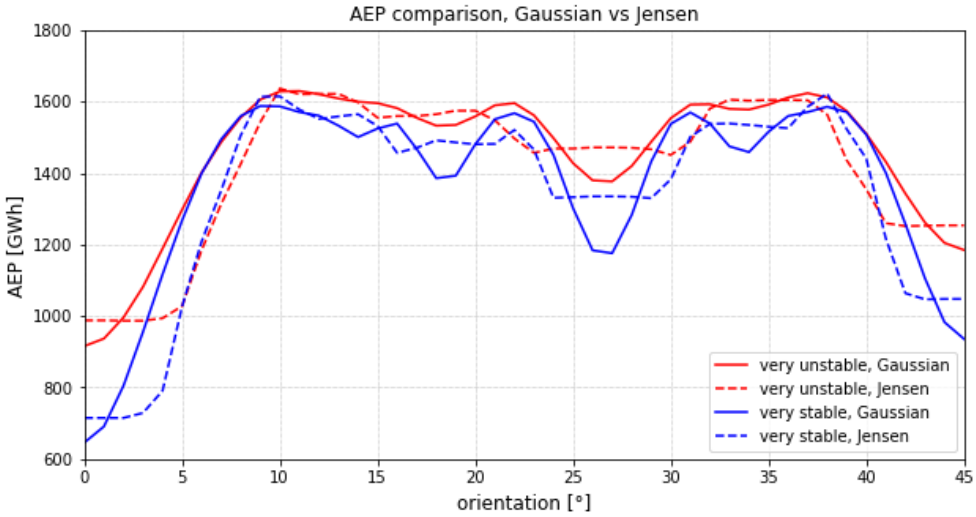

Figure 4.2. A comparison between the Gaussian (full lines) and the Jensen (dashed lines) wake model, showing the AEP for the very unstable (red) and very stable (blue) case of one wind direction.

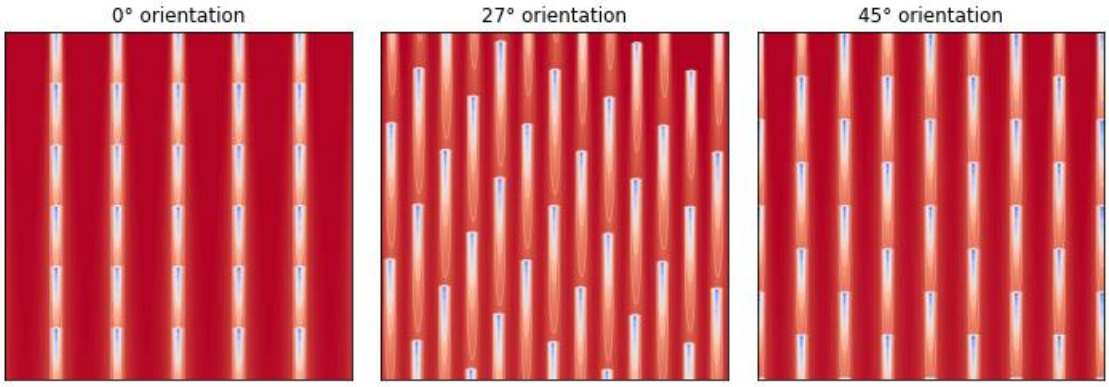

Figure 4.3. A visualization of three orientations for which the turbines are aligned with the wind direction.

4.2.2 Velocity deficit in the wake

The second step of the validation is to determine the velocity deficit in the wake. The velocity deficit is determined for three stability conditions for both the Gaussian and the Jensen wake model at downwind distances from 3D to 11D. The results are shown in figure 4.4. For the Gaussian model, the velocity deficit is distributed according to a Gaussian distribution over the width of the wake at any downwind distance. This means that the velocity deficit is highest at the wake centerline and decreases radially outwards. For this comparison, only the velocity deficit at the wake centerline is compared. Again, the focus is on the differences between the stability conditions for each model, rather than the differences between the values found for the two models. The velocity deficit is expressed as a fraction of the ambient wind speed. As an example, if the ambient wind speed is 12 m/s and the measured wind speed is 9 m/s, the velocity deficit is 0.25.

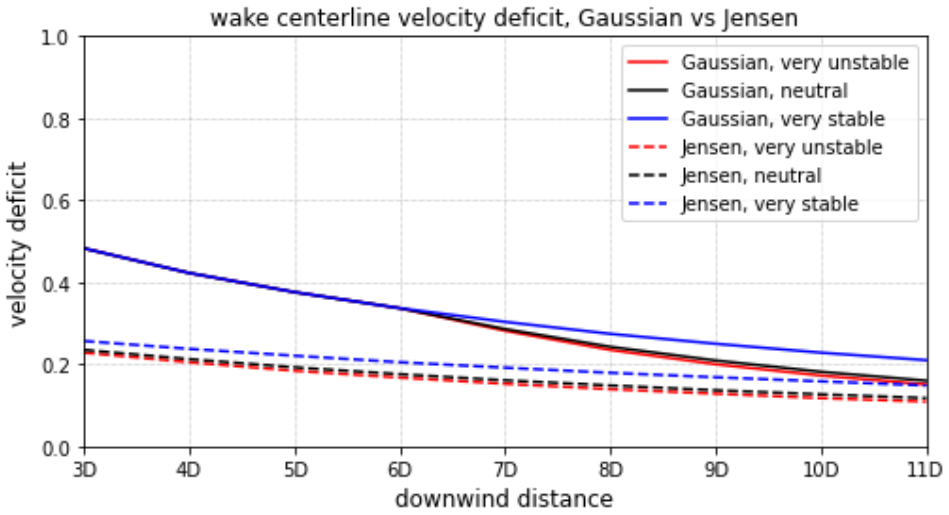

Figure 4.4. The wake centerline velocity deficit as a function of downwind distance expressed in rotor diameter D. The velocity deficits obtained with the Gaussian and the Jensen model are compared for three stability conditions: very unstable (z/L = -1), neutral (z/L = 0), and very stable (z/L = 1).

There are three observations made from the results shown in figure 4.4. The first is that the velocity deficit for the Gaussian model is significantly higher than for the Jensen model, especially for small downwind distances. This is as expected, since this comparison is only for the wake centerline, for which the velocity deficit is highest in the Gaussian wake model. This is also, again, the reason why in section 4.2.1 the AEP for the Gaussian model is lower for orientations that align exactly with the wind direction. The second is that the difference in velocity deficit between the neutral and the stable conditions is much larger than the difference between the neutral and the unstable conditions. This finding is true for both the Gaussian and the Jensen model and is consistent with previous findings. The third, and most important observation is that for the Gaussian model there is no difference in the velocity deficit between the three stability conditions for downwind distances smaller than 6D. This finding is a direct result of the way in which the stability-dependency is implemented in the model in FLORIS. As explained in section 4.1, the growth rate k^* only affects the far-wake region of the model. To implement stability-dependent effects in the near-wake region, the constants α and β would have to be considered in the calibration of the stability-dependent model. The development of such a detailed model is beyond the scope of this thesis. A more practical reason to only implement far-wake stability effects is that in wind farm design, turbine spacing is generally large enough to avoid near-wake effects. It is clear from the results that for the Gaussian model the stability conditions only affect the velocity deficit for downwind distances larger than 6D. This implies that, according to the parameters changed in FLORIS, the transition between the near-wake and the far-wake region is around 6D. This is unexpected, as it is in contrast with the commonly found value of around 3D for the transition between these two regions (Zhang et al., 2012). The fact that these stability effects only start developing so far downwind, could have an influence on the results obtained using this new stability-dependent model. This is because the default turbine spacing used in this thesis is 7D, while it is clear from figure 4.4 that the differences in velocity deficit between the stability conditions are relatively small for a 7D downwind distance, compared to for example the 9D distance. This finding could mean that stability effects become more important for wind

farms with larger turbine spacings. In section 4.4, the effect of turbine spacing on the potential AEP gain is analyzed in more detail.

4.3 Potential AEP gain with stability-dependent Gaussian model

To quantify the potential benefits of considering stability effects in the optimization process, the potential AEP gain is determined using the stability-dependent Gaussian wake model. The method is the same as in chapter 3, with the only difference being the model that is used. The two cases that are tested are the extreme case found in case 3, in which there are two wind directions with a 40° angle between them, and the semi-realistic case used in case 4. These two cases are chosen, because the extreme case provides an upper limit on the potential AEP gain and the semi-realistic case provides a more realistic indication of the potential AEP gain for real applications.

4.3.1 AEP results for case 3 wind conditions

The potential AEP gain is determined for the extreme case presented in case 3 in section 3.4.2. The wind conditions in this case consist of two wind directions with an angle of 40° between them. One of these wind directions is very unstable ($z/L = -1$) and one is very stable ($z/L = 1$). The wind speed is 9 m/s. The AEP results for each orientation from 0° to 90° are shown in figure 4.5. The potential AEP gain for this case is 1.0%, which is achieved by changing the orientation from 32° to 58°. The result is significantly lower than the 9.2% that is found in section 3.4.2, using the Jensen model.

4.3.2 AEP results for case 4 wind conditions

The potential AEP gain is determined for the wind conditions of the semi-realistic case 4 presented in section 3.5. The biased distribution of stability conditions, shown in figure 3.11, is used for this analysis. The uniform distribution is not considered, since it already resulted in a very low AEP gain using the Jensen model. The AEP results for the neutral and the non-neutral (biased) stability conditions are shown in figure 4.6. It is clear from this figure that there is almost no difference between the peak values for the neutral and the non-neutral conditions. The result is a potential AEP gain of 0.0%, meaning that there is no benefit in considering stability conditions for this case. This result is explained by the fact that in this case, the stable wind directions are also the wind directions with the highest wind speeds and the highest occurrence, as is visible from the wind rose in figure 3.11. In section 3.3.2 it is concluded that the stable wind directions are likely to play a dominant role in the optimal layout, due to the fact that minimizing losses for stable winds is more beneficial than maximizing gains from unstable winds. In this case, the optimal layout that is obtained under the assumption of neutral stability conditions is mostly determined by the 210°, 240°, and 270° wind directions. However, when considering stability conditions, these are also the exact wind directions for which there are stable conditions. This means that the consideration of stability conditions does not change the optimal layout, and therefore there is also no gain in considering these stability effects for this case.

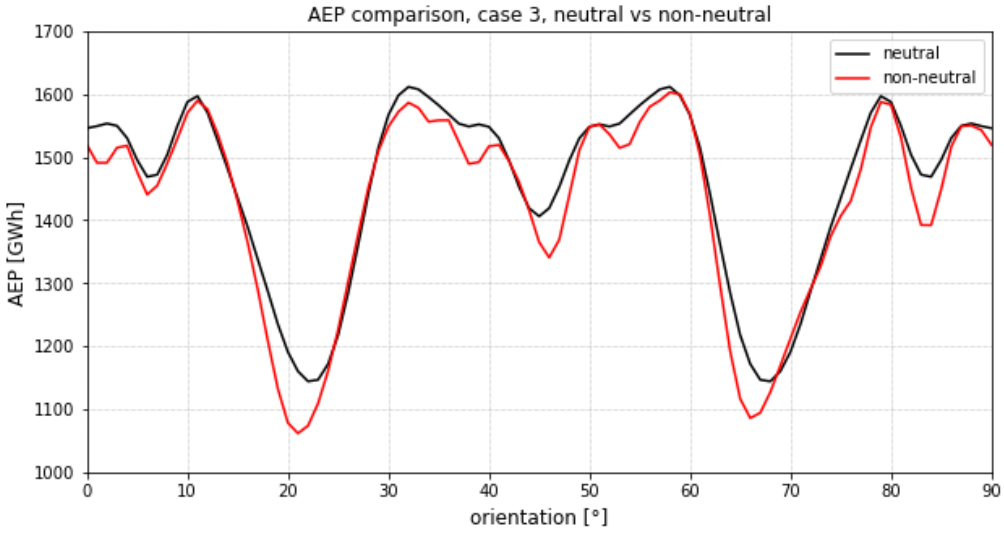

Figure 4.5. The AEP results for orientations from 0° to 90° for the neutral and non-neutral case 3.

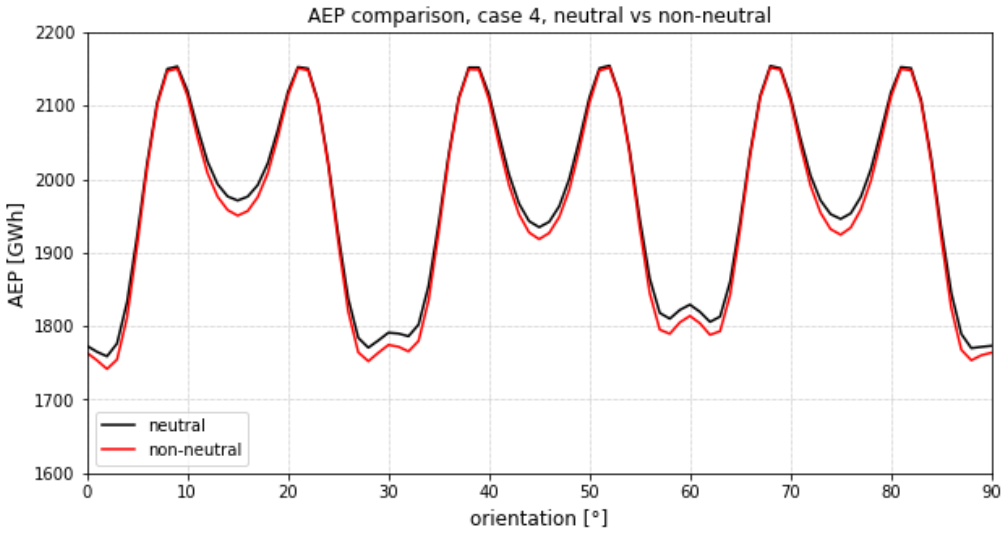

Figure 4.6. The AEP results for orientations from 0° to 90° for the neutral and non-neutral case 4.

In section 2.4 the relation between atmospheric stability and wind speed is described. It is shown that unstable conditions are more common for low wind speeds and stable conditions are more common for intermediate to high wind speeds. The stability conditions used in case 4 follow this trend, with the higher wind speeds having more stable conditions. The fact that the potential AEP gain for this case is 0.0% is not very promising for the overall expected benefits of considering stability effects in layout optimization. This is because in an optimization that is done under the assumption of neutral stability, the highest wind speeds are likely to play a dominant role in the resulting layout. These higher wind speeds, however, also are more likely to be stable and therefore it is likely that the consideration of these stability conditions will not change the resulting optimal layout significantly.

To confirm whether this alignment of the high wind speeds with the stable conditions is indeed the reason why potential AEP gain is zero, another final test case is used. In this final case, the stability conditions of case 4 are flipped, with the unstable conditions becoming stable and vice versa. These wind conditions are no longer considered semi-realistic, as the lower wind speeds are now more likely to be stable than the higher wind speeds. The expectation is that, since the stable conditions are no longer in the same wind direction as the high wind speeds, the potential AEP gain should be higher. The results, however, again show a potential AEP gain of 0.0% for this case. This does not necessarily have to mean that the hypothesis that stable winds play a dominant role in the resulting optimal layout is false. It does indicate, however, that it is likely that there are other factors causing the potential AEP gain to be significantly lower than the values found using the Jensen model in chapter 3. One such a factor could be turbine spacing, as it is shown in section 4.2 that the difference between the velocity deficits is relatively small for the chosen turbine spacing of 7D. In section 4.4, the turbine spacing and ambient wind speed are varied to determine the influence of these parameters on the potential AEP gain.

4.4 Influence of turbine spacing and ambient wind speed on AEP gain

To determine the influence of other parameters on the potential AEP gain, the turbine spacing and the wind speed are varied in this section. The stability conditions from case 2 are used, in which there are two wind directions, one stable and one unstable, with a 30° angle between them. The turbine spacing is varied from 3D to 11D and the wind speed is varied from 8 m/s to 16 m/s. The results of these two tests are shown in figure 4.7 and are discussed in the following sections.

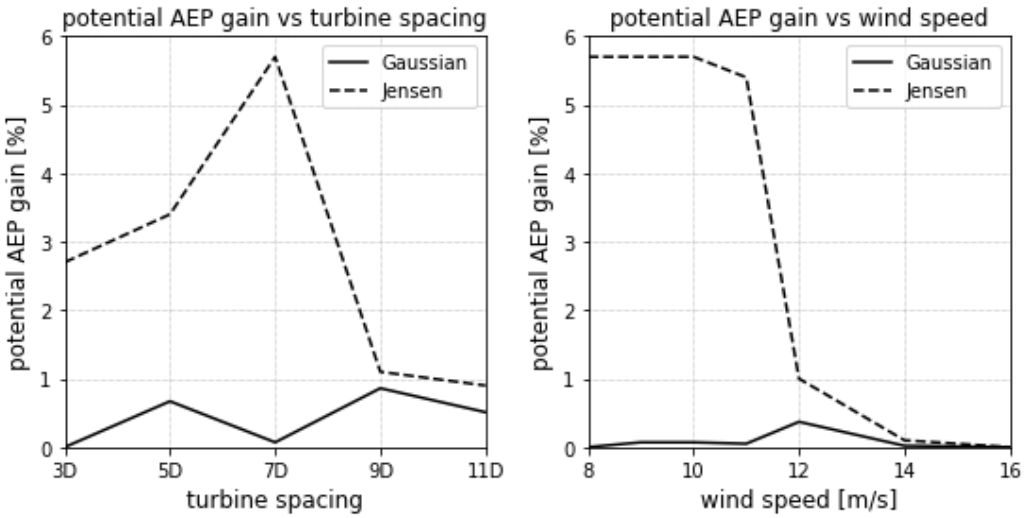

Figure 4.7. The potential AEP gain versus the turbine spacing (left) and versus the ambient wind speed (right).

4.4.1 Turbine spacing results

The first test consists of a variation of the turbine spacing from 3D to 11D. It is found in section 4.2.2 that the difference in velocity deficit between stable and unstable conditions is larger for larger downwind distances when using the Gaussian wake model. It is therefore expected that the potential AEP gain would be larger for cases with large turbine spacings, as the effects of the different stability conditions would be more pronounced in these cases. The results, however, show that there is no such relation between the turbine spacing and the potential AEP gain. In fact, there does not seem to be any specific relation whatsoever. For the Gaussian model, the AEP gain increases for both a decrease of 7D to 5D and for an increase from 7D to 9D. The AEP gain then decreases when increasing or decreasing the turbine spacing even further. It seems to be a coincidence for this specific case that the AEP gain is relatively low for the default turbine spacing of 7D. For the Jensen model, the opposite is true, since the potential AEP gain is highest for a turbine spacing of 7D. The AEP gain then decreases for both an increased and a decreased turbine spacing. This further supports the conclusion that there is no direct relation between the AEP gain and the turbine spacing, at least for this specific case. Note that this does not mean that the turbine spacing is not important for a wind farm layout, as clearly the AEP per wind turbine is higher for wind farms with a larger turbine spacing. However, for this thesis the main focus is on whether the consideration of stability effects is relevant, and for that purpose there does not seem to be an indication that this consideration is specifically relevant for wind farms with certain turbine spacings.

Another interesting finding is that the optimal orientation, and thus the resulting layout, is different for the Gaussian and the Jensen model when using the default turbine spacing of 7D. For the Jensen model the optimal orientation is 23° and for the Gaussian model this optimal orientation is 53°. This is an important result, as it means that the choice of the wake model has a significant impact on the resulting optimal layout, which is obviously not preferred. It is also found that with increased turbine spacings of 9D and 11D, the resulting optimal orientation of the two models are much closer again. For both these cases the optimal orientation is 22° for the Gaussian model and 23° for the Jensen model. It is therefore reasonable to assume that the 53° orientation from the 7D Gaussian case is wrong, which is also supported by the earlier finding in section 4.2.2, regarding the relatively small difference in velocity deficits for the 7D downwind distance. It is concluded that the simple stability-dependent Gaussian wake model, as proposed in this thesis, should not be used for turbine spacings up to 7D, as the differences between the stability conditions are not sufficiently reflected for these values. An improved version could be developed in FLORIS using a more elaborate calibration that includes the near-wake region parameters.

4.4.2 Ambient wind speed results

The second test consists of a variation of the ambient wind speed from 8 m/s to 16 m/s. The rated wind speed of the used wind turbine is 11.4 m/s and most cases presented so far use a default wind speed of 9 m/s. The results of the Gaussian model, presented in figure 4.7 (right), show a remarkably low potential AEP gain for all wind speeds. This is likely due to the fact that the default turbine spacing of 7D is used

for this test, while for this specific turbine spacing the AEP gain is coincidently very low for the Gaussian model, which is also shown in figure 4.7 (left). For the Jensen model, however, there is a clear trend in the potential AEP gain for increasing wind speeds. The AEP gain drops significantly when the ambient wind speed becomes larger than the rated wind speed. This difference is largest between 11 m/s and 12 m/s, at which the AEP gain decreases from 5.4% to 1.0%. The observed trend is explained by the fact that the difference in velocity deficits between the stable and the unstable case is not relevant anymore when the wind speed is sufficiently high. For high wind speeds, as long as the resulting wind speed at subsequent wind turbines is larger than the rated wind speed, the produced power is the same for both stable and unstable conditions. This is not true for lower wind speeds, as a slightly higher wind speed due to unstable conditions, leads to a slightly higher power production, compared to the stable or neutral case. This means that the consideration of stability effects is more important for wind speeds below the rated wind speeds, which is reflected by the high potential AEP gain. The upper limit for this test is a wind speed of 16 m/s, at which the potential AEP gain is 0.0%. For this wind speed the resulting AEP is practically the same for each orientation. This means that all wind turbines are operating at rated power, regardless of the orientation or the stability condition. In these conditions, there is clearly no benefit in considering the stability conditions, which is reflected by the AEP gain of 0.0%.

The ambient wind speed of 14 m/s resulted in an interesting finding that is highlighted in this final section. The AEP results for each orientation are shown in figure 4.8 for both the Jensen and the Gaussian model. It is noted again that the wind conditions for case 2 consist of one unstable wind in the 165° direction and one stable wind in the 195°. This means that if the orientation is 15°, the stable wind is aligned with the wind farm, and if the orientation is 75°, the unstable wind is aligned with the wind farm. Both the Jensen and the Gaussian wake model show that under the assumption of neutral stability, the 15° and the 75° orientation are the same due to symmetry. However, when stability effects are considered in the non-neutral case, it becomes clear that the 15° orientation results in a much lower AEP than in the neutral case, while the 75° orientation results in a higher AEP. It is also clearly visible that the loss in AEP due to stable conditions is significantly greater than the gain in AEP due to unstable conditions. This finding does not affect the potential AEP gain, since the optimal orientation is clearly not one of these two orientations. By just looking at the low potential AEP gain, it seems as if stability effects are negligible for scenarios with high wind speeds, but it is clear from figure 4.8 that the stability conditions and specifically the stable winds can still have a significant impact on the AEP.

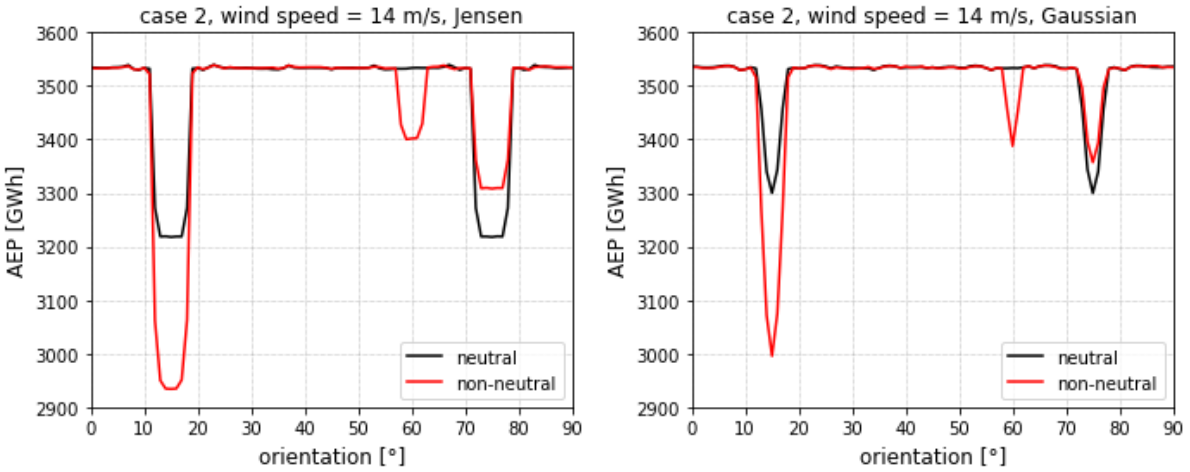

Figure 4.8. The AEP per orientation for the stability conditions of case 2 with an ambient wind speed of 14 m/s using the Jensen model (left) and the Gaussian model (right).

4.5 Chapter conclusions

In this section, the main results and conclusions from this chapter are summarized.

- For case 1, the stability-dependent Gaussian model shows good agreement with the Jensen model. The AEP difference between the two models is largest for orientations in which the wind direction is aligned with the wind farm. For these orientations, the Gaussian model results in a minimum AEP for the exact orientation of alignment, whereas the Jensen model results in a low AEP for a small range of orientations around that exact orientation.

- The velocity deficit at the wake centerline is significantly higher for the Gaussian model than for the Jensen model. The difference in velocity deficit between the neutral and stable conditions is larger than the difference between neutral and unstable conditions, for both the Jensen model and the Gaussian model.

- For the Gaussian model, there is no difference in velocity deficit between the different stability classes for downwind distances smaller than 6D. This is a direct result of the method used to implement the stability-dependent effects, which is only applied to the far-wake region. However, it was not expected that these effects would only become apparent after such a large distance, as the transition between near-wake and far-wake is generally considered to be around a 3D downwind distance.

- The potential AEP gain is determined using the Gaussian model and is 1.0% for the extreme case with a 40° angle in case 3 and 0.0% for the semi-realistic case 4. These results are significantly lower than the values found using the Jensen model, which are 9.2% and 0.7%, respectively.

- There seems to be no relation between the potential AEP gain and the turbine spacing for both the Jensen and the Gaussian model. There is no indication that the consideration of stability effects is more important for wind farms with certain turbine spacings.

- The Gaussian model gives a different optimal orientation than the Jensen model for turbine spacings up to 7D. For larger turbine spacings, both models show similar results. This is the result of the fact that differences between the velocity deficits between the different stability conditions are not developed enough for small downwind distances. The stability-dependent Gaussian model should therefore not be used for wind farms with turbine spacings smaller than or equal to 7D.

- Using the Jensen model, the potential AEP gain drops significantly for ambient wind speeds greater than 12 m/s. For wind speeds greater than 16 m/s, this AEP gain is reduced to zero. When the reduced wind speed in the wakes at subsequent turbines is larger than the rated wind speed, the difference between stable and unstable conditions is no longer relevant for the resulting AEP. No significant relation between the potential AEP gain and the ambient wind speed is found for the Gaussian model, due to the AEP gain being too low for all wind speeds.

5. Stability-dependent layout optimization for a real site using meteorological data

The main goal of this chapter is to quantify the potential benefits of considering stability in the layout optimization process by determining the potential AEP gain for a real site using meteorological data. The data is taken from the Dutch Offshore Wind Atlas (DOWA), which is developed by KNMI and consists of 10 years (2008-2017) of meteorological data in a large domain centered around the Netherlands.

In section 5.1, more information is given about the used database. In section 5.2, the wind conditions and stability conditions are determined. The method to determine the stability conditions is explained and the binning of the input parameters is described in detail. Some considerations regarding the computation time are also mentioned. In section 5.3, the wind conditions and stability conditions are analyzed. The wind rose and stability rose are presented, along with a wind speed distribution and a bin-based normalized stability distribution. In section 5.4, the AEP and optimization results are presented.

5.1 Meteorological data

The meteorological data used in this chapter is taken from the Dutch Offshore Wind Atlas (DOWA). The DOWA is one of the databases developed by KNMI, the meteorological institute of the Netherlands, and provides a 10 year (2008-2017) wind climatology for the North Sea. The DOWA can be seen as an updated version of the KNMI North Sea Wind (KNW) Atlas, as it provides a better hourly correlation with measurements and climatological information for heights up to 600 m, instead of 200 m. The KNW Atlas, however, consists of 40 years of data and is therefore preferred in applications that require long-term statistical data such as extreme wind speeds. The dataset in DOWA is developed using the numerical weather model HARMONIE and is validated with satellite measurements, met masts and LiDAR measurements. The data consists of hourly information on a 2.5 km square grid, which can be downscaled to 60 seconds and a 100 m grid. The DOWA subdomain consists of 217 by 234 grid points and is centered around Cabauw in the Netherlands. The location selected for this chapter is at grid point (48,64), which is positioned slightly northeast of the Borssele offshore wind farm. The location is shown on a map in figure 5.1 (Google, n.d.). There is no particular reasoning for choosing this specific site, other than there already being a wind farm at this location.

Figure 5.1. A map of the southern coast of the Netherlands, showing the location of the chosen site. (Google, n.d.)

5.2 Determining the wind conditions

In this section it is described how the meteorological data is processed to be used for the AEP calculations and the layout optimization process. First, the calculation of the stability conditions is explained. Then, the binning of all wind condition parameters is described. Finally, an important trade-off between accuracy and computation time is introduced.

The stability conditions for the obtained data are determined and expressed in the non-dimensional Obukhov length. To do this, the bulk Richardson number is first determined and used in combination with the assumption that $z/L \approx 10\ Ri_B$, which is taken from Cañadillas et al. (2020). To calculate the bulk Richardson number, given in equation 2.17, the following parameters are required from the data. Firstly, the virtual potential temperature difference $\Delta\theta_v$ between the surface and hub height needs to be determined. This requires the air temperature, air pressure and specific humidity at both the surface and at hub height. The expressions for the potential temperature and the virtual potential temperature are given in equations 2.14 and 2.15, respectively. Secondly, the wind speed difference Δu between the surface and hub height is required. The wind speed at the surface is considered to be zero, therefore only the wind speed at hub height is required. Thirdly, the height difference Δz between the surface and hub height is required, which is simply the hub height of 90 m.

The wind condition parameters that are required for the AEP calculations in the layout optimization process are the wind direction, the wind speed, and the stability condition. Each parameter is divided into bins and the values for these parameters are checked for each data point. Every check adds one count to a combination of these bins to find the frequency of occurrence for every possible combination of wind conditions. The binning of the wind direction turns out to have a strong impact on the optimization results, as is explained in more detail in section 5.4. Therefore, both bin sizes of 15° and 5°

are used. The bin size of 15° results in a total number of 24 wind direction bins, while the bin size of 5° results in a total number of 72 wind direction bins. The bins are center-valued and the first bin starts at 0°, such that for the 5° bin size all data points between -2.5° and +2.5° are added to this bin (including -2.5° and excluding +2.5°). The binning of the wind speed is the same for all presented results. The step size between the bins is not constant, therefore the binning is described in more detail. Firstly, there are two bins for wind speeds below the cut-in wind speed of 3 m/s and above the cut-out wind speed of 25 m/s. The bin with wind speeds below the cut-in wind speed is shown in the wind statistics plots in section 5.3, however, it is not used in the AEP calculations to reduce the computation time. The bin with wind speeds above the cut-out wind speed is not shown, since only 103 out of 87673 data points have a wind speed above 25 m/s. Secondly, there are twelve bins with a bin size of 1 m/s ranging from 3-4 m/s up to 14-15 m/s. Thirdly, there are five bins with a bin size of 2 m/s ranging from 15-17 m/s up to 23-25 m/s. The bin size for wind speeds up to and slightly over the rated wind speed is chosen to be smaller, since for these wind speeds small changes have a larger impact on the resulting AEP than for wind speeds well exceeding the rated wind speed. The total number of wind speed bins is 19. However, the cut-in and cut-out bins are not used in the AEP calculations, effectively reducing the number of bins to 17. The binning of the stability conditions is based on the stability classes presented in table 3.1. There is one bin for each stability class, resulting in a total of 5 bins consisting of the very unstable, unstable, neutral, stable, and very stable conditions. The total number of bins and therefore the number of possible combinations of wind conditions is either 6120 or 2040, depending on the choice of the wind direction bin size of 5° or 15°, respectively.

The computation time is directly and almost linearly related to the number of bins used. Using a wind direction bin size of 5° instead of 15° results in a computation time that is roughly three times as long. However, the 5° bin size is generally preferred, as it provides a more accurate representation of real wind conditions as an input to the optimization process. To allow the use of a 5° bin size, without having excessively long computation times, another method is applied. First of all, since there are so many combinations of very specific wind conditions, it is likely that there are some combinations for which there are no counts. An example of this would be a wind condition in any arbitrary wind direction, with a wind speed of 24 m/s and a stability condition that is very unstable. To reduce the number of bins to be used as an input for the optimization process, any bins that have a count of zero are removed. For the wind direction bin size of 5°, this reduces the total number of bins to 4142. However, this reduced total number of bins is still too large, therefore the applied method is extended to not only remove bins that have a count of zero, but to also remove bins that have a count below a specified minimum. For example, using a wind direction bin size of 5° and a count minimum of 10, the total number of bins is further reduced from 4142 to 1942. For a wind direction bin size of 15°, removing all empty bins reduces the total number of bins from 2040 to 1508, and applying a count minimum of 10 further reduces this number to 1023 bins. The problem with this method, however, is that valid data points are removed. Using a count minimum of 10 and a wind direction bin size of 5° , roughly 10.1% of the data points are removed just to reduce the computation time. This problem appears to be smaller for the wind direction bin size of 15°, for which only 2.7% of the valid data points are removed. Unfortunately, the data points

that do get removed are also likely to be the more uncommon wind conditions, such as very stable conditions or very high wind speeds, which are expected to have the largest impact on the resulting layout. On the other hand, these specific bins also have a very low frequency of occurrence and therefore are expected to have a small impact on the resulting AEP. The choice of the count minimum is a direct trade-off between accuracy and applicability. It is clear that the consideration of this count minimum is important, and the chosen value is therefore explicitly mentioned with each of the presented results in section 5.4. Finally, it is worth noting that applying a count minimum of 1 is the same as only removing the empty bins, therefore the number of valid data points is not reduced with a count minimum of 1.

5.3 Analysis of the wind conditions

In this section, the wind conditions for the chosen site are presented. As is done in previous cases, the wind rose and the stability rose are shown. Additionally, the wind speed distribution and the stability distribution per wind speed are given.

The wind rose and the stability rose for the chosen site are shown in figure 5.2. It is clear that the southwest wind direction is the most common, which is quantified by the fact that 33.0% of all data points are between 195° and 255° (225°±30°). The southeast wind direction on the other hand is the least common, with only 8.7% of all data points being in the range of 105° to 165° (135°±30°). As a comparison, in a uniform case the number of data points in such a range would be 16.7%. The stability conditions at this site are predominantly unstable, with 72.2% of all data points being in the (very) unstable range. The unstable condition seems to be the most dominant stability class for all wind directions, however, it appears to be less dominant for the most common wind directions. For the southwest wind direction, the unstable and very unstable conditions comprise 56.4% of all data points, while for the north wind direction, 88.0% of all data points are either unstable or very unstable. This difference in occurrence of unstable conditions is likely the result of differences in average wind speeds between the mentioned wind directions. It is mentioned in section 2.4 that unstable conditions tend to favor low wind speeds, while stable conditions tend to favor intermediate to high wind speeds. For the southwest wind direction, the average wind speed is 11.6 m/s, while for the north wind direction, the average wind speed is 7.7 m/s. This seems to confirm the general trend that unstable conditions favor lower wind speeds. The average wind speed over all data points is 9.5 m/s.

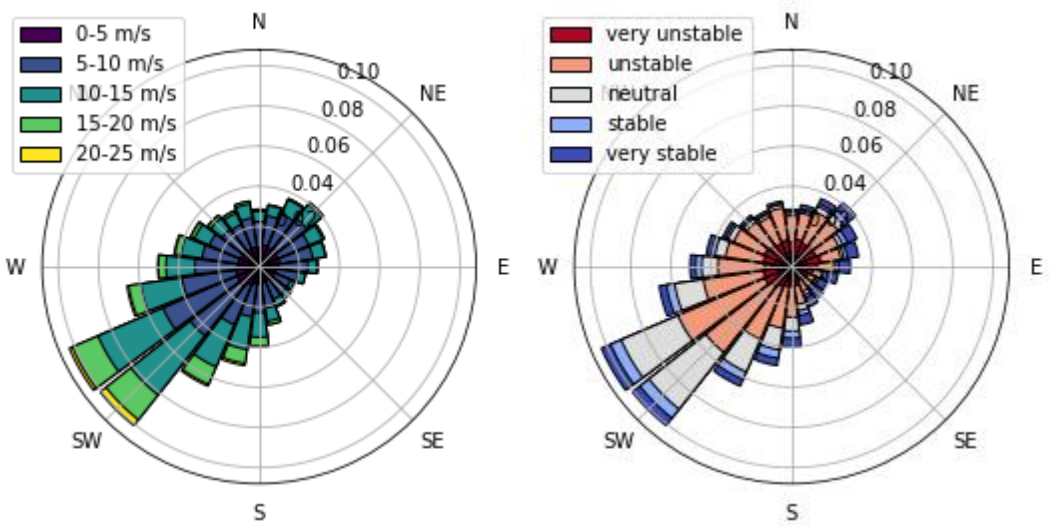

Figure 5.2. The wind rose (left) and the stability rose (right) for the chosen site.

The wind speed distribution is shown in figure 5.3. In this figure, the stability conditions per wind speed are also shown. To further analyze the occurrence of different stability conditions for different wind speeds, the bin-based normalized stability distribution is shown in figure 5.4. Both plots clearly show that unstable conditions are dominant for this particular site, as is also observed from the stability rose in figure 5.2. It is remarkable, however, that the frequency of stable conditions does not increase with increasing wind speeds. It is mentioned in section 2.4 that stable conditions are generally considered to be more common for intermediate to high wind speeds. From figure 5.4, it is clear that the frequency of unstable conditions is reduced significantly for higher wind speeds, which is expected. However, the frequency of stable conditions is also reduced for higher wind speeds, which is not expected. It is not concluded that the resulting stability conditions are wrong because of this finding. No research is found that shows similar graphs for any sites near the chosen site, and it is therefore difficult to compare these results with other findings. The results, especially regarding the stable conditions, are interesting and there is of course a possibility that something went wrong in determining the stability conditions. One likely error could be that the boundaries of the stability classes are not chosen appropriately. The used range for the stable class is $0.1 < z/L < 0.5$. A quick test showed that reducing this lower boundary to 0.01 results in a slight increase in the frequency of stable conditions for higher wind speeds. This could be an indication that this is a better choice for the value of the boundary. It is decided, however, to keep the boundaries of the stability classes consistent with previous chapters.

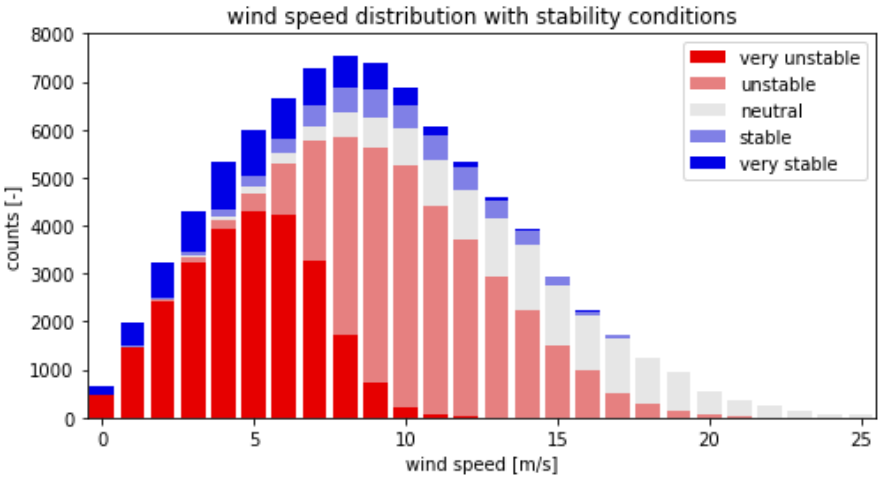

Figure 5.3. The wind speed distribution and stability conditions for the chosen site.

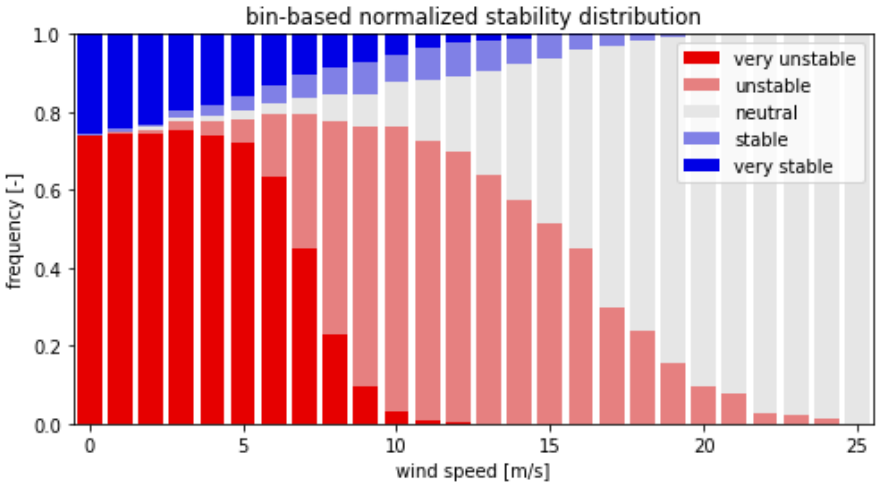

Figure 5.4. The bin-based normalized stability distribution for the chosen site.

5.4 Results

In this section, the AEP results for the chosen site are presented. This includes a comparison of the neutral and non-neutral stability conditions, the obtained optimal orientation, and the potential AEP gain. In section 5.2, it is mentioned that the choice of the wind direction bin size has a strong impact on the resulting optimal layout. Before presenting the final results, it is important to clarify how this choice affects the optimal orientation and how some input parameters can even result in an incorrect optimal layout. This clarification is done using an example in which the wrong input parameters are chosen.

The AEP results of the first example are shown in figure 5.5. For this calculation, a wind direction bin size of 15° is used, the wind farm orientation is changed in steps of 1° from 0° to 90°, and a count minimum of 20 is applied to the wind conditions. The difference in AEP between the neutral and the non-neutral stability conditions is not necessarily important for this example, but they are still both shown for consistency with other AEP plots. What is important, however, is the large reoccurring fluctuation that is clearly visible for both stability cases. The AEP varies significantly from roughly 1600 GWh to 1800 GWh,

with the lowest values occurring at multiples of 15° and the highest values occurring in the middle of those intervals. These results suggest that any orientation that is in the middle of those 15° intervals is the optimal orientation for this wind farm, as the resulting AEP is almost exactly the same for all peaks. It is clear that this conclusion is wrong, and that the behavior of the shown AEP results is due to the choice of the wind direction bin size of 15°. It is now explained why this is the case and what is changed regarding the input parameters to resolve this problem. By using a 15° bin size to define the wind conditions, the wind input that is used by the model in the AEP calculations is limited, such that wind can only come from those directions that are multiples of 15°. This means that when rotating the wind farm for different orientations, there will only be cases in which the wind is aligned with the wind farm at those same intervals of 15°. Any time the wind is aligned with the wind farm, the AEP drops significantly, which is clearly represented by the lows in figure 5.5. Naturally, it is beneficial to prevent these aligned wind conditions. Therefore, the optimal orientations that result from this case are those orientations that are the furthest away from having any aligned winds, which are the orientations that are exactly between the multiples of 15°. These results can be understood and explained, based on the used input parameters. However, they cannot be practically applied since the conclusion of the optimal orientation is not a result of simulating realistic wind conditions. In reality, the wind does not only come from specific wind directions and therefore the conclusion should not be the result of such a limitation in the simulation method. A solution to this problem is to only consider orientations that are aligned with the wind direction bins. An additional benefit of this solution is that it also reduces the number of orientations that have to be checked, therefore reducing the computation time.

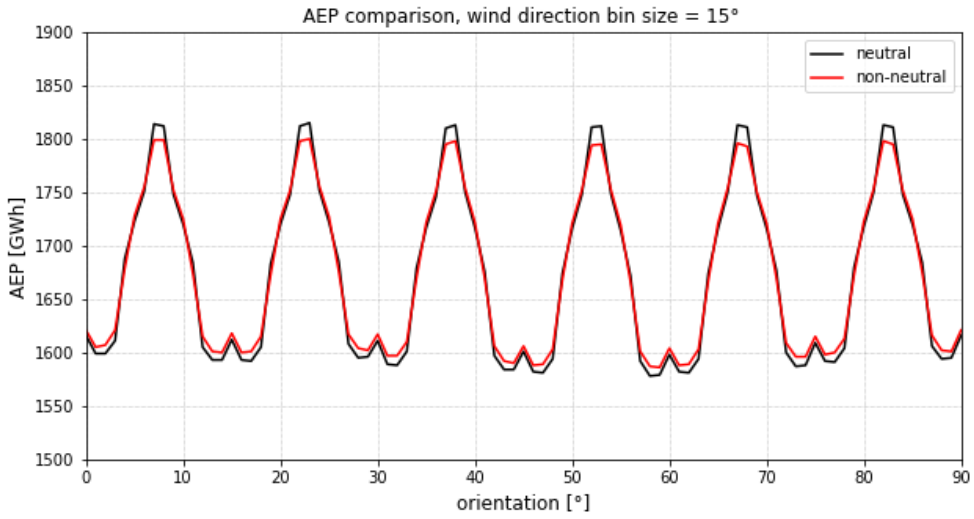

Figure 5.5. The AEP results for the neutral and non-neutral stability conditions for the chosen site. The wind direction bin size is 15° and the orientation is changed in steps of 1°.

The AEP results for the chosen site are shown in figure 5.6. The wind direction bin size is reduced to 5°, the orientation is changed in steps of 5° from 0° to 90°, and a count minimum of 1 is applied. The results clearly show a minimum AEP at the 50° and 55° orientations. This is expected, as the wind rose shows that the most common wind directions are 225° and 240°, which are aligned with the wind farm at orientations of 45° and 60°. Note that rotating the wind farm clock-wise by 45° means that it is aligned

with the NE direction, but also with the SW direction. The optimal orientation for this case is either the 0° or the 15° orientation, which both result in an AEP of 1699 GWh for the non-neutral case. The minimum AEP for the non-neutral case is 1684 GWh and is obtained at both the 50° and the 55° orientation. It is remarkable that the minimum and the maximum AEP are so close together, with only a 15 GWh difference between them. The neutral and the non-neutral case are also close together, with the neutral case having a 4 GWh lower AEP than the non-neutral case. The lower overall AEP for the neutral case is explained by the fact that the stability conditions for this specific site are predominantly unstable. The potential AEP gain, which is arguably the most important parameter for this study, is found to be 0.0% for this case. There is no benefit in considering the stability conditions for this case, since the resulting optimal orientation is the same as is obtained using the assumption of neutral stability.

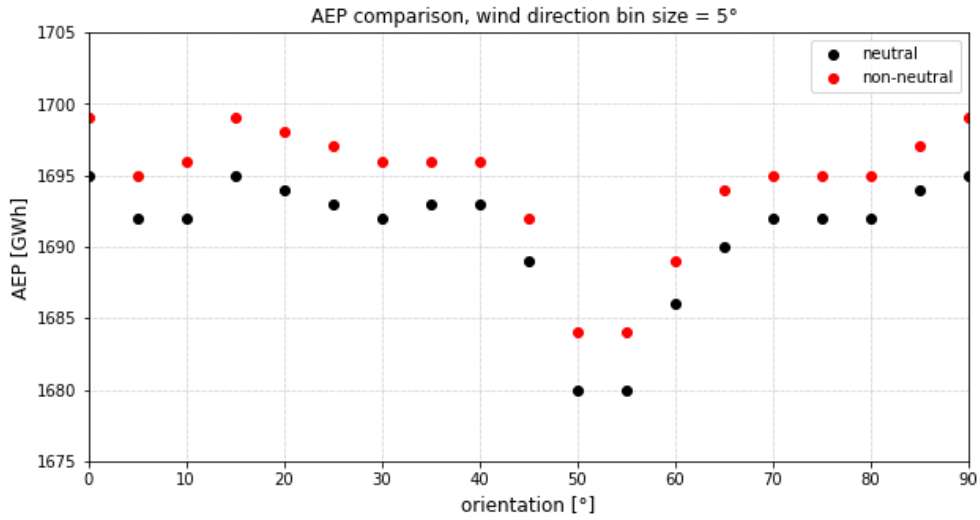

Figure 5.6. The AEP results for the neutral and non-neutral stability conditions for the chosen site. The wind direction bin size is reduced to 5° and the orientation is changed in steps of 5°.

5.5 Chapter conclusions

In this section, the main results and conclusions from this chapter are summarized.

- The wind conditions for the chosen site, which is near the Borssele offshore wind farm in the Netherlands, show that the southwest wind direction is most common, with 33% of all data points being winds from roughly this direction. The southeast wind direction is the least common, with only 8.7% of all data points showing winds from this direction.

- The wind conditions are predominantly unstable, with 72.2% of all data points being in either the unstable or very unstable range. The average wind speed for all data points is 9.5 m/s. For the southwest wind direction, the average wind speed is 11.6 m/s and 56.4% of all data points are (very) unstable. For the north wind direction, the average wind speed is 7.7 m/s and 88.0% of all data points are (very) unstable. This is consistent with the fact that unstable conditions favor lower wind speeds.

- The stability distribution shows a decrease of unstable conditions with increasing wind speed, as expected. However, it also shows an unexpected decrease of stable conditions with increasing wind speed. This outcome could be a result of a too high lower boundary for the stable class, as a short test showed that reducing this lower boundary results in a slight increase in stable conditions with increasing wind speed.

- The step size of the orientations in the layout optimization must be equal to the wind direction bin size. If these two parameters do not have the same step size, the resulting optimal layout is biased towards orientations that are exactly between two wind direction bins. This is because the wind farm is then oriented in such a way that it avoids any aligned wind directions.

- The optimal orientation for the chosen site is determined to be either 0° or 15°. The AEP results show that the minimum AEP is obtained for the 50° and 55° orientations. This is expected, since for these orientations the wind farm is aligned with the most common wind directions.

- The potential AEP gain for the chosen site is 0.0%. The AEP difference between the tested orientations is remarkably small, with only a 15 GWh difference between the maximum and minimum AEP. The difference between the neutral and non-neutral case is even smaller, being only 4 GWh. This finding means that there is no benefit in considering the stability conditions in the layout optimization process for this case.

6. Conclusions and Recommendations

In this chapter, the main conclusions of each chapter are summarized in section 6.1. A general conclusion is given in section 6.2. Some recommendations for future projects are given in section 6.3.

6.1 Summary

In this section, the main conclusions of each chapter are summarized.

6.1.1 Layout optimization with stability-dependent Jensen wake model

The main goal of chapter 3 is to use a simple optimization method to determine the potential AEP gain that can be achieved by considering atmospheric stability effects in the wind farm layout optimization process. A stability-dependent Jensen wake model is developed in FLORIS, a wake modeling utility for Python, by introducing a stability-dependent wake decay coefficient. The layout optimization method is based on only changing the orientation of the wind farm, while keeping the number of rows, the number of turbines per row, and the turbine spacing fixed. The optimal orientation and potential AEP gain is determined for four cases, ranging from as basic as possible to semi-realistic.

Case 1 consists of just one wind direction with one stability condition, which is either neutral, very stable, or very unstable. The potential AEP gain for case 1 is 7.4%. Case 2 consists of two wind directions with a 30° angle between them. One wind direction is very stable, and one wind direction is very unstable. The potential AEP gain for case 2 is 5.6%. Case 3 also consists of two wind directions, however in this case the goal is to find the angle between any two wind directions that results in the highest possible potential AEP gain. The potential AEP gain for case 3 is 9.2%, which is obtained at an angle of 40°. Finally, case 4 consists of semi-realistic wind conditions, for which two different stability distributions are tested. The first is a uniform stability distribution, which resulted in a potential AEP gain of 0.1%. The second is a biased stability distribution, for which the potential AEP gain is 0.7%.

The results of the first cases look promising, showing high AEP gains by considering the stability effects. However, as soon as semi-realistic wind conditions are used in the optimization method, this potential AEP gain quickly drops to effectively zero for a uniform stability distribution. Only in the case of an extremely biased stability distribution, in which certain wind directions only have stable conditions and other wind directions only have unstable wind conditions, a potential AEP gain of 0.7% is obtained. It can be argued, of course, that a 0.7% increase in AEP is still a huge benefit to any real wind farm. However, it should also be noted that these wind conditions are still far from realistic, as the stability distribution for the biased case is made specifically to try to maximize the AEP gain for the given wind speed distribution and wind rose. It is expected that in a real case the potential AEP gain is likely to be closer to 0.1%. The benefits of considering stability effects in the layout optimization process are therefore expected to be insignificant.

There are some other conclusions made in this chapter that are not specifically about the benefits of considering stability effects, but rather about the impact of the different stability classes and the stability distribution on the resulting optimal layout. Firstly, it is found that the stability distribution has the largest impact on the optimal layout when there are specific wind directions that have specific stability conditions. This means that stability effects are only likely to play a role in the layout optimization, when certain wind directions are dominantly stable or unstable, for example due to some geographical features. Secondly, it is found that stable conditions play a dominant role in determining the optimal layout. The benefit of reducing wake overlap is greater for stable winds than for unstable winds, which results in the stable winds having a larger impact on the resulting optimal layout.

6.1.2 Layout optimization with stability-dependent Gaussian wake model

The main goal of chapter 4 is to develop a stability-dependent Gaussian wake model and to compare its performance with the stability-dependent Jensen wake model. The Gaussian wake model is made stability-dependent using the growth parameter k^*. The value of the growth parameter is changed based on the stability class, which is done by applying a scaling factor to the wake expansion parameters k_a and k_b in FLORIS. The scaling factor is determined for each stability class and is based on a calibration using the stability-dependent Jensen model. This calibration is done using 12 cases, consisting of different wind roses, stability conditions, and wind farm layouts.

A validation of the modified Gaussian wake model is done by comparing the AEP results per orientation with the Jensen wake model for the case of one wind direction. The results show good agreement between the two models for most orientations. The Gaussian model is less sensitive to small changes in the orientation, which is a direct result of the Gaussian distribution of the velocity deficit over the width of the wake. The Jensen model, on the other hand, has a more plateau-like curve for the AEP plot. This is the result of the constant velocity deficit over the width of the wake. The differences between the AEP results for the very stable and very unstable conditions are very similar when comparing the Gaussian model and the Jensen model. The velocity deficits in the wake centerline are also compared. For large downwind distances, the differences between the velocity deficits for very stable and very unstable conditions show good agreement between the two models. However, it is found that for the Gaussian model, a difference between deficits for stable and unstable conditions only starts to develop for downwind distances greater than 6D. This is unexpected, as the stability-dependency is implemented in the far-wake region of the model, and the transition between the near-wake and far-wake region is generally considered to be around the 3D downwind distance.

The stability-dependent Gaussian wake model is applied to case 3 and case 4. For case 3, the extreme case with a 40° angle is used, and the resulting potential AEP gain is 1.0%. For case 4, the biased stability distribution is used, and the resulting potential AEP gain is 0.0%. These results are significantly lower than the values found using the Jensen model, which are 9.2% and 0.7%, respectively. The influence of the turbine spacing and ambient wind speed on the potential AEP gain is also studied. For the ambient wind speed, it is found that using the Jensen model, the potential AEP gain is reduced significantly for

wind speeds greater than 12 m/s. The Gaussian model did not show this, because the overall AEP gains are too low for all considered wind speeds. No significant relation between the turbine spacing and the potential AEP gain is found for both the Jensen and the Gaussian model. The Gaussian model resulted in different optimal orientations than the Jensen model for turbine spacings up to 7D. For larger turbine spacings, both models show similar results in terms of the optimal layout. It is concluded that the developed stability-dependent Gaussian wake model should not be used for wind farms with turbine spacings smaller than or equal to 7D.

6.1.3 Stability-dependent layout optimization for a real site using meteorological data

The main goal of chapter 5 is to quantify the benefits of considering atmospheric stability in the layout optimization process by determining the potential AEP gain for a real case using meteorological data. The approach is mostly the same as is described in chapter 3; the stability-dependent Jensen wake model is used, and the optimization method consists of using a fixed layout for which only the orientation is changed. The most important difference with previous cases is that the wind conditions in this case are based on meteorological data, which is obtained from the Dutch Offshore Wind Atlas (DOWA). The location of the chosen site is grid point (48,64) of the DOWA subdomain and is just northeast of the Borssele offshore wind farm in the Netherlands. To determine the stability conditions, the bulk Richardson number is calculated and used to determine the non-dimensional Obukhov length.

The wind conditions are predominantly unstable, with 72.2% of all data points being in either the unstable or very unstable range. The average wind speed for all data points is 9.5 m/s. For the southwest wind direction, which is the most common wind direction, the average wind speed is 11.6 m/s and 56.4% of all data points are (very) unstable. For the north wind direction, the average wind speed is 7.7 m/s and 88.0% of all data points are (very) unstable. These findings are consistent with the general idea that unstable conditions favor lower wind speeds. The stability distribution also shows a decrease of unstable conditions with increasing wind speed, as expected. However, it also shows an unexpected decrease of stable conditions with increasing wind speed. This outcome could be the result of a too high lower boundary for the stable class, as a short test showed that reducing this lower boundary results in a slight increase in stable conditions with increasing wind speed.

It is found that the step size of the orientations in the layout optimization must be equal to the size of the wind direction bins. If these two parameters do not have the same size, the resulting optimal layout is biased towards orientations that are exactly between two wind direction bins. This is because the wind farm is then oriented in such a way that it avoids any aligned wind directions. This finding resulted in a reduction of the wind direction bin size from 15° to 5° and an increase in the orientation step size from 1° to 5°. The optimal orientation for the chosen site is determined to be either 0° or 15°, as both orientations result in the same AEP. The minimum AEP is obtained for the 50° and 55° orientations. This is expected, since for these orientations the wind farm is aligned with the most common wind directions. The AEP difference between the tested orientations is remarkably small, with only a 15 GWh difference between the maximum and minimum AEP. The difference between the neutral and non-neutral case is

even smaller, being only 4 GWh. The potential AEP gain for this case is 0.0%. This result means that there is no benefit in considering the stability conditions in the layout optimization process for this case.

6.2 General conclusion

The main goals of this thesis are to determine the effects of atmospheric stability on the optimal layout of a wind farm and to quantify the potential benefits of considering stability conditions in the layout optimization process. Stability conditions affect the wake recovery within a wind farm. Unstable conditions have an improved wake recovery, while stable conditions have a reduced wake recovery. This means that unstable conditions are generally more beneficial than stable conditions for wind energy production. The stability-dependent wake recovery is implemented in wake models using a stability-dependent wake decay coefficient for the Jensen wake model, and a stability-dependent growth parameter for the Gaussian wake model.

An analysis of the effects of the different stability conditions on the optimization process shows that stable conditions are likely to play a dominant role in the resulting optimal layout. When considering stability effects as an additional factor in wind farm layout optimization, there are two different ways of applying the added stability conditions. The first is to maximize the AEP by maximizing the positive effects of unstable wind directions. The second is to maximize the AEP by minimizing the negative effects of the stable wind directions. Unstable conditions are beneficial due to the improved wake recovery, however, this also means that any wake overlap on subsequent turbines results in smaller power deficits than for neutral or stable conditions. Stable conditions, on the other hand, have a reduced wake recovery and any wake overlap results in large power deficits, compared to neutral or unstable conditions. The benefit of reducing wake overlap is therefore larger for stable conditions than for unstable conditions. This means that the resulting layout is primarily optimized for stable wind directions, even if it means that the unstable wind directions have more wake overlap.

It is concluded that the benefits of considering stability effects in the layout optimization are likely to be insignificant. The initial results, which are obtained from hypothetical cases with unrealistic wind conditions, look promising. These cases all show that by considering stability effects the AEP can be increased by more than 5%. However, as soon as more realistic wind conditions are used, the potential AEP gain is quickly reduced to almost zero. The conclusion is supported by two main arguments. The first argument is that the differences between stability conditions in real applications is too small. Even if a given site would have a wide range of very stable and very unstable conditions, it is still likely that the stability distributions for the different wind directions are similar. The stability conditions could possibly have a significant impact on the resulting optimal layout when there are certain wind directions that have a completely different stability distribution than most other wind directions. Such wind conditions are unlikely, but can occur for example at sites with very distinct geographical features, such as mountains or land-sea transitions. The second argument is that even under the assumption of neutral stability, it is likely that the layout is already optimized for stable conditions. If a wind farm is optimized for a given site that has certain dominantly stable wind directions, it is likely that these wind directions

play a dominant role in the resulting optimal layout. However, it is also known that stable conditions generally occur more frequently in intermediate to high wind speeds. This means that these dominantly stable wind directions are also likely to be the wind directions with the highest wind speeds. If no stability effects are considered, the layout optimization is based on the wind directions that are most common and on the wind directions that have the highest wind speeds. The result is that the wind directions that play a dominant role in the neutral layout optimization, are the exact same wind directions that play a dominant role in the layout optimization in which stability effects are considered. This means that even under the assumption of neutral stability, the layout is already optimized for stable conditions, therefore the consideration of stability effects has no significant impact on the resulting optimal layout.

6.3 Recommendations

In this section, recommendations for future projects are given regarding the developed stability-dependent Gaussian wake model, the layout optimization method, and the chosen site for the real case.

Two recommendations are given for possible improvements to the stability-dependent Gaussian wake model introduced in this thesis. The results of the stability-dependent Gaussian wake model show that the stability effects only start to develop for downwind distances larger than 6D. This is a direct result of the simple method used to implement the stability effects in the model. The growth parameter is only made stability-dependent for the far-wake region. However, with a more advanced method the stability conditions could also be implemented in the near-wake region. This should result in a more realistic behavior, as the differences between velocity deficits for the different stability conditions should then develop at smaller downwind distances. Another improvement would be to directly base the stability-dependency of the wake parameters on values found in literature. In the presented model, the values for the scaling factor of the growth parameter are based on a calibration of the stability-dependent Jensen wake model. The literature used to develop this Jensen model is also based on the stability effects within the Jensen model. It is likely more accurate to base the stability-dependent growth parameter on literature that uses the Gaussian wake model in combination with atmospheric stability effects, such as the work of Krutova et al. (2020) or Habiboella (2019).

The layout optimization method used in this thesis is very simplistic and there are other optimization methods that can be used. The used optimization method assumes a fixed layout of the wind farm and only allows changing in the orientation. This method gives a clear and simple quantification of the change in the resulting layout. However, there are also some clear downsides of using this method. Firstly, it is likely that the square grid layout is not the optimal layout, regardless of the orientation that is used. It could be that there are more subtle changes resulting from the consideration of stability effects, for example that rows should be further apart, or that the angle of the grid should not be 90°. It is not possible to find such changes in the optimal layout with the used method. Secondly, for many wind farm projects there is an assigned area that can be used for the placement of wind turbines. In real

applications, the goal is therefore generally to optimize the layout of a wind farm for a specific area. Rotating the entire wind farm is not possible for such real applications, as doing so significantly changes the boundaries of the wind farm. Ideally, the layout optimization method should therefore take the boundaries of the assigned area into account and only optimize the position of wind turbines within that area. A solution is to use a traditional optimization method, for which the boundaries can be set and the position of each individual wind turbine is optimized.

The final case presented in this thesis uses wind conditions that are based on a meteorological data from a chosen site. The results show that the potential AEP gain for this specific site is 0.0% and it is concluded that there are no benefits in considering stability conditions in the layout optimization process. However, it is also said that there could be a potential benefit for sites that have certain characteristics in their stability distributions. An example of a cause for such stability distributions is a distinct geographical feature, such as a mountain or a land-sea transition. It could be interesting to find meteorological data for sites that have such features. The used method can be applied to sites that have unique stability distributions to determine if there are any cases for which the consideration of stability effects does have a significant impact on the resulting AEP.

References

Abkar, M., & Porté-Agel, F. (2015). Influence of atmospheric stability on wind-turbine wakes: A large-eddy simulation study. *Physics of Fluids*, *27*(3). Scopus. https://doi.org/10.1063/1.4913695

Alblas, L., Bierbooms, W. A. A. M., & Veldkamp, D. (2014). Power output of offshore wind farms in relation to atmospheric stability. *Journal of Physics: Conference Series 555 (2014) 012004*. https://doi.org/10.1088/1742-6596/555/1/012004

Archer, C. L., Colle, B. A., Veron, D. L., Veron, F., & Sienkiewicz, M. J. (2016). On the predominance of unstable atmospheric conditions in the marine boundary layer offshore of the U.S. northeastern coast. *Journal of Geophysical Research: Atmospheres*, *121*(15), 8869–8885. https://doi.org/10.1002/2016JD024896

Ainslie, J.F. (1982). *Comparison of wake models for computing interactive effects between wind turbines*. CEBG.

Barthelmie, R. J., Hansen, K., Frandsen, S. T., Rathmann, O., Schepers, J. G., Schlez, W., Phillips, J., Rados, K., Zervos, A., Politis, E. S., & Chaviaropoulos, P. K. (2009). Modelling and measuring flow and wind turbine wakes in large wind farms offshore. *Wind Energy*, *12*(5), 431–444. https://doi.org/10.1002/we.348

Barthelmie, R.J., Frandsen, S., Rathmann, O., Hansen, K., Politis, E., Prospathopoulos, J., Schepers, J., Rados, K., Cabezon, D., Schlez, W., Neubert, A., & Heath, M. (2011). *Flow and wakes in large wind farms: Final report for UPWIND WP8*.

Barthelmie, R. J., & Jensen, L. E. (2010). Evaluation of wind farm efficiency and wind turbine wakes at the Nysted offshore wind farm. *Wind Energy*, *13*(6), 573–586. https://doi.org/10.1002/we.408

Bastankhah, M., & Porté-Agel, F. (2014). A new analytical model for wind-turbine wakes. *Renewable Energy*, *70*, 116–123. https://doi.org/10.1016/j.renene.2014.01.002

Borvarán, D., Peña, A., & Gandoin, R. (2020). Characterization of offshore vertical wind shear conditions in Southern New England. *Wind Energy*. Scopus. https://doi.org/10.1002/we.2583

Brand, A. J. (2008). *Offshore Wind Atlas of the Dutch part of the North Sea*. ECN.

Cañadillas, B., Foreman, R., Barth, V., Siedersleben, S., Lampert, A., Platis, A., Djath, B., Schulz‐Stellenfleth, J., Bange, J., Emeis, S., & Neumann, T. (2020). Offshore wind farm wake recovery: Airborne measurements and its representation in engineering models. *Wind Energy*, *23*(5), 1249–1265. https://doi.org/10.1002/we.2484

Chamorro, L. P., & Porté-Agel, F. (2010). Effects of Thermal Stability and Incoming Boundary-Layer Flow Characteristics on Wind-Turbine Wakes: A Wind-Tunnel Study. *Boundary-Layer Meteorology*, *136*(3), 515–533. https://doi.org/10.1007/s10546-010-9512-1

DTU Wind Energy. (n.d.). *Wind resource assessment, siting & energy yield calculations - Wake Effect Model*. Technical University of Denmark, Department of Wind Energy. Retrieved March 29, 2021, from https://www.wasp.dk/wasp#details__wakeeffectmodel

Emeis, S. (2010). A simple analytical wind park model considering atmospheric stability. *Wind Energy*, *13*(5), 459–469. https://doi.org/10.1002/we.367

Emeis, S. (2018). *Wind Energy Meteorology: Atmospheric Physics for Wind Power Generation* (2nd ed.). Springer International Publishing. https://doi.org/10.1007/978-3-319-72859-9

FLORIS. (2020). Version 2.2.0 (2020). Available at https://github.com/NREL/floris

Frandsen, S. (1992). On the wind speed reduction in the center of large clusters of wind turbines. *Journal of Wind Engineering and Industrial Aerodynamics*, *39*(1), 251–265. https://doi.org/10.1016/0167-6105(92)90551-K

Frandsen, S., Barthelmie, R., Pryor, S., Rathmann, O., Larsen, S., Højstrup, J., & Thøgersen, M. (2006). Analytical modelling of wind speed deficit in large offshore wind farms. *Wind Energy*, *9*(1–2), 39–53. https://doi.org/10.1002/we.189

Gaumond, M., Réthoré, P.-E., Ott, S., Peña, A., Bechmann, A., & Hansen, K. S. (2014). Evaluation of the wind direction uncertainty and its impact on wake modeling at the Horns Rev offshore wind farm. *Wind Energy*, *17*(8), 1169–1178. https://doi.org/10.1002/we.1625

Ghaisas, N. S., Archer, C. L., Xie, S., Wu, S., & Maguire, E. (2017). Evaluation of layout and atmospheric stability effects in wind farms using large-eddy simulation. *Wind Energy*, *20*(7), 1227–1240. https://doi.org/10.1002/we.2091

Global Wind Energy Council. (2021). *Global Wind Report 2021.* Retrieved July 2, 2021, from GWEC website: https://gwec.net/global-wind-report-2021/

Google. (n.d.). [Google Maps, map of southern coast of the Netherlands]. Retrieved July 1, 2021, from https://www.google.com/maps/@51.8509012,3.8184327,9z

Guo, N., Zhang, M., Li, B., & Cheng, Y. (2021). Influence of atmospheric stability on wind farm layout optimization based on an improved Gaussian wake model. *Journal of Wind Engineering and Industrial Aerodynamics*, *211*, 104548. https://doi.org/10.1016/j.jweia.2021.104548

Habiboella, A.A. (2019). *Jensen-Gaussian wake model extension considering the Atmospheric Boundary Layer effects for the Wind Farm Layout Optimization* [Master Thesis]. TU Delft.

Högström, U. (1988). Non-dimensional wind and temperature profiles in the atmospheric surface layer: A re-evaluation. *Boundary-Layer Meteorology*, *42*(1), 55–78. https://doi.org/10.1007/BF00119875

Højstrup, J. (1983). *Nibe wake, part one*. Internal technical report, Risø.

Holtslag, M. C., Bierbooms, W. A. A. M., & van Bussel, G. J. W. (2014). Estimating atmospheric stability from observations and correcting wind shear models accordingly. *Journal of Physics: Conference Series*, *555*, 012052. https://doi.org/10.1088/1742-6596/555/1/012052

Jensen, N. O. (1983). *A note on wind generator interaction*. Risø National Laboratory. https://orbit.dtu.dk/en/publications/a-note-on-wind-generator-interaction

Jonkman, J., Butterfield, S., Musial, W., & Scott, G. (2009). *Definition of a 5-MW Reference Wind Turbine for Offshore System Development* (NREL/TP-500-38060, 947422; p. NREL/TP-500-38060, 947422). https://doi.org/10.2172/947422

Katic, I., Højstrup, J., & Jensen, N. O. (1987). A Simple Model for Cluster Efficiency. *In W. Palz, & E. Sesto (Eds.), EWEC'86. Proceedings. Vol. 1*, 407–410.

King, J., Fleming, P., King, R., Martínez-Tossas, L. A., Bay, C. J., Mudafort, R., & Simley, E. (2020). Controls-Oriented Model for Secondary Effects of Wake Steering. *Wind Energy Science Discussions*, 1–22. https://doi.org/10.5194/wes-2020-3

KNMI. (2018). Dutch Offshore Wind Atlas - time series files from 2008-2017 at 10-600 meter height at individual 2,5 km grid location. https://dataplatform.knmi.nl/dataset/dowa-netcdf-ts-singlepoint-1

Krutova, M., Paskyabi, M. B., Nielsen, F. G., & Reuder, J. (2020). Evaluation of Gaussian wake models under different atmospheric stability conditions: Comparison with large eddy simulation results. *Journal of Physics: Conference Series*, *1669*, 012016. https://doi.org/10.1088/1742-6596/1669/1/012016

Martínez-Tossas, L. A., Annoni, J., Fleming, P. A., & Churchfield, M. J. (2019). The aerodynamics of the curled wake: A simplified model in view of flow control. *Wind Energy Science*, *4*(1), 127–138. https://doi.org/10.5194/wes-4-127-2019

Paulson, C. A. (1970). The Mathematical Representation of Wind Speed and Temperature Profiles in the Unstable Atmospheric Surface Layer. *Journal of Applied Meteorology (1962-1982)*, *9*(6), 857–861.

Peña, A., & Rathmann, O. (2013). Atmospheric stability-dependent infinite wind-farm models and the wake-decay coefficient. *Wind Energy*, *17*(8), 1269–1285. https://doi.org/10.1002/we.1632

Peña, A., Réthoré, P.-E., & Rathmann, O. (2014). Modeling large offshore wind farms under different atmospheric stability regimes with the Park wake model. *Renewable Energy*, *70*, 164–171. https://doi.org/10.1016/j.renene.2014.02.019

Rodrigo, J. S., Arroyo, R. C., Gancarski, P., Guillén, F. B., Avila, M., Barcons, J., Folch, A., Cavar, D., Allaerts, D., Meyers, J., & Dutrieux, A. (2018). Comparing Meso-Micro Methodologies for Annual Wind Resource Assessment and Turbine Siting at Cabauw. *Journal of Physics: Conference Series*, *1037*, 072030. https://doi.org/10.1088/1742-6596/1037/7/072030

Salimi, M. (2016). *Modelling atmospheric stability effects on wakes by actuator disk simulations* [Master Thesis]. TU Cottbus.

Samorani, M. (2010). The Wind Farm Layout Optimization Problem. *Handbook of Wind Power Systems, Energy Systems*. https://doi.org/10.1007/978-3-642-41080-2_2

Schmidt, J., Chang, C.-Y., Dörenkämper, M., Salimi, M., Teichmann, T., & Stoevesandt, B. (2016). The consideration of atmospheric stability within wind farm AEP calculations. *Journal of Physics: Conference Series*, *749*, 012002. https://doi.org/10.1088/1742-6596/749/1/012002

Stevens, R., Graham, J., & Meneveau, C. (2014). A concurrent precursor inflow method for Large Eddy Simulations and applications to finite length wind farms. *Renewable Energy*, *68*, 46–50. https://doi.org/10.1016/j.renene.2014.01.024

Stull, R. (2017). *Practical Meteorology: An Algebra-based Survey of Atmospheric Science*. University of British Columbia. https://www.eoas.ubc.ca/books/Practical_Meteorology/

UNFCCC. (n.d.). *The Paris Agreement.* United Nations Framework Convention on Climate Change. Retrieved July 2, 2021, from https://unfccc.int/process-and-meetings/the-paris-agreement/the-paris-agreement

Vermeulen, P.E.J., Builtjes, P., Dekker, J., & van Bueren, G. (1979). *An experimental study of the wake behind a full scale vertical-axis wind turbine.* TNO-report, No. 79-06118.

Wharton, S., & Lundquist, J. K. (2012). Assessing atmospheric stability and its impacts on rotor-disk wind characteristics at an onshore wind farm. *Wind Energy*, *15*(4), 525–546. https://doi.org/10.1002/we.483

World Wind Energy Association. (2020). *Global Statistics 1980-.* Retrieved from WWEA website: https://library.wwindea.org/global-statitistics-1980/

Zhang, W., Markfort, C. D., & Porté-Agel, F. (2012). Near-wake flow structure downwind of a wind turbine in a turbulent boundary layer. *Experiments in Fluids*, *52*(5), 1219–1235. https://doi.org/10.1007/s00348-011-1250-8

APPENDIX A:
NREL 5MW reference turbine specifications

The NREL offshore 5-MW baseline wind turbine is described briefly in section 2.5.1. This wind turbine model is the default model in the wake modeling utility FLORIS, which is also developed by NREL. Gross properties of the wind turbine, such as rotor diameter and rated wind speed, are given in table A.1. Steady-state responses, including the power curve and the thrust curve, are given in figure A.1.

Table A.1. Gross properties of the NREL offshore 5-MW baseline wind turbine. (Jonkman et al., 2009)

Rating	5 MW
Rotor Orientation, Configuration	Upwind, 3 Blades
Control	Variable Speed, Collective Pitch
Drivetrain	High Speed, Multiple-Stage Gearbox
Rotor, Hub Diameter	126 m, 3 m
Hub Height	90 m
Cut-In, Rated, Cut-Out Wind Speed	3 m/s, 11.4 m/s, 25 m/s
Cut-In, Rated Rotor Speed	6.9 rpm, 12.1 rpm
Rated Tip Speed	80 m/s
Overhang, Shaft Tilt, Precone	5 m, 5º, 2.5º
Rotor Mass	110,000 kg
Nacelle Mass	240,000 kg
Tower Mass	347,460 kg
Coordinate Location of Overall CM	(-0.2 m, 0.0 m, 64.0 m)

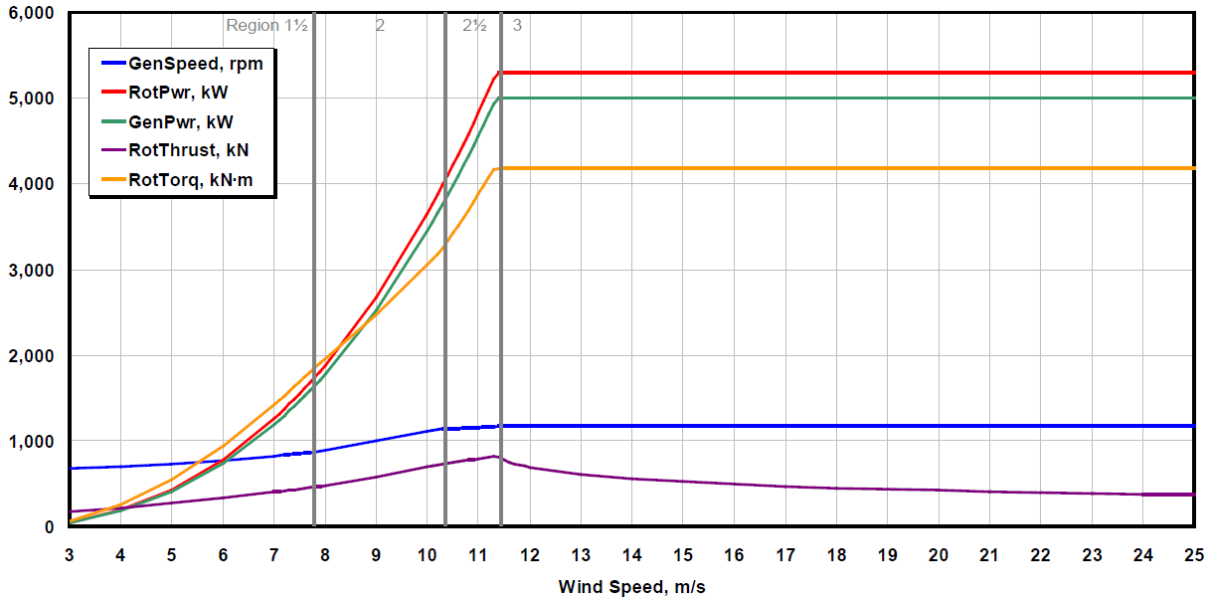

Figure A.1. Steady-state responses as a function of wind speed. (Jonkman et al., 2009)